

Dissertation
submitted to the
Combined Faculties for the Natural Sciences and for Mathematics
of the Ruperto-Carola University of Heidelberg, Germany
for the degree of
Doctor of Natural Sciences

presented by
Diplom-Chemieingenieur - Per Hillertz,
Master of Science in Chemical Engineering,
Born in: Göteborg, Sweden

Oral examination:.....

Advances in Fragment-Based Drug Discovery: *studies of cAMP-dependent protein-kinase A using X-ray-crystallography, surface-plasmon-resonance and high compound concentration assays.*

Referees: Prof. Dr. Irmgard Sinning
Prof. Dr. Klaus Scheffzek

TABLE OF CONTENTS

ACKNOWLEDGEMENTS	5
ABSTRACT	7
ZUSAMMENFASSUNG	8
LIST OF FIGURES	9
LIST OF TABLES	10
LIST OF SYMBOLS, ABBREVIATIONS, AND ACRONYMS	10
CHAPTER 1	12
INTRODUCTION	12
1.1. Fragment-based lead discovery (FBLD)	12
1.2. Applications of FBLD	19
1.3. Protein Kinases and PKA	21
1.3.1. PKA - the cAMP-dependent protein kinase	23
1.3.2. Protein kinases and FBLD.....	26
1.3. The aim of this study	26
CHAPTER 2	28
MATERIALS AND METHODS	28
2.1. Materials.....	28
2.1.1. Chemicals	28
2.1.2. Inhibitors	28
2.1.3. Protein, human-PKA	29
2.1.4. Experimental buffers, solutions, and materials	29
2.1.5. Computer software	34
2.2. Methods.....	35
2.2.1. Protein crystallography.....	35
2.2.2. Surface-Plasmon-Resonance analyses	42
2.2.3. Biochemical assays at high fragment concentrations.....	57
2.2.4. Fragment-library design	59
CHAPTER 3	62
RESULTS	62
3.1. FBLD involving SPR, HCA, and Protein Crystallography.....	62
3.1.1. Results of Surface-Plasmon-Resonance (SPR) analyses.....	62
3.1.2. High-compound-Concentration biochemical Assays.....	74

3.1.3. Protein crystallography.....	75
3.1.4. A Review of selected results	78
3.2. Results obtained by employing available biochemical-assay data in the protein-crystallographic analyses.....	83
CHAPTER 4	89
DISCUSSION.....	89
4.1 Conclusions	98
BIBLIOGRAPHY	100
APPENDIX 1	112
APPENDIX 2	115
APPENDIX 3	118

ACKNOWLEDGEMENTS

First, I would like to thank Djordje Musil for granting me the opportunity to come to his lab for my doctoral studies. It has been several very nice years and I cannot express just how much I have appreciated the time I spent here. He never failed to take the time to explain the work involved and discuss the problems that turned up and the opportunities available for solving them. A better and nicer supervisor would be hard to find. I would also like to thank Prof. Dr. Irmgard Sinning for allowing me to join her group as a doctoral student. I thank her for the practical support, friendliness, and help during my work on my doctoral dissertation.

I would like to thank the various departments and groups at MerckSerono for all the help and guidance I received during my work there and the very pleasant atmosphere. Special thanks are due Verena Dresing, Martin Lehmann, Ulrich Grädler, Thorsten Knöchel, and Judith Schmiedel of the X-ray team, as well as Jörg Bomke, Andreas Schönemann, Norbert Avemarie, and Yvonne Bischoff of the BIACORE-team. I would also like to thank ITC-team members Ansgar Wegener, Eva-Maria Leibrock, and Gerlinde Bönisch, as well as Protein-Purification Group members Dirk Müller-Pompalla, Jens Hannewald, Stephan Keller, Stefan Jäkel, and colleagues, both for their help with the work involved and the nice breakfasts and friendly atmosphere that prevails in the Q27-building. I would like to further thank the other students in the various departments at MerckSerono and specially thank Dirk Vocke and student colleagues at the Oncology Department and, of course, Judith Schmiedel and Silvia Santos at the MIB-Department. Collaborating with them has been a valuable experience.

I am also very grateful to Mireille Krier, Gerhard Barnickel, Michael Krug, Christian Herhaus, Ulrich Grädler, Paul Czodrowski, Thomas Grombacher, Anja Heydebreck, Christian Griebel, Frank Morawietz, Friedrich Rippmann, and colleagues at the Bioinformatics and Chemoinformatics Department for their assistance and the collegial ambience. Thanks for all the help and guidance during my work there and for familiarizing me with the fragment-docking and library-generation approaches.

I would also like to thank the numerous persons at the Medicinal-Chemistry Department who always had answers to my questions regarding the chemistry of the structures of the complexes formed by the various fragments and proteins. Special thanks are due Günther Hölzemann, Alfred Jonczyk, Dieter Dorsch, Margarita Wuchrer-Plietker, Dirk Finsinger,

Michel Calderini, Mathias Osswald, and Hans-Peter Buchstaller for their discussions and answers to various questions regarding the fragments involved.

I would also like to thank the numerous persons at the Screening Department who explained matters related to screening, biology, and chemical compounds. Thanks also for the nice parties they organized, which were great. Thanks are also due the Oncology Department, with special thanks to Frank Zenke, who invariably took the time to elucidate matters related to protein kinase and various topics related to my oncological work. At the Oncology Department, I would also like to thank Christina Esdar and Christiane Amendt for allowing me to participate in the work of their Disease-Project Teams, which I greatly appreciated. I thoroughly enjoyed working with them. Thanks also to the various members of the teams involved. I had a great time there and learned a lot from working with them.

My special thanks to Prof. Dr. Gerhard Klebe and all of the members in his group at Marburg University. Sascha Brass, Tobias Craan, Helene Krüger, Patrick Pfeffer, Gerd Neudert, Tina Ritschel, and Jark Böttcher are but a few of the numerous group members who made my collaborations with them an exhilarating experience. Thanks also to Lars Neumann and Doris Hafebradl at Proteros Biostructures GmbH for the fruitful work and discussions of fragment screening.

My special thanks to Djordje Musil, Matthias Frech, and Jörg Bomke for all the help, support, straight answers, and suggestions for corrections while I was finishing this dissertation. Special thanks are also due Jens Hannewald for allowing me to stay at his place and the great grill parties we had. Thanks also to Verena Dresing for allowing me to use her apartment while she was away.

Someone who means a lot to me, helped me, supported me in all sorts of ways, and, in the end, had to read and reread this dissertation countless times, is Sofia. Thank you for your patience and understanding. I would also like to thank my family and friends, all of whom mean a lot to me and have helped me in various ways. For example, my grandmother used to say that no one bothers about how long it took to accomplish something, just how well it was done.

Thanks again to all of you for a truly great time.

ABSTRACT

Development of a new, or candidate, therapeutic drug is a challenging process that must ensure that favorable target selectivity, potency, pharmacokinetics, and pharmacodynamics, as well as lack of toxicity, all fall within the therapeutic window. During the hit-optimization stage, the focus shifts toward optimizing potency and target selectivity. Fragment-based methods have recently been developed to the point where they represent a promising strategy in drug discovery, where a variety of biophysical techniques may be employed for fragment library screening and characterizing hit-fragments. Hit-fragments deduced from fragment-based screenings typically have ligand efficiencies (LE) exceeding those of average HTS-hits. Structure data on the complexes formed by fragment-target-protein structures yield a much-better starting point for hit optimization and lead discovery.

This dissertation presents two fragment-screening studies. Under the first, surface-plasmon-resonance (SPR) analyses and biochemical assays at high compound concentrations (HCA) were employed in primary screenings of protein-kinase A (PKA) that were followed by X-ray crystallographic determinations of the structures of the PKA-fragments involved. The aim of that study was testing the characteristics, outcomes, and limits of both SPR and HCA as fragment-screening methods, as well as estimating hit rates that could be confirmed by X-ray crystallographic analyses. Under the second, in-house, biochemical-assay data were used for selecting the fragment-like inhibitors of PKA to be subjected to X-ray crystallographic structure determinations. The biochemical-assay data involved were taken from screening campaigns, such as high-throughput screenings (HTS), or other, available, in-house, biochemical-assay runs. The goal there was estimating the extent to which existing HTS-data might be utilized for obtaining three-dimensional, fragment-target, protein structure data, without need for conducting any additional fragment-screening runs.

Following screening a library of 257 fragment-like compounds using SPR and HCA, a total of 26 hit-fragments were chosen for X-ray structure determinations, which yielded the structures of nine fragment-PKA-structures. Under the second approach, 67 fragments exhibiting > 50 % inhibitions taken from the available, in-house, biochemical-assay data were selected for structure determinations, which yielded the structures of 21 fragment-PKA-complexes. Both approaches yielded respectable hit rates and descriptions of the characteristics of numerous fragment-protein interactions. The structural information and data on fragment-target-protein complexes gained from those two setups might well accelerate the drug-discovery process throughout the pharmaceutical industry.

ZUSAMMENFASSUNG

Die Entwicklung eines neuen therapeutischen Arzneimittels ist ein umfassender Prozess. Sie schließt umfangreiche Studien von Wirksamkeit, Selektivität, Pharmakokinetik, Pharmakodynamik und Toxizitätsbestimmungen ein. Während der Hit-Optimierungsstufe liegt der Fokus auf der Optimierung von Bindungsaffinität und Selektivität. Als vielversprechende Strategie werden seit kurzem Fragment-basierte Studien als neue Methode im Bereich der Wirkstoffidentifizierung angewendet (Fragment Based Drug Discovery - FBDD). Dabei kommen eine Vielzahl biophysikalischer Technologien für das sogenannte Fragment-Screening und die Charakterisierung von Hit-Fragmenten zum Einsatz. Die im Fragment-Screening gefundenen Hit-Moleküle haben in der Regel eine höhere Ligand-Effizienz (LE) als HTS-hits. Die nachfolgende Aufklärung des Bindungsmodus der Fragment-Hits im Proteintarget durch Röntgenstrukturanalyse ist essentieller Bestandteil des Fragment-Screenings. Die Strukturdaten dieser Fragment-Target-Proteinstrukturen gebildet geben einen viel besseren Ausgangspunkt für die folgende Hit-Optimierung durch rationales Design.

Die vorliegende Dissertation präsentiert zwei Fragment-basierte Studien zum Screening von Protein-Kinase A (PKA) Inhibitoren. Zuerst wurden Oberflächen-Plasmon-Resonanz (Surface Plasmon Resonance - SPR) Analysen und biochemische Inhibitionsmessungen bei hohen Fragment Konzentrationen (High Concentration Assay - HCA) durchgeführt. Danach erfolgte die Strukturbestimmung der PKA-Fragment Komplexe mit Hilfe der Röntgenstrukturanalyse.

Das Ziel dieser Studie war die Prüfung der Kenndaten, Ergebnisse und Grenzen von SPR und HCA als Fragment-Screening-Methoden, sowie die Bestätigung der Fragment-hits durch Röntgenstrukturanalyse. In der zweiten Studie wurden Daten eines bei Merck etablierten biochemischen Assays für die Fragmentwahl herangezogen und ebenfalls die Struktur dieser Fragment-PKA Komplexe kristallographisch bestimmt. Die biochemischen Inhibitionsdaten werden parallel zu den Screening-Kampagnen, wie z. B. High-Throughput-Screening (HTS) und anderen Merck internen Tests erfasst. Ziel war es, zu klären, in welchem Umfang bestehende HTS-Daten ohne zusätzliches Fragment Screening für den Erhalt von dreidimensionalen Fragment-Target-Protein-Struktur-Daten genutzt werden können.

Es wurde eine Bibliothek von 257 Fragment Molekülen mittels SPR und HCA gescreent. Aus den Ergebnissen wurden insgesamt 26 Hit-Fragmente für X-ray Bestimmungen gewählt, woraus neun Fragment-PKA-Strukturen gelöst werden konnten. Im zweiten Ansatz wurden 67 Fragmente für die Röntgenstrukturanalyse ausgewählt, die in den biochemischen Inhibitionsmessungen eine mehr als 50%ige Hemmungen der PKA Substrat-Phosphorylierung zeigten. Aus diesem Ansatz ergaben sich 21 Fragment-PKA-Komplex Strukturen. Beide Ansätze ergaben beachtliche Trefferquoten und interessante Bindungsmodi der Fragment-Protein-Interaktionen. Die in dieser Arbeit identifizierten Fragmente und Proteinstrukturen zeigen den Erfolg Fragment-basierter Methoden in der Wirkstoffforschung.

LIST OF FIGURES

Fig. 1. Illustration of the expansion of the chemical space covered under FBLD	13
Fig.2. Diagrammatic representation of a model molecular framework.....	15
Fig.3. Workflow for a fragment-based lead-discovery project.	17
Fig.4. Examples of two approaches to upgrading fragments into lead molecules.	18
Fig.5. Protein kinases and phosphatases	22
Fig.6. The catalytic sub-unit of PKA.	25
Fig.7. The ATP binding pocket in cAMP-dependent protein-kinase A.	26
Fig.8. Solubility plot for proteins.	36
Fig. 9. Schematic of the SPR-fragment technique.	43
Fig.10. SPR-detection.....	43
Fig.11. A sample SPR-sensorgram.....	44
Fig.12. The five detection areas employed in immobilizing protein on the sensor chip.....	47
Fig.13. Sensorgrams for the positive-control samples employed in screening and hit characterization.	63
Fig.14. A plot of the responses obtained from fragment screenings.....	64
Fig.15. Sensorgrams of a fragment that interacted with both PKA and CA.	65
Fig.16. Sensorgrams of a typical hit-fragment.	66
Fig.17. Sensorgrams of fragments exhibiting promiscuous binding.....	67
Fig.18. The results of SPR-hit characterizations.	68
Fig.19. An example of a fragment that exhibited transient binding and was assigned an estimated affinity.....	69
Fig.20. Sensorgrams for a fragment exhibiting transient binding, but for which no K_D was computed.	70
Fig.21. Sensorgrams of fragments exhibiting promiscuous binding.....	71
Fig.22. Sensorgrams of a superstoichiometric binder.	72
Fig.23. Sensorgrams of a fragment undergoing pseudo-irreversible binding to the protein involved.	73
Fig.24. Sensorgrams of a fragment exhibiting concentration-dependent aggregation.....	74
Fig.25. HCA hit-characterization data for two fragments.....	75
Fig.26. The binding modes of the nine hit-fragments to PKA.	77
Fig.27. Binding data for fragment 6.....	79
Fig.28. Binding data for fragment 19.....	80

Fig.29. Binding data for fragment 20.....	81
Fig.30. Binding data for fragment 57.....	82
Fig.31. Sample fragments selected for protein crystallography.....	83
Fig.32. The ATP binding pocket in cAMP-dependent protein-kinase A.....	84
Fig.33. A depiction of the overlappings of fragments bound in the A-zone of PKA.....	85
Fig.34. Binding to the BP-I-pocket and K-zone of PKA.. ..	86
Fig.35. The three conformations of Thr-183 in PKA.....	86
Fig.36. Interactions occurring in the E ₀ - and R-zones	87
Fig.37. Glycine-rich loop conformations.	88
Fig.38. A schematized depiction of fragment-fragment and fragment-protein interactions....	91
Fig.39. Fragment binding modes overlapped by known PKA-inhibitor molecules.....	97

LIST OF TABLES

Table 1. Fragment-molecule selection criteria.....	16
Table 2. Clinical and preclinical candidates derived from fragments.....	19
Table 3. Classifications of protein kinases into subfamilies.....	22
Table 4. Criteria for SPR fragment screening hit selection.....	66
Table 5. An overview of the protein-crystallography studies conducted under the present approach to FBLD.....	76
Table 6. Selective interactions observed in conjunction with screenings	78
Table 7. An overview of fragment-protein interactions.....	84
Table 8. The methods employed in, and the results obtained from, the two FBLD-approaches involved.....	89
Table 9. Binding modes for the nine fragments involved	112
Table 10. The results of the X-ray-crystallographic investigations conducted.....	115
Table 11. Characterization data for all those fragments contained in the library	118

LIST OF SYMBOLS, ABBREVIATIONS, AND ACRONYMS

Å	Ångström (10 ⁻¹⁰ m)
ATP	adenosin triphosphate
cAMP	3', 5'-cyclic adenosin monophosphate
Da	Dalton
<i>E. coli</i>	<i>Escherichia coli</i>
EDTA	ethylenediaminetetraacetic acid
FBDD	fragment-based drug discovery

FBLD	fragment-based lead discovery
Fc	computed structure factor
Fo	empirically observed structure factor
HTS	high-throughput screening
Kd	dissociation constant
λ	wavelength
LE	ligand efficiency
MWT	molecular weight
NMR	nuclear magnetic resonance
PDB	protein database
PEG	polyethylene glycol
PKA	protein-kinase A
R	ideal-gas constant
RO3	rule of three
SAR	structure-activity relationship
T	temperature

LIST OF SYMBOLS AND ABBREVIATIONS DESIGNATING AMINO ACIDS AND PROTEIN RESIDUES

Alphabetic Symbol	Abbreviation	Chemical Name
A	Ala	alanine
C	Cys	cysteine
D	Asp	aspartic acid
E	Glu	glutamic acid
F	Phe	phenylalanine
G	Gly	glycine
H	His	histidine
I	Ile	isoleucine
K	Lys	lysine
L	Leu	leucine
M	Met	methionine
N	Asn	asparagine
P	Pro	proline
Q	Gln	glutamine
R	Arg	arginine
S	Ser	serine
T	Thr	threonine
V	Val	valine
W	Trp	tryptophan
Y	Tyr	tyrosine
X	(varies)	protein residue
Aa		amino acid

Chapter 1

INTRODUCTION

1.1. FRAGMENT-BASED LEAD DISCOVERY (FBLD)

The development of new therapeutic drugs requires the maturation of chemical compounds possessing attributes that makes them effective medications. Specificity, potency, bioavailability, duration of action, and lack of toxicity are some of the parameters that have to be considered and optimized in the course of designing drug molecules and that define the final characteristics of drug-like compounds. The challenge in preclinical drug discovery research is identifying the optimized molecular properties involved.

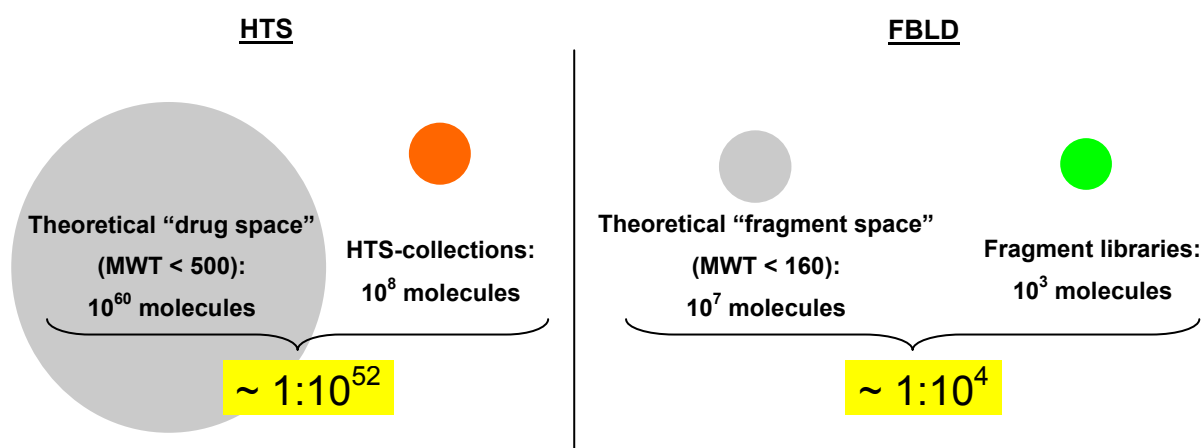
Screening large collections of compounds is a leading paradigm for identifying new starting points for developing drug molecules. Under screening campaigns, large collections of molecules are rapidly tested for activity against targets using high-throughput screening (HTS) techniques. Compounds identified as hits are characterized and upgraded by pharmaceutical chemists in order to arrive at drug-like properties (Jhoti, 2005).

Upgrading compounds listed in screening libraries leads to the development of molecules that are characterized as “lead-like.” Lead-like molecules possess a majority of the parameters of drug-like compounds, but lack final proof that they are optimal choices. The concepts “lead-like” and “drug-like” have been developed in order to describe what constitutes good leads for drug development, and imply cutoff points in the physicochemical profiles of the compounds involved that will limit their complexity, for example, confine their molecular weights to values < 400 (Hann and Tudor, 2004)

Recently, there has been increasing interest in a new approach to generation of lead-like molecules based on identification of small molecules termed “fragments” (Davies, et al., 2004). Such fragments have low molecular weights, typically less than 300 Da, and usually

contain fewer functional groups (Hartshorn, et al., 2005). Employment of fragments in drug development is alternatively referred to as “fragment-based lead discovery (FBLD), “fragment-based drug discovery,” (FBDD) or “fragment screening.”

Employment of FBLD has revealed several key factors that are critical in the case of fragment-based approaches and distinguish them from other hit-identification techniques. The first is a more-efficient probing of the chemical space (Jahnke and Erlanson, 2006). Screening collections of smaller molecules allows more efficiently covering the chemical space involved, which may be exemplified by comparing a library of fragment molecules with a library of molecules that might have come from an HTS-collection program. The theoretical total number of prospective fragment molecules composed of twelve or fewer heavy atoms, excluding three-member and four-member ring structures, has been estimated to be 10^7 , while the total number of prospective drug-like molecules, i.e., molecules composed of thirty or fewer heavy atoms, has been estimated to exceed 10^{60} (Jahnke and Erlanson, 2006). A fragment-compound library listing fewer molecules than a library listing molecules obtained from an HTS-collection can therefore represents a basis for screening more of the chemical space falling within the applicable molecular-weight range. Fig.1 depicts the definitions of chemical space employed in HTS and FBLD.



Source: Fragment-Based Approaches in Drug Discovery, (2006), Wiley VCH

Fig. 1. Illustration of the expansion of the chemical space covered under FBLD (Jahnke and Erlanson (2006)). The estimated, theoretical drug space covers 10^{60} molecules (Jahnke and Erlanson, 2006), while the theoretical fragment space covers 10^7 molecules, which leads to a greatly condensed compound collection, or library, capable of covering larger portions of the chemical space when working with FBLD-approaches.

The second results from the fact that smaller molecules are better able to adapt their interactions to suit conditions in targets’ binding pockets, which leads to fragment binding

efficiencies per atom, which might also be termed “ligand efficiencies” (LE), that are at least equal to those for larger hit-molecules. Fragment LE are defined as their Gibbs free energy, ΔG , divided by the total number of heavy atoms, i.e., atoms heavier than hydrogen, #HA, that they incorporate (Hopkins, 2004), i.e.:

$$LE = \frac{\Delta G}{\#HA} = \frac{R \cdot T \cdot \ln K_D}{\#HA} \quad (\text{Eq. 1})$$

Application of alternative approaches to screening for drug-target interactions provides supplementary data of use in searches for chemical scaffolds. Since fragment molecules have properties that differ from those of typical HTS-hits, employing fragments could benefit both novelty and downstream intellectual-property rights in conjunction with optimizations of hits targeted at arriving at marketable drugs (Albert, et al., 2007). The aim is finding small scaffolds that might serve as starting points for synthetic efforts to arrive at compounds other than those listed in HTS compound pools.

The emergence of low-affinity fragments as prospective starting points for pharmacological optimizations necessitates a re-evaluation of the generally accepted criteria governing compounds regarded as screening hits. Even low-affinity compounds might represent viable candidates for admission to the relevant chemical space. If a rational hypothesis for elaboration of the compounds involved can be formulated, low-affinity fragments might also support the discovery of new active drug ingredients. FBLD’s ability to supply that information is dictated by the detection limits of the techniques employed, which has been a key factor in the development of FBLD-methods. Technical advances and the availability of more-sensitive detection systems have allowed development of various methods for characterizing a large number of low-affinity interactions. In many cases, the techniques involved have been developed in conjunction with fragment-based studies.

In general, the objective of screening campaigns is sifting out numbers of compounds covering chemical spaces that will be sufficient for supplying data that may be utilized in creating drugs that will be effective against specific targets. The numbers of compounds involved must fall within testable ranges for the particular targets and methods employed. Numerous examples of fragment libraries have been mentioned in the literature. Although they typically cover fewer than 1,000 fragment molecules (Reynolds, et al., 2008), some cover several thousand molecules (Jahnke and Erlanson, 2006; Hartshorn, et al., 2005). The essential properties of the fragments covered must be accurately known and reliable. High

fragment solubility and presence of no more than a few reactive groups represent fragment properties of importance when endeavoring to avoid interferences with screening assays, thereby minimizing the numbers of false positives and false negatives that arise during screening (Jahnke and Erlanson, 2006). Suitable fragment solubilities are thus one of the most-important fragment properties (Di and Kerns, 2006). Concentrated stock solutions should have solubilities therein falling within the range 10^{-1} M – 1 M (Ciulli and Abell, 2007). The purities and chemical stabilities of fragment molecules are also important. A "rule of three" (RO3) has been derived from analyses of a diverse set of hit-fragments identified as such against a range of targets (Congreve, et al., 2003). That study indicated that hit-fragments appeared to track just a few molecular properties. The RO3 defines the molecular weights (MWT) of fragments as less than 300Da, the computed octanol/water partition coefficient (clogP) as equal to, or less than, 3, the total number of hydrogen-bond acceptor and donors (HBA and HBD, respectively) as equal to, or less than, 3, and the total number of rotatable bonds (NROT) as equal to, or less than, 3. It also suggests that the total polar surface areas (TPSA) of the individual molecules involved are equal to, or less than, 60 \AA^2 (cf. Table 1). Further suggestions for fragment properties of interest have been based on designs for a fragment "molecular framework" (Bemis and Murcko, 1996; Bemis and Murcko, 1999; Bohacek, et al., 1996). Combinations of ring systems, subring systems, linker atoms, and side chains may be utilized for generating complex chemical conformations. Once their patternings have been deduced, drug designers may apply them in various ways, for example, to designing a fragment-molecule library. Fig.2 depicts a sample design for a molecular framework.

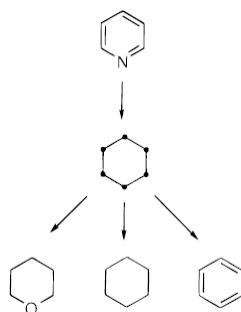


Fig.2. Diagrammatic representation of a model molecular framework (Bemis and Murcko, 1996). The structure framework of a six-member ring has been utilized for forming several, different, six-member, ring scaffolds. Employment of various molecular frameworks allows assembling a wide variety of chemical scaffolds for use in FBLD-approaches.

Examples of recently developed criteria that have been incorporated into the designs of fragment libraries are synthetic tractability, increased scaffold coverage, or the availability of close molecular analogs (Schnur, 2008; Gillet, 2008; Jahnke and Erlanson, 2006; Leach, et al.,

2006). An example of a tractable synthetic chemical group is a fragment having a carboxylic acid appendage that might provide a handle for further chemical upgradings in conjunction with fragment optimizations (Jahnke and Erlanson, 2006). However, such approaches need to be handled with care, since it is likely that tractable chemical groups provide key interactions with target proteins that would be removed by chemistry that makes use of their tractability. Furthermore, fragments should not contain any reactive chemical groups. Groups or chemical scaffolds that randomly react with numerous targets are usually termed “frequent hitters” (Roche, et al., 2002) or “bad functional groups” (BFGs). Table 1 lists several selection criteria applying to fragment molecules.

Table 1. Fragment-molecule selection criteria. There are several approaches to designing fragment libraries, where the “rule of three” (RO3) is commonly employed. Empirical parameters, such as fragment solubilities, purities, and chemical stabilities, are collected and evaluated. Certain molecular frameworks may be used. Further approaches are usage of chemical handles or targeted libraries for certain protein classes. The parameters involved are frequently derived from *in-silico*/computational approaches, combined with manual inspections.

Rule of Three	Experimental Factors	Other Factors
Molecular weight < 300 Da	Solubility in stock solutions (10^{-1} M - 1 M)	Molecular frameworks
clogP < 3	Solubility in buffering solutions (10^{-3} M - 10^{-2} M)	Exclusion of reactive groups
HBA < 3	Chemical purity	Chemical handles
HDB < 3	Chemical stability	Fragment analogs available
NROT < 3	Commercial availability	A library targeted against a specific class of proteins
TPSA < 60 \AA^2		

Since fragment affinities frequently fall within the μM - mM concentration range, fragment-screening methodologies must be able to detect fragment binding constants over that concentration range. Most detection techniques also require binding-site occupancies of > 20 % for reliable identifications of ligand binding (Jahnke and Erlanson, 2006). Employment of high fragment concentrations will thus be necessary. Detection of relatively weak interactions and high fragment concentrations imposes stringent demands upon screening and characterization methods. Experimental methods, such as nuclear magnetic resonance (NMR), surface plasmon resonance (SPR), mass spectrometry (MS), biochemical assays and protein crystallography, represent screening methods that have been mentioned in conjunction with FBLD-applications (Zartler and Shapiro, 2005). Technical progress in those areas has led to their successful employment in FBLD-applications, which, in turn, has led to FBLD acquiring greater acceptance as a further tool of use in early-stage, preclinical, drug discovery.

In most cases, the characteristics of the fragment-target interactions involved will fail to meet the criteria demanded of lead-like or drug-like compounds. Chemical synthesis is then applied in order to manipulate and upgrade fragment properties in order to yield sustainable series of chemical leads (Leach, et al., 2006). Fragments may be viewed as building blocks that may be combined or elaborated on in order to form more-potent, more-attractive, lead compounds. Numerous approaches have been applied to the identification and elaboration of fragment molecules. Fig.3 presents an example of a workflow chart for a typical fragment-based lead-discovery project.

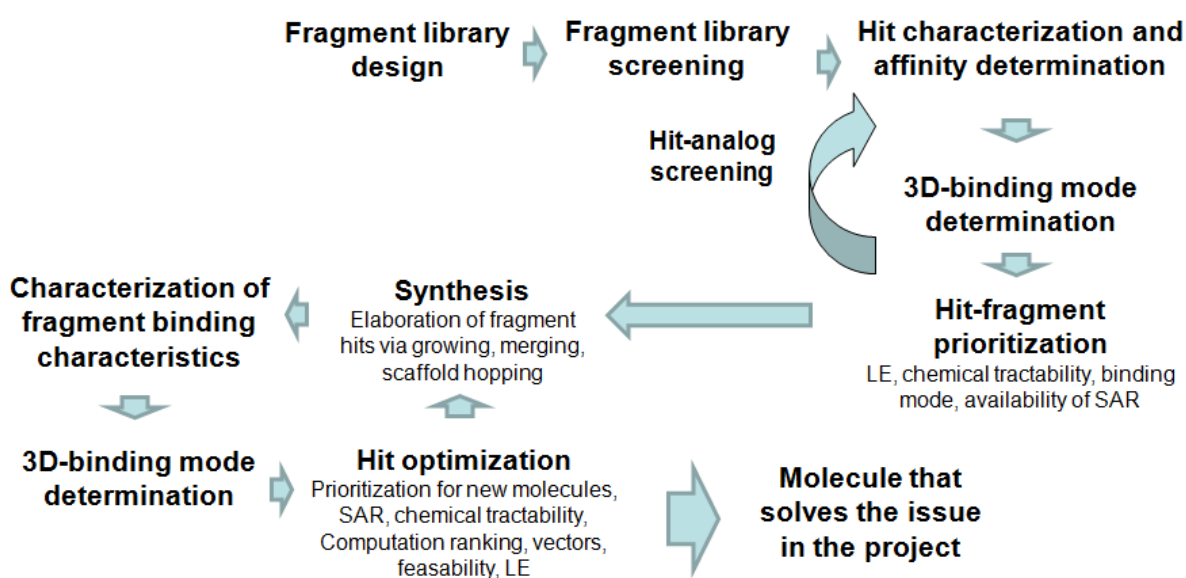


Fig.3. Example of a workflow for a fragment-based lead-discovery project. Example diagram of a workflow and screening cascade for the case where target structure information is available (Jahnke and Erlanson, 2006). A library is designed and an initial screening subsequently detects fragment hits, which is followed by a characterization of the hit-fragments involved in order to determine their affinities. X-ray crystallography is then applied in order to determine their 3D-binding modes on the target. A decision-making point, where the data must be analyzed in order to decide on the next approaches, such as pharmacological studies, to be employed then arises. For example, ligand efficiencies (LE) might be computed and analogs of the hits subjected to testing. The fragments involved then enter the optimization cycle, where x-ray crystallographic analyses, binding-constant determinations, and pharmacological syntheses are employed in order to optimize molecules and arrive at compounds that are more lead-like.

One approach depicted in Fig.3 is searching for molecular analogs to hit-fragments. Molecules that are structurally similar to hit-fragments are identified and tested for activity against the target in order to discover molecules having binding affinities better than those of initial hits (Carr, et al., 2005). Such minor structure modifications allow arriving at structure-activity relationships (SAR) centered on initial fragment hits. The aim there is assessing the latent efficiencies of molecular chemical cores, e.g., assembling a pharmacophore. The pharmacophore/fragment may then be employed in several ways, e.g., employed in computational approaches or synthetic-chemistry approaches.

Several common means for utilizing hit-fragments for developing lead molecules are those termed “fragment growing,” “fragment merging,” and “fragment linking,” along with the employment of fragments in “scaffold hopping.” Fragment growing utilizes the fragments involved as starting points, where fragment molecules are modified, or grown, such that they pick up more interactions in binding pockets and acquire greater affinities for targets, while simultaneously retaining the properties of lead-like or drug-like substances. Available structure-activity relationships (SAR) may be utilized for designing the stages in fragment-growing procedures. Fragment linking represents yet another approach, under which fragments that bond to distinct zones on binding pockets are detected using protein crystallography. The fragments involved are then linked such that their initial binding modes are preserved and the affinities of the resultant complexes will be optimized. An extraordinary approach to fragment linking, termed “fragment self-assembly,” has been exemplified by the use of *in-situ* chemistry, where two fragments were linked together in a protein-binding pocket. A retrosynthetic-fragment approach has been described as utilizing pre-existing lead series from the pharmacological literature for deriving fragments focused on specific targets (Hajduk, 2006). Lead molecules are broken down into their key fragments and regrown in order to arrive at new chemical scaffolds that fit into protein-binding sites. Fig.4 illustrates the fragment-growing and fragment-linking approaches to fragment optimization.

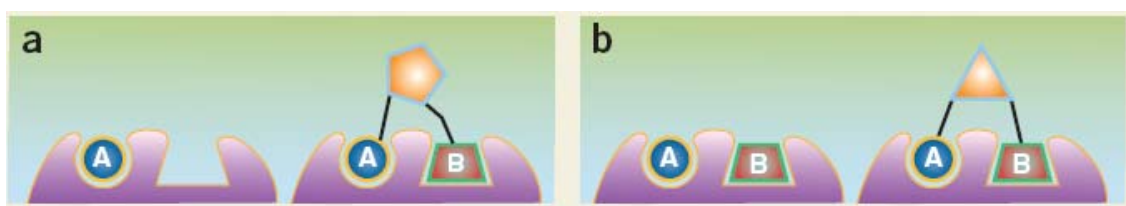


Fig.4. Examples of two approaches to upgrading fragments into lead molecules. (a) Fragment growing, where molecule A is detected under a fragment screening and then grown into sub-pocket B on the target. **(b)** Fragment linking, where molecules A and B are detected under a fragment screening and then linked together using a chemical-linker's moiety.

Pharmaceutical companies, biotechnology companies, and university research groups have all reported several successful examples of FBLD over the past few years.

Table 2 summarizes the progress made by the initial compounds discovered, on their way to clinical trials.

Table 2. Clinical and preclinical candidates derived from fragments (Congreve, et al., 2008).

Compound	Company	Target	Progress
LY-517717	Lilly/Protherics	FXa	Phase 2
PLX-204	Plexxikon	PPAR-agonist	Phase 2
ABT-263	Abbott	Bcl-XL	Phase 1/2a
AT9283	Astex	Aurora	Phase 1/2a
ABT-518	Abbott	MMP-2 and 9	Phase 1
AT7519	Astex	CDKs	Phase 1
PLX-4032	Plexxikon	B-RafV600E	Phase 1
SGX523	SGX Pharmaceuticals	MET	Phase 1
SNS-314	Sunesis	Aurora	Phase 1
NVP-AUY922	Vernalis/Novartis	HSP90	Phase 1
AT9311/LCQ195	Astex/Novartis	CDKs	preclinical
AT13148	Astex	PKB/Akt	preclinical
AT13387	Astex	HSP90	preclinical
PLX-4720	Plexxikon	B-RafV600E	preclinical
RO6266	Roche	P38	preclinical
SGX393	SGX Pharmaceuticals	BCR-AblT315I	preclinical

1.2. APPLICATIONS OF FBLD

FBLD challenges the techniques and methods utilized in current drug-discovery projects. Methods, such as NMR, SPR, ITC, and protein crystallography, have been optimized to the point where they are robust and meet the requirements for detecting weak fragment-protein interactions (Jahnke and Erlanson, 2006). The term “biophysical methods” may be applied to grouping those methods that have also gained greater importance in the field of modern drug discovery. In this dissertation, surface-plasmon-resonance (SPR) analyses, enzymatic high compound concentration assays (HCA), and protein crystallography have been applied to investigations of fragment-protein interactions.

Detection of ligand-protein binding events using SPR-instrumentation has made major strides during recent years. Lower signal/noise ratios have allowed detecting molecules whose molecular weights fall within the 100-Da – 300-Da range. Technological advances have also simplified the handling of large numbers of compounds dissolved in DMSO. SPR-methods

have meanwhile been developed to the point where they represent feasible options for studying interactions between fragment molecules and target proteins (Lundqvist, 2005).

The SPR-approach utilized in this dissertation immobilizes proteins on the sensor chip's surface and injects fragments in a stream flowing across its surface and employs a method termed "direct-binding assay," under which responses are proportional to the quantities of fragments bound to the proteins resident on its surface (Karlsson, et al., 2000; McDonnell, 2001; Deinum, et al., 2002). Use of SPR in FBLD has been previously reported in various studies (Edwards, et al., 2007; Cannon and Myszka, 2002; Geschwinder, et al., 2007; Hämäläinen, et al., 2008; Boehm, et al., 2000; Metz, et al., 2003; Neumann, et al., 2005; Papalia, et al., 2006; Nordin, et al., 2005). SPR can simultaneously provide data on bond formation, binding stoichiometry, binding selectivity, and estimated affinities, which has made it a method frequently utilized in FBLD (Huber, 2005; Geschwinder, et al., 2007; McDonnell, 2001; Deinum, et al., 2002).

Recently, the approach to finding new starting points via screening large compound libraries has come to be most widely employed in drug-discovery programs. Most current drug-discovery programs include assays based on inhibition or stimulation of a biochemical/enzymatic mechanism of molecular targets. High-throughput methods, such as HTS, are utilized for screening libraries covering several hundred thousand compounds for activity against the intended targets. HTS-hits usually have binding constants falling in the nM-range or low μ M-range, while the aim of fragment screening is detecting bonds having binding constants extending up to the high- μ M-range and mM-range. In order to detect bonding at such high affinities, ligand concentrations also must reach such high concentrations. The biochemical assays employed in the case of fragments are therefore often termed "high-concentration biochemical assays" (HCA) or "high-concentration screening" (HCS) assays. One advantage of HCA fragment assays is that they may be readily employed in a similar manner for screenings conducted in conjunction with HTS-campaigns, since the fragment-HCA involved do not require substantial lengths of time for assay development. FBLD-efforts that employ HCA-methods are thus subject less throughput limitations (Barker, et al., 2006), which may allow relatively rapid pursuit of wider explorations of fragment chemical-space diversities and follow-up methods, such as fragment-analog approaches (Hesterkamp and Whittaker, 2008; Gribbon and Sewing, 2008).

Protein crystallography is utilized for determining the three-dimensional bonding modes of fragments on target proteins at the atomic-site level. Knowledge of 3D-binding modes facilitates upgrading fragment molecules into lead-like molecules. Recent developments and improvements in protein crystallography have led to an optimized protein-crystallography workflow and faster determinations of 3D-structures, which has also benefited the implementation of protein crystallography as a tool in FBLD (Blundell, 2001; Gill, et al., 2005; Nienaber, et al., 2000; Sharff and Jhoti, 2003; Hartshorn, et al., 2005). Furthermore, protein crystallography has also been used as a lone technique in FBLD-approaches (Blundell, 2001; Gill, et al., 2005; Nienaber, et al., 2000; Sanders, et al., 2004; Bosch, et al., 2006). Protein crystallography has been used to reveal several interesting fragment-compound bonding modes and been applied as a research tool for developing drugs for a range of various targeted diseases (Erlanson, 2006; Carr, 2007; Norman, 2007; Erlanson, 2004; Howard, et al., 2006; Frederickson, et al., 2008; Warner, et al., 2006; Hohwy, et al., 2008). The growing numbers of therapeutic targets whose crystalline structures have been determined also increase the number of prospective applications of protein crystallography to FBLD.

1.3. PROTEIN KINASES AND PKA

Approximately 2 % of the genes in the human genome encode for protein kinases (Manning, et al., 2002). Those enzymes constitute one of the largest gene families and are crucial to the regulation of various cellular processes. Furthermore, those enzymes play an important role in cell growth and cell-signaling transduction (Taylor, et al., 2004). The primary function of protein kinases is catalyzing the phosphoryl transfer of the γ -phosphate group on adenosine triphosphate (ATP) to the hydroxyl group of a recipient substrate, which occurs as a response, following receipt of a signal from an upstream, signaling protein.

Protein phosphatases are the antagonists of protein kinases and counteract protein kinases by detaching their appended phosphate groups and terminating transmission of signals induced by the phosphorylation (cf. Fig.5). Protein substrates, including the protein kinases situated thereon, will be toggled between active and inactive conformational states, depending upon their degree of phosphorylation (Akamine, et al., 2005; Hunter, 1995).

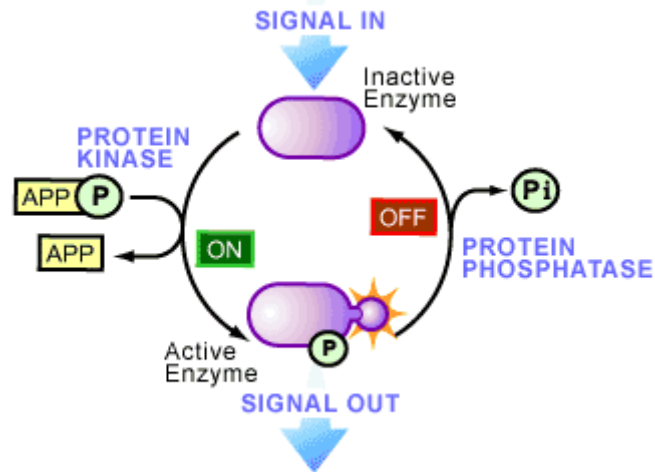


Fig.5. Protein kinases and phosphatases. Protein kinases and phosphatases regulate biological signals by acting as enzymes that catalyze phosphorylation and dephosphorylation in biological organisms. Phosphorylation catalyzed by protein kinases retransmits incoming signals by activating the protein kinases' substrates. Signal transmission will be terminated by dephosphorylation (inactivation) of their substrates, a reaction catalyzed by protein phosphatases.

The 518 protein kinases known to be present in the human genome have been classified by comparing their sequences, which has allowed identifying protein-kinase families (Hanks, et al., 1988; Hanks and Hunter, 1995). Characterizations of human protein kinases have been designated “the human kinome” (Liu and Gray, 2006). A classification based on the amino-acid sequence of the catalytic domain (or kinase domain) has segregated protein kinases into ten, distinct subgroups (Hanks and Hunter, 1995). The cAMP-dependent protein kinase (PKA) utilized in the studies reported in this dissertation belongs to the AGC-kinase family.

Table 3. Classifications of protein kinases into subfamilies (Hanks and Hunter, 1995).

- AGC-family (63 members)
- CAMK-family (74 members)
- CK1-family (12 members)
- CMGC-family (61 members)
- RGC-family (5 members)
- STE-family (47 members)
- TK-family (90 members)
- TKL-family (43 members)
- aPK (40 members)
- Other protein kinases (83 members)

More than 400 human diseases have been directly or indirectly connected to protein kinases. It is also estimated that more than one-quarter of all pharmaceutical drug targets are protein kinases (Liu and Gray, 2006). Protein-kinase activity is controlled and regulated. However, perturbations of protein-kinase signaling by mutations and other genetic alterations can result in deregulation of kinase activity and the onset of tumorigenesis, which can cause malignant transformations (Pawson, 1994; Hunter, 2000; Reed, 1999). The design of small molecules in conjunction with cancer-drug discovery is aimed at inhibiting such tumorigenic activity. It is generally believed that targeting protein kinases in conjunction with drug discovery can retard tumor growth. Compounds are designed to inhibit those protein kinases that have been identified as therapeutic targets. (Blume-Jensen and Hunter, 2001; Katayama, et al., 2008; Hünenberger, et al, 1999; Melnikova and Golden, 2004).

All protein kinases bind ATP and the ATP-pockets of the various protein kinases therefore contain many similar structures, which has raised concerns regarding whether protein kinases might be targeted using ATP-competitive inhibitors, without resulting in severe side effects. Nonspecific bonding by designed drug molecules to protein kinases other than those targeted could alter pathways of importance to normal cell signaling, and thus cause undesired side effects. As of the late 1980s, no protein-kinase inhibitors had entered human clinical trials. The matter of specificity, along with the relatively high ATP-concentrations (2 mM – 10 mM) present in cells raised questions regarding how competitive bonding to ATP-pockets should be addressed. A milestone in that process was the discovery of the rapamycin molecule. Rapamycin was initially found to have immunosuppressant properties due to its bonding to the cytosolic protein kinase, mTOR (or FKBP-12), and was approved for clinical use for preventing rejections following kidney transplantations in 1999. However, rapamycin was shown to inhibit tumor growth and approved for clinical use in the treatment of cancer (Davies, et al., 2000). A review of small-molecule inhibitors targeting protein kinase was published by Cherry and Williams (2004).

1.3.1. PKA - the cAMP-dependent protein kinase

The cAMP-dependent protein kinase (PKA) is one of the most commonly characterized of the protein kinases. PKA has served as a prototype for the extensive protein-kinase family (Taylor, et al., 2004). The catalytic subunit of PKA represents a prominent example of how a protein kinase both recognizes its substrates as well as inhibitors. It also shows how the enzyme moves through the stages of catalysis (Hünenberger, et al, 1999).

Early research revealed how the different zones and residues of PKA affect the kinetics and affinity of the phosphotransfer reaction occurring between protein kinase and its various substrates (Kemp, et al., 1977). Furthermore, PKA was the first protein kinase whose 3-dimensional structure became known, a finding that has had an enormous impact on modern protein-kinase drug discovery (Cohen, 2002). PKA is unique among protein kinases due to the fact that the full-length, single-chain protein kinase is constitutively active in monomeric form and possesses only a single folding domain that consists of the core kinase catalytic domain and N-terminal and C-terminal extensions (Breitenlechner, et al., 2005). In its inactive state, PKA exists as a heterotetramer having two dimeric regulatory (R) subunits and two catalytic (C) subunits. Activation is achieved when cAMP bonds to those regulatory subunits (Choe, et al., 2006), which leads to the C-subunits being liberated from the R-subunits. After that, the C-subunits can bind ATP and interact with substrates. The catalytic subunit of PKA is potently inhibited (confined to the low-nM range) by a number of synthetic derivatives (Congreve, et al., 2005). In comparison, ATP forms bonds with an affinity (K_D) falling within the 10- μ M –20- μ M range. Fig.6 presents an overview of the structure elements/segments involved and a description of the binding pocket of PKA's catalytic subunit.

The overall structure patterns occurring in PKA are similar to those of other protein kinases. Fig.6 is confined to depicting an overall description of protein kinase's catalytic subunits, which are formed by two lobes designated the "small lobe" and the "large lobe." A cleft, in which the ATP-nucleotide bonds, is formed between the two lobes. The two lobes are connected by a hinge segment that anchors and stabilizes the bonding of the nucleotide. Bonding of the nucleotide illustrates how several parts of the ATP binding cleft interacts with ATP-molecules. For example, a loop formed in PKA by residue 49-57 generates several phosphate interactions via its backbone. That loop has a structure, the glycine-rich loop, containing several glycine residues. An ion pair is formed between the nucleotide and the amine group on the catalytically important lysine residue in PKA, Lys-72, which is strongly preserved in protein kinases. The adenine ring of the nucleotide is situated deep within the pocket and forms two hydrogen bonds with the hinge segment. A further interaction with the residue Thr-183 present in PKA transpires. The magnesium ions are cofactors in kinase activity and bind via the aspartic acid present in *DFG-motifs*, Asp-184, the asparagine residue, Asn171, present in PKA's catalytic loops, and the γ -phosphate, present in PKA's ATP-molecules (Congreve, et al., 2005).

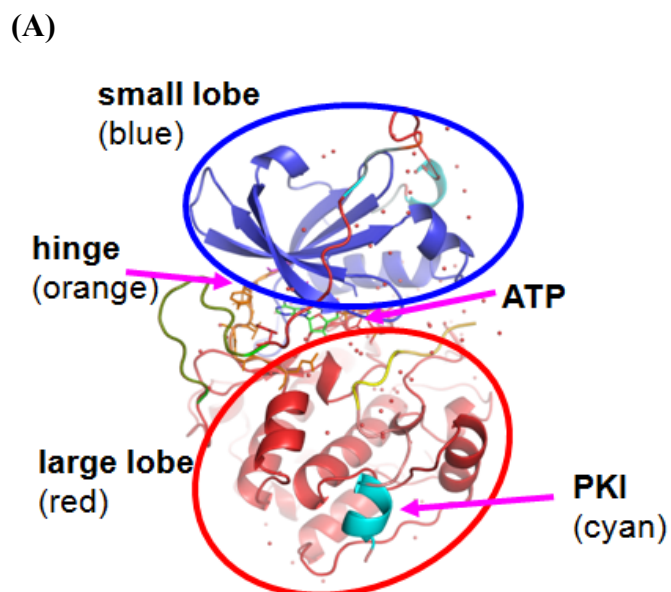
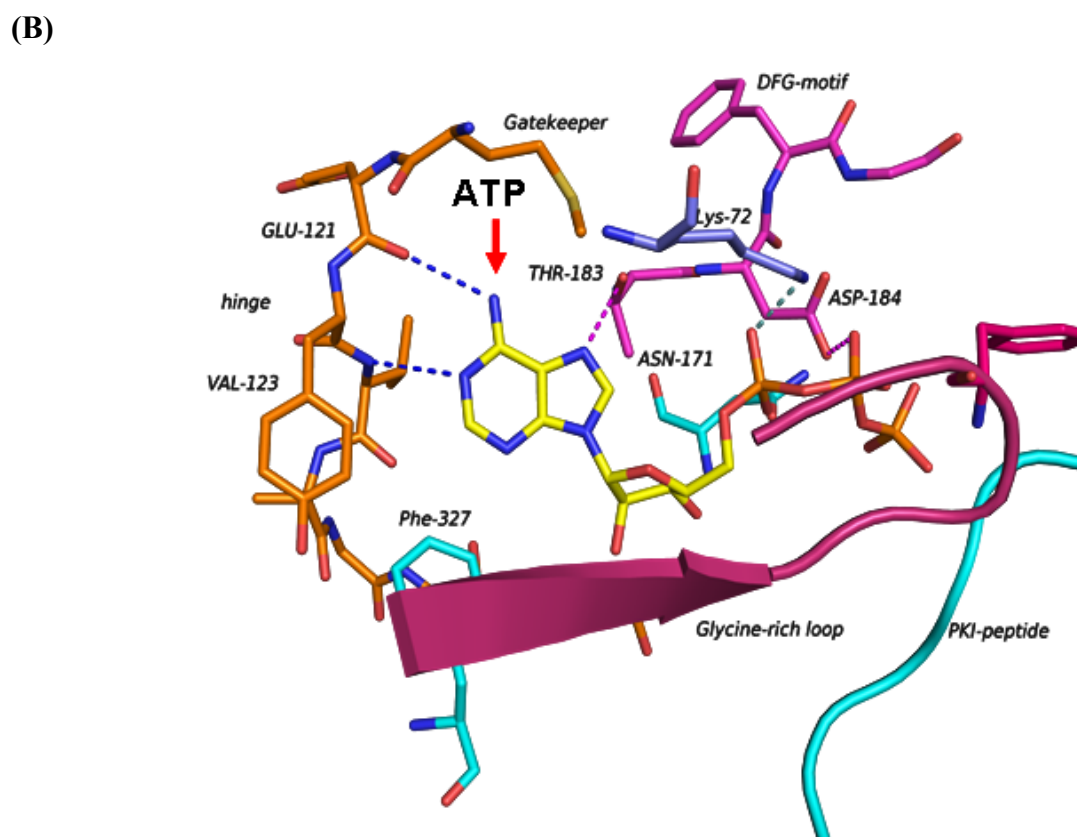


Fig.6. The catalytic sub-unit of PKA. (A) An overview orientation image where the small lobe (blue) and the large lobe (red) are shown. The ATP binding cleft/pocket and the hinge zone are pointed out (orange). (B) A detailed image of the ATP binding mode in the catalytic subunit of PKA. Structure elements are marked and a selection of the interactions picked up by the ATP molecule is shown. The adenine moiety forms two hydrogen bonds with the hinge (orange) and interacts with the residue Thr-183 (purple). The phosphate groups interact with Lys-72 (blue) and the DFG-motif (purple). Both the glycine-rich loop (purple) and the PKI-peptide (light-blue) cover the ATP-pocket.



Another overview of the ATP binding pockets present in protein kinases has been published by Liao (2007) and defines several subpockets commonly addressed by small molecules binding to protein kinases (cf. Fig.7). ATP binding pockets on PKA are subdivided into various zones designated A, K, R, P, E₀, E₁, BP-I, and BP-II.

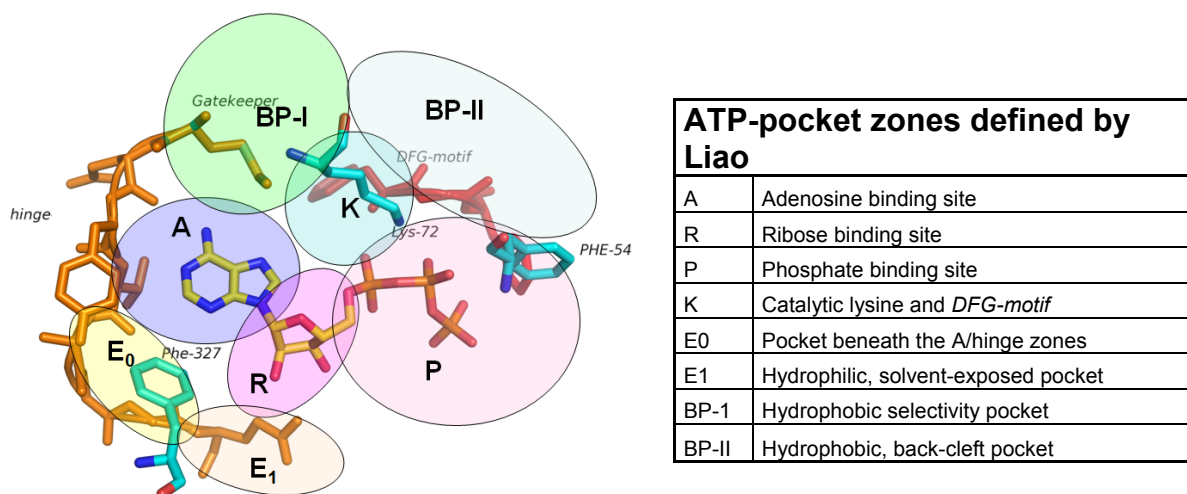


Fig.7. The ATP binding pocket in cAMP-dependent protein-kinase A. An illustration of the zones defined by Liao for describing its ATP-pocket. Their designations are listed in the table at right. When ATP binds, the adenosine moiety is situated in the A-zone. The ribose is situated in the R-zone. Phosphate groups bind in the P-zone. BP-I- and BP-II-zones are situated above the A-zone in this view. The K-zone is situated between the A-, R-, BP-I-, and BP-II-zones. The E₀- and E₁-pockets are situated beneath the A- and R-zones, which are described as being hydrophilic, solvent-exposed zones.

1.3.2. PROTEIN KINASES AND FBLD

Extensive research has been devoted to the development of small-molecule drugs that target the ATP binding pocket in protein kinases. Fragment-based approaches have thus also been employed for detecting new chemical scaffolds in the protein-kinase drug-discovery field. The literature is replete with reports on fragment screenings targeting protein kinases that have led to development of potent inhibitors in conjunction with various projects (PKB: (Donald, et al., 2007; Saxty, et al., 2007); p38 MAP: (Gill, et al., 2005); c-Src: (Taylor, et al., 2007); c-Met, aurora kinases: (Jhoti, et al., 2007); CK2, PDK1, and CHK1: (Hajduk and Greer, 2007); CDK2: (Congreve, et al., 2003); JNK3: (Fejzo, et al., 2003); and adenosine kinase (Hajduk, et al., 2000)).

It has been pointed out that protein kinases contain the 21st-century's most-interesting drug targets (Cohen, 2002). Programs aimed at finding new chemical scaffolds that interact with the ATP-pockets or other parts of proteins are thus of great interest, and FBLD offers one way of approaching that field of research (Lindsay, 2005).

1.3. THE AIM OF THIS STUDY

The pharmaceutical industry aims to increase the rate at which drug-discovery processes develop new, active, drug ingredient. Fragment-based lead discovery (FBLD) has been chosen as a tool for use in that effort and is emerging as an approach to small-molecule drug

discovery. Employment of FBLD has led to experimental techniques that allow characterizing interactions between low-molecular-weight fragments and disease target protein attracting greater interest on the part of those working in the drug-discovery field. Characterizations of the interactions between molecular fragments and target proteins can aid efforts to understand how results obtained from FBLD can aid the drug-discovery process. In the early days of such studies, the respective techniques involved were employed in investigations of various approaches to FBLD. However, no detailed characterizations of fragment-screening data obtained from combinations of them have been published to date. These studies therefore combined characterizations of the respective results obtained from surface-plasmon-resonance (SPR) analyses, high-compound-concentration biochemical assays (HCA), and protein crystallography. This study combines those techniques with the results of a second approach and discussions regarding how results extracted from available interaction data can make FBLD more useful in the development of new drugs. The outcomes, limits, and hit rates resulting from employment of those techniques in FBLD will also be discussed.

The goals of this study were:

- examining the characteristics, outcomes, and limits that result when SPR and HCA are employed as fragment-screening methods,
- estimating screening hit rates that could be confirmed by protein-crystallography studies,
- identifying fragment-like compounds that might serve as starting points for drug-discovery programs, and
- assessing how available assay data might be of use in efforts to create fragment-protein complexes.

Chapter 2

MATERIALS AND METHODS

2.1. MATERIALS

2.1.1. CHEMICALS

All standard chemicals were either purchased from Calbiochem, Darmstadt, Germany, or requisitioned from in-house inventories maintained at Merck, Darmstadt, Germany, unless otherwise stated.

2.1.2. INHIBITORS

2.1.2. SMALL-MOLECULE INHIBITORS

Solid-state H-89 (CAS 127243-85-0), packed in vials containing 1 mg per vial, was purchased from Calbiochem. All other inhibitors and compounds were requisitioned from MerckSerono's in-house inventories and either dissolved in "remp solution," yielding 10-mM concentrations in 100 % DMSO, or employed in solid form in quantities of < 10 mg per compound.

2.1.2.1. PEPTIDE INHIBITOR

Solid-state PKI (Calbiochem), packed in vials containing 1 mg per vial.

Sequence: Thr-Tyr-Ala-Asp-Phe-Ile-Ala-Ser-Gly-Arg-Thr-Gly-Arg-Arg-Asn-Ala-Ile (6-22)

<http://www.merckbiosciences.co.uk/product/539684>

MWT: 1,868.1 Da

CAS 121932-06-7

2.1.3. PROTEIN, HUMAN-PKA

2.1.3.1. SEQUENCE

MGNAAAAKKGSEQESVKEFLAKAKEDFLKKWESPAQNTAHLDQFERIKTLGTGSFG
 RVMLVKHKETGNHYAMKILDKQKVVKLKQIEHTLNEKRILQAVNFPFLVKLEFSFKD
 NSNLYMVM EYVPGGEMFSLRIRGRFSEPHARFYAAQIVLTFEYLHSLDLIYRDLKPE
 NLLIDQQGYIQVTDGFAKRVKGRWTLCGTPEYLAPEIILSKGYNKAVDWWALGV
 LIYEMAAGYPPFFADQPIQIYEKIVSGKVRFP SHFSSDLKDLLRNLLQVDLTKRFGNLK
 NGVNDIKNHKWFATTDWIAIYQRKVEAPFIPKFKGPGDTSNFDDYEEEEIRVSINEKC
 GKEFSEF

MWT: 40.56 kDa

2.1.4. EXPERIMENTAL BUFFERS, SOLUTIONS, AND MATERIALS

All buffers were prepared in the form of aqueous solutions. NaOH (2-M) and HCl (2-M) were employed for adjusting buffer pH.

2.1.4.1. PROTEIN CRYSTALLOGRAPHY

Protein-purification buffer	<i>30.4 mg/ml PKA</i> 5 mM Mes 5-mM bis-tris-propane/HCl 75 mM LiCl 0.1 mM EDTA 1 mM DTT pH: 6.9
Protein-crystallization buffer	5 mM MES 5 mM bis-tris-propane 75 mM LiCl 1 mM DTT 0.1 mM EDTA
Protein-crystallization additives	1.4 mM MEGA-8 (Hampton Research, detergent screen I) 1.5 mM PKI peptide inhibitor 15 % – 25 % ethanol or methanol

Protein-crystallization and data-collection materials	24-well VDX-plate, with sealant (Hampton Research) Siliconized-glass cover slides (Hampton Research) Seed-bead kit (Hampton Research) Vortexer (VWR International) Centrifuge (Eppendorf 5415) Seeding tool (Hampton Research) Cryoloop, installed (Hampton Research)
Crystal cross-linking	100 % gluteraldehyde <i>Protein crystallization buffer</i> Microbridges (Hampton Research) Cryoloop, installed (Hampton Research)
Crystal-stabilizing buffer/compound-soaking buffer	<i>70 % protein-crystallization buffer</i> 30 % ethanol or methanol Cryoloop, installed (Hampton Research)
Cryoprotectant conditioner	20 % L-(+)-2,3 butanediol (FLUKA #18967) 20 % ethanol <i>60 % protein-crystallization buffer</i> Cryoloop, installed (Hampton Research)
Data collection	Cryoloop, installed (Hampton Research) Rigaku MicroMax microfocus X-ray generator (Rigaku Americas Corporation) R-axis IV++ detector (Rigaku Americas Cooperation) PX-I and PX-II sources (SLS) Pilatus detector (Brönnimann, et al., 2006)

2.1.4.2. SURFACE-PLASMON-RESONANCE ANALYSES

2.1.4.2.1. GENERAL MATERIALS

BIACORE A-100	BIACORE
Series-S CM5 sensor chip	BIACORE
BIAnormalizing solution	BIACORE
BIAmaintenance kit	BIACORE
HBS-N buffer	BIACORE

Buffer stock solution	1 M HEPES 1.5 M NaCl pH: 6.8
PKA-protein, in buffer	30.5 mg/ml PKA 5 mM Mes 5 mM bis-tris-propane/HCl 75 mM LiCl 0.1 mM EDTA 1 mM DTT pH: 6.9
CA-protein, in buffer	30 µg/ml CA (BIACORE, S-51 training kit) Acetate buffer, pH: 5.5 (BIACORE)

2.1.4.2.2. PROTEIN IMMOBILIZATION

Normalizing solution	BIACORE
EDC	BIACORE
NHS	BIACORE
Ethanolamine	BIACORE
Running buffer used during protein immobilization	100 mM HEPES (buffer "A") 150 mM NaCl (buffer "A") 0.005 % Tween 20 2 mM MgCl ₂ pH: 6.8
Protein (PKA) immobilization buffer	10 mM bis-tris-propane 200 µM ATP 2 mM MgCl ₂
Protein (CA) immobilization buffer	Acetate buffer, pH: 5.5 (BIACORE)

2.1.4.2.3. COMPOUND SCREENING AND CHARACTERIZATION

Running buffer	100 mM HEPES (buffer "A") 150 mM NaCl (buffer "A") 0.005 % Tween 20 2-mM MgCl ₂ pH: 6.8 2 % DMSO
Sample-preparation buffer	100 mM HEPES (buffer "A") 150 mM NaCl (buffer "A") 0.005 % Tween 20 2 mM MgCl ₂ pH: 6.8
Positive-control sample (PKA)	<i>1 mg H-89 dissolved in DMSO to yield a:</i> 1-mM solution in 100% DMSO (stock solution) <i>Diluted in sample-preparation buffer:</i> 2 μM H-89 2 % DMSO
Positive-control sample (CA)	10 mM furosemide (BIACORE, S-51 training kit) 100 % DMSO <i>Diluted in sample-preparation buffer:</i> 20 μM furosemide (BIACORE) 2 % DMSO (Merck)
Negative-control sample	<i>Running buffer</i>
Solvent-correction setup	<i>Sample preparation buffer containing</i> 1.2 % DMSO 1.4 % DMSO 1.6 % DMSO 1.8 % DMSO 2.0 % DMSO 2.2 % DMSO 2.4 % DMSO

	2.6 % DMSO 2.8 % DMSO
Compound-screening preparation	10 mM compound in “remp-tube” 100 % DMSO <i>Diluted in sample preparation buffer:</i> 200 μ M compound 2 % DMSO
Compound-characterization preparation	Solid-state compound dissolved in stock solutions 100 mM compound in 100 % DMSO <i>Diluted in sample preparation buffer:</i> 1 mM compound 2 % DMSO <i>1:1-dilution in sample preparation buffer in ten increments:</i> 1.0 mM compound, 2 % DMSO 500 μ M compound, 2 % DMSO 250 μ M compound, 2 % DMSO 125 μ M compound, 2 % DMSO 62.5 μ M compound, 2 % DMSO 37.25 μ M compound, 2 % DMSO 15.63 μ M compound, 2 % DMSO 3.91 μ M compound, 2 % DMSO 1.95 μ M compound, 2 % DMSO

2.1.5. COMPUTER SOFTWARE

Library-generation and virtual-screening software	<p>ZINC (UCSF, http://zinc.docking.org/) (Irwin and Shoichet, 2005)</p> <p>ISIS Base (MDL Information Systems, Inc.)</p> <p>ISIS Draw (MDL Information Systems, Inc.)</p> <p>Accord for Excel (Accelrys, Inc.)</p> <p>MOE (Chemical Computing Group, Inc.)</p> <p>SpotFire (Tibco Software, Inc.)</p>
SPR-software	<p>BIACORE A-100 Control</p> <p>BIACORE A-100 Evaluation</p> <p>BIACORE T-100 Control</p> <p>BIACORE T-100 Evaluation</p> <p>BIACORE S-51 Control</p> <p>BIACORE S-51 Evaluation</p> <p>BIACORE 3000 Control</p> <p>BIACORE 3000 Evaluation</p> <p>Accord for Excel</p> <p>ISIS Base (MDL Information Systems, Inc.)</p> <p>ISIS Draw (MDL Information Systems, Inc.)</p>
Protein-crystallography software	<p>ADXV (The Scripps Research Institute)</p> <p>XDS (Kabsch, 1993)</p> <p>Mosflm, Version 7.0.4 (Leslie, 1992)</p> <p>HKL2000, Version 0.97.647 (Otwinowski, et al., 1997)</p> <p>d*Trek, Version 9.9.2L (Pflugrath, 1999)</p> <p>CNS/CNX (Brunger, et al., 1998)</p> <p>Molrep (Vagin, 1997)</p> <p>CCP4 Suite (STFC Daresbury Laboratory)</p> <p>WhatIF (Vriend, 1990)</p> <p>COOT (Emsley and Cowtan, 2004)</p> <p>PyMol (DeLano, 2002)</p>
General software	<p>Microsoft Office (Microsoft Corporation)</p> <p>Adobe Acrobat 8.0 (Adobe Systems, Inc.)</p>

2.2. METHODS

Every molecular-biology protocol employed during cloning and purification has been described in detail by Yonemoto and by Engh (Yonemoto, 1997; Engh, 1996). MerckSerono's in-house Protein-Expression Department and Purification Department were commissioned to perform that work. In brief, the catalytic subunit of human PKA was expressed in cytosolic expressions in *E-coli* BL21 (DE3) cells. Expressed biomass was purified by affinity chromatography and ion-exchange chromatography. Protein purification yielded approximately 20 mg of protein per 200 g of biomass. The purified protein was divided into two batches and concentrated to 20.5 mg/ml and 30.4 mg/ml, respectively, and stored in the protein-purification buffer following plunge-freezing in liquid nitrogen at -80°C .

2.2.1. PROTEIN CRYSTALLOGRAPHY

Crystals and Symmetry

In FBLD, protein crystallography is utilized for describing fragments' three-dimensional binding modes in proteins. Protein crystals are formed when protein molecules precipitate out of solutions in the form of well-ordered solids. The orderings involved are three-dimensional arrays of atoms and molecules forming infinitely repeatable building blocks (asymmetric units) arranged in accordance with well-defined symmetries (65 distinct space groups in the case of proteins, 230 such altogether). A single asymmetric unit contains all of the information available on the crystal, where one or more protein molecules will be packed into each cell, depending upon the particular packing symmetry involved.

Protein crystallography is reliant upon the availability of protein crystals that may be analyzed by means of X-ray diffraction. Experiments are necessary in order to determine suitable conditions for the formation of well-ordered protein crystals. Solutions of proteins are brought to the saturation point in order to cause nucleation and arrive at well-regulated crystal growth (McPherson, et al., 1995). The experimental parameters involved, such as solution pH, temperature, and ionic strength, are then optimized. Choices of protein buffer solutions, precipitate reagents, salts, and detergents also affect crystal growth (McPherson, 1982). Protein purities and concentrations also play important roles in efforts to obtain high-quality protein crystals. Fig.8 presents a solubility plot illustrating the protein-crystallization process.

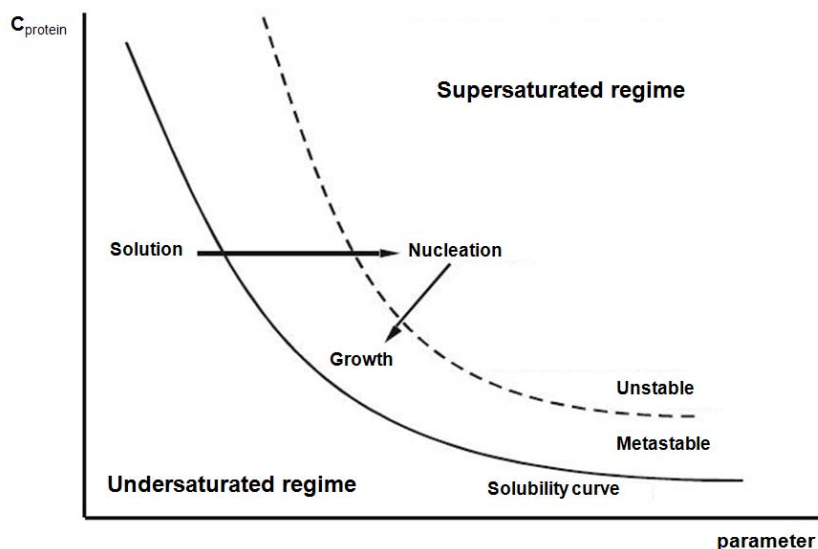


Fig.8. Solubility plot for proteins. A plot of dissolved-protein concentration, C_{protein} , against salt concentration or other parameter. Protein crystals begin to form at supersaturation levels below those at which nucleation occurs. Once nucleation occurs, dissolved-protein concentration declines. The solution then enters the metastable zone and stable protein-crystal growth sets in. The protein that subsequently precipitates out attaches itself to the surfaces of nuclei, allowing larger crystals to form.

Automating crystallization experiments has become a common approach to determining suitable crystallization conditions. Robots capable of servicing several hundred to more than one-hundred thousand experimental setups daily have made large-scale, automated, crystallization experiments possible (Kuhn, et al., 2002). Techniques for automating the design of the chemical structures of proteins that will be soluble up to high concentrations and suitable for use in crystallization experiments are also available (Gilbert and Albala, 2002; Lesley, 2002). Investigations involving large numbers of experimental setups may also be conducted in more highly automated manners by taking advantage of advances in the areas of crystal storage and automated monitoring of experimental runs. A comprehensive review of crystallization techniques appears in the volume edited by Bergfors (Bergfors, 1999).

PKA-crystallization

cAMP-dependent protein kinase (PKA) must be regarded as one of the most-accurately characterized protein kinases, in view of the large number of published studies regarding it. The structure conformations, protein expressions, purification stages, and crystallization conditions have all been optimized for numerous, distinct sets of assay parameters. Employment of the resultant experimental conditions and PKA as target in order to characterize fragment-protein interactions were regarded as the best choice for the work undertaken in conjunction with the present dissertation.

PKA-crystallization protocols have been described by Bonn, et al. (2006), where purified protein at a concentration of 30.4 mg/ml was thawed following storage at -80°C . The protein vials employed contained 25 μl protein per vial. MEGA-8 and PKI peptide inhibitor were added to the protein and the mixture diluted in protein-crystallization buffer to a theoretical protein concentration of 17 mg/ml. The solution was then centrifuged at 20°C and 6,000 g for 1 minute in an Eppendorf 5415D centrifuge. Adhering droplets were set to have volumes of 1 μl . They therefore contained 17 mg/ml PKA, 5 mM MES, 5 mM bis-tris-propane (pH: 6.5), 75 mM LiCl, 0.1 mM EDTA, 1 mM DTT, and 1.5 mM PKI (5-24) peptide. The adhering droplets were then equilibrated at 4°C over a grid consisting of 15 % – 25 % (v/v) methanol and ethanol. Streak-seeding was conducted approximately 1 hour after commencement of the experiment using crystals that had been grown a few days earlier on a setup employing the same conditions, but without employment of streak-seeding. Seed crystals were collected by mixing adhering droplets containing crystals in a 1:1-ratio with crystal-stabilizing solution. The adhering droplets involved, which had volumes of approximately 2 μl , were then transferred to an Eppendorf seed-bead kit (Hampton Research) and vortexed for two minutes on a VWR International vortexer. Dipping a seeding tool into the Eppendorf seed-bead kit and streak-seeding droplets adhering to the crystallization plate resulted in overnight growth of PKA-crystals.

2.2.1.1. FRAGMENT SOAKING AND COCRYSTALLIZATION

Various methods may be employed for forming fragment-protein complexes. The protein may be co-expressed with the ligand, the ligand may be added at the protein-purification stage, cocrystallization may be utilized, or protein crystals may be soaked in a solution of the ligand (Hassel, et al. 2007). In the case of the type of setup involved here, both soaking and cocrystallization methods have been employed, but the soaking method has been that most extensively employed. Under the soaking method, protein crystals are soaked in a solution containing ligand molecules. Ligand molecules then diffuse into protein-binding sites, where they bind protein molecules to the latter, due to a particular mode of interaction. One of the major aspects to be considered when working with fragments is the need for obtaining sufficiently high occupancies of protein-binding sites. Protein crystallography involves coherently accumulating diffraction signals from the protein molecules present in crystals. Fragment molecules present in protein-binding pockets should therefore contribute to coherently accumulated diffraction signals. If the occupancies of protein-binding pockets are too low, fragment electron densities will not be observed. A rule-of thumb in protein

crystallography is employing fragment concentrations that are at least five times those needed for affinity. However, it has been found that when protein crystallography is utilized in FBLD, the solubilities of the fragments involved frequently limits the fragment concentrations that may be employed.

The soaking procedures employed

Fragment concentrations in the 100-mM, 100 % DMSO, stock solutions were diluted to the soaking concentrations in crystal-stabilizing buffers. Soaking investigations were conducted on an adhering-droplet setup, where 2- μ l droplets containing the compound-soaking solution and 300 μ l – 500 μ l crystal-stabilizing buffer were inserted into the well in order to preclude the adhering droplets drying out. The fragment concentration in the soaking solution was 5 mM in 5 % DMSO. Soaking was conducted for approximately 24 h at 4°C. Crystals were initially transferred from crystallizing droplets to the soaking solution. Those transferrals were cautiously conducted in order to avoid damaging the crystals. Soaked crystals were briefly immersed in the cryoprotectant solution (20 % ethanol, 20 % L-(+)-2,3-butanediol, and 60 % well solution taken from the wells where crystals had grown) prior to plunge-freezing them in liquid nitrogen at – 80°C. All transferrals of the crystals were conducted via the Hampton Research cryoloop that had been installed on the setup.

Soaking conditions were individually optimized for each fragment, where a second or third round of soaking proved necessary. An initial stage involved a switch to employing higher compound/DMSO-concentrations (20 mM compound in 20 % DMSO). In addition, soaking periods were extended to as long as four days, depending on crystal stabilities in the compound-soaking solution. Crystal stability was manually checked under a microscope at intervals of approximately 24 h, 48 h, and 72 h.

Crosslinking PKA-crystals

The protein crystals obtained were not always stable under the soaking conditions employed. Many of them either broke or failed to yield diffraction patterns during soaking investigations. One way to eliminate such crystal instability is cross-linking the protein crystals (Lusty, 1999; Cohen-Hadar, et al., 2006; Roy and Abraham 2003), which stabilizes them and allows making more changes in protein structures without destroying the crystals involved, which, in turn, can increase success rates in efforts aimed at obtaining the structures of complexes.

The cross-linking conducted utilized glutaraldehyde and was applied to those cases where initial soakings had led to PKA-crystals losing their diffraction patterns. The PKA-crystals involved were emplaced in droplets adhering to cover slides containing 2 μl crystal-stabilizing solution suspended above a Hampton Research microbridge. 300 μl – 400 μl crystal-stabilizing solution was transferred to the well in order to prevent droplets from drying out. 8 μl glutaraldehyde was transferred to the microbridge and the PKA-crystals were immersed in evaporating glutaraldehyde for 2 h at 4°C. The PKA-crystals involved were then transferred to the compound-soaking solution. Investigations of the diffraction patterns of each such PKA-crystal following soaking revealed that the various soakings employed had damaged them.

2.2.1.2. X-RAY DATA COLLECTION AND STRUCTURE DETERMINATION

In 1896, Röntgen published a paper reporting the properties of X-rays, including their failure to demonstrate interference, reflection, or refraction effects on ordinary optical apparatus. In 1912, von Laue was able to show that X-rays yielded diffraction patterns due to interferences with the lattice spacings of a $\text{CuSO}_4 \cdot 5\text{H}_2\text{O}$ -crystal. In that same year, Bragg was able to provide a valid explanation for the incidence of spots on X-ray-diffraction patterns and the new science of X-ray crystallography was born. Röntgen's observations also led to him concluding that no substance can be utilized for focusing X-rays. However, diffracted X-rays may be combined analytically with the aid of computers, provided that X-ray-diffraction patterns are measurable. X-ray-diffraction experiments allow measuring the intensities of diffracted X-rays. However, recording diffraction patterns destroys all information on the relative phases of the diffracted X-rays that produced them. Since knowledge of both the phases and intensities of the diffracted X-rays is essential to reconstructing the images of diffracting objects, determining their phases represents the fundamental problem in all crystallographic analyses.

Bragg's law describes X-ray scattering by crystals in terms of reflections from crystal planes. Crystal planes illuminated at a grazing angle of incidence, θ , scatter X-rays at an angle of reflection that is also equal to θ . The incident and diffracted rays and the normals to the diffracting planes all lie in the same plane. Constructive interference between rays scattered from adjacent crystal planes will only occur if the path difference between the rays equals an integral number of wavelengths. If the spacing of adjacent crystal planes is d , the path differ-

ence between two rays, ray 1 and ray 2, will be $AB + BC = 2d \sin \theta = n\lambda$. For constructive interference, we then have that

$$2d \sin \theta = n\lambda, \quad (\text{Eq. 2})$$

where λ is the X-ray wavelength and n is an integer.

Since the interaction between X-rays and matter is weak, interactions between single molecules and X-rays are unobservable. Molecules must therefore be crystallized, i.e., arranged in regular arrays, which will cause the scattering from any, given molecule to be reinforced by that from all other molecules. The diffraction patterns of molecular crystals may be referred to as their “molecular transforms,” i.e., the Fourier transforms of the molecules contained in the crystals. The three-dimensional lattices of molecules in crystals give rise to diffraction patterns, where the location of each spot thereon is governed by the underlying molecular transform at that location. In general, every part of molecules contributes to every part of diffraction patterns. Conversely, in order to reconstruct molecules’ structures from their diffraction patterns, it will be necessary to measure the intensity of every spot on their diffraction patterns. When an X-ray beam interacts with matter, scattering occurs from two types of processes, coherent scattering and incoherent scattering. The electromagnetic field of the incident X-ray beam forces the electrons in the matter involved into oscillations at the same frequency as that of the incident beam. All rays scattered by a given electron will thus have the same phase relative to the incident beam, and the resultant scattering will be coherent. The intensity of the scattered beam is inversely proportional to the mass of the scattering entity. The fact that the proton mass is approximately 2,000 times the electron mass thus explains why only the electrons in crystals contribute to coherent scattering. In X-ray crystallography, the incoherent scattering is much weaker than the correlated, coherent scattering and is thus usually ignored.

The total intensity scattered by a crystal is the sum of the intensities of all rays scattered by all unit cells involved. The von Laue equations are mathematical relations that describe that summation in three-dimensional space. Knowledge of proteins’ diffraction patterns and applications of Fourier transforms will allow computing their crystalline structures. However, the phase problem remains to be solved. In order to compute their electron densities, the phases of all diffracted waves will be needed. The phase problem may be solved by different

methods, Patterson summation, direct methods, heavy-atom isomorphous replacement, or by analyzing anomalous scattering patterns. Molecular replacement can employ homologue crystalline structures in order to obtain phases via Patterson summation. The phases obtained for the homologue structure are utilized as initial estimates of phases for the unknown structure. That model is termed the “phasing model” and is mapped onto the unit cell of the unknown structure. Computing the Patterson functions for a random cell and superimposing them allows determining the orientations of the two models. Once a set of initial phases has been obtained, a trial structure may be configured and improvements and thermal parameters that will bring it into the closest-possible conformity with reality sought. “Reality,” as used here, means the set of observable amplitudes/intensities contained in the X-ray diffraction pattern in question. Observed and computed structure factors should agree, to within the tightest tolerances possible. The progress of refinements at each stage is usually assessed in terms of a reliability index, R, or R-factor, which is given by

$$R = \frac{\sum(|F(h, k, l)|_{obs} - |F(h, k, l)|_{calc})}{\sum|F(h, k, l)|_{obs}}, \quad (\text{Eq. 3})$$

where F_{obs} are the observed structure factors and F_{calc} are those obtained from the computational model. A cross-validation scheme based on the so-called R-free factor (Brünger, 1992) employs a test-data set that is ignored under the refinements, but for which an R-factor is computed, provides indications regarding how well the model predicts empirical observations that were not used in fitting the model to the empirical data. Since the differences between the conventional R-factor and the R-free factor, R-free – R, are partly a measure of the extent to which the model overfits the empirical data, they should be small.

There are several means for refining the protein structure model. The phases involved may be refined, they may be extended to higher resolutions, and the fit of the model to computed electron densities may be improved. Knowledge of protein chemistry is required there, and the improvements obtained will depend upon the correctness of the interpretations of electron-density data. Such incremental refinements are typically pursued with the aid of computer programs that have been specially developed for use in protein crystallography.

PKA-data collection and structure refinements

X-ray diffraction data was collected following transferrals of PKA-crystals to the cryoprotectant solution and plunge-freezing in liquid nitrogen. The PKA-crystals were cooled by a 100-K stream of liquid nitrogen while X-ray-diffraction data was being collected. The Swiss Light Source (SLS) PXI and PXII beamlines and in-house MerckSerono rotating-anode source were employed as X-ray sources. The in-house source employs graphite, monochromatized CuK α radiation from an RU 200 rotating-anode generator (Rigaku, Tokyo, Japan). The in-house detector is a Rigaku R-AXIS IV X-ray detector, and, at SLS, the Pilatus detector at PXI was employed in collecting diffraction data. Data reduction was conducted using XDS, HKL2000 (Otwinowski, et al., 1997), or d*Trek. Data were integrated and scaled using HKL2000, XDS, d*Trek, SCALA, and MOSFLM. All structures were derived from molecular replacements employing Molrep. The initial molecular-replacement model employed was the PKA-structure 1ATP (Zheng, et al., 1993), downloaded from PDB (Bernstein, et al., 1997), with ligand and water molecules removed. Structure-model refinement and ligand fitting employed CNX (Brunger, et al., 1998) and COOT (Emsley and Cowtan, 2004). Following ligand fitting, subsequent cycles of model adjustment and refinement were carried out using COOT and CNX. Refined protein structures were checked and validated using WhatIF (Vriend, 1990).

2.2.2. SURFACE-PLASMON-RESONANCE ANALYSES

Surface-plasmon-resonance (SPR) analysis is an optical technique that measures changes in refractive index close to a sensor's surface employing the evanescent-wave phenomenon. In the case of the setup employed for this dissertation, the target protein (PKA) is immobilized on the sensor's surface and molecules (fragments) are injected into a stream flowing over the sensor's surface. The fragments thus interact with the target protein and generate a response that was recorded in real time. Fig. 9 schematically depicts the basic interactions involved.

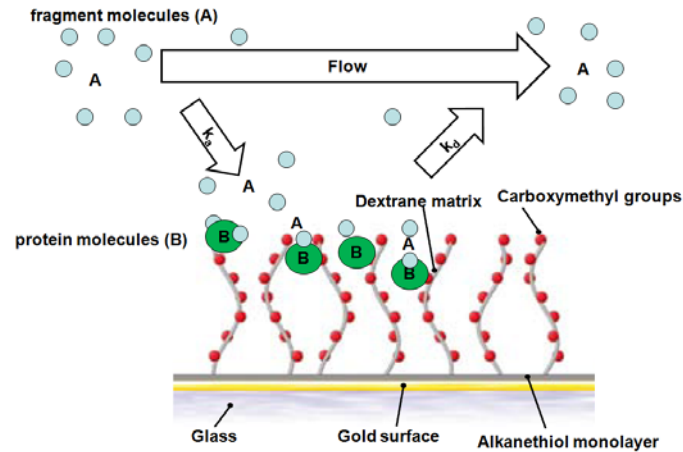


Fig. 9. Schematic of the SPR technique. Protein molecules (B) are attached to the dextrane matrix on the sensor's surface. Fragment molecules (A) are injected into a stream passing over the sensor's surface. k_a and k_d are intrinsic rate constants that describe the formation of complexes involving the fragments (A) and the protein (B). (adapted from a figure appearing in Myszkka, (1997))

Detection relies upon surface plasmon resonance (SPR), an electron-charge-density wave phenomenon that arises at the surface of a metallic film when light is reflected at the film under conditions of total internal reflection (TIR). The resonance is due to transformations of the energies and momentum of incident photons into surface plasmons, which depends upon the refractive index of the medium on that side of the film opposite that from which the incident light is reflected. SPR monitors interactions between the protein and the fragments by measuring the changes in solute concentration occurring at the latter surface due to the interactions taking place between the protein and fragments. The result is a change in the surface-plasmon-resonance signal, expressed in response units (RU) (cf. Fig.10).

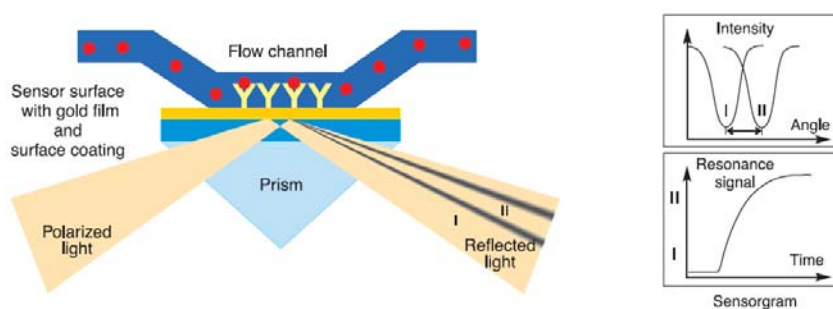


Fig.10. SPR-detection. Interactions between fragments injected into the flow channel and proteins attached to the sensor's surface cause a change in the refractive index of the underlying material, close to its upper surface, which alters the angle of incidence (SPR-angle) required for generating SPR. The SPR-angle is monitored in the form of a resonance signal, expressed in RU, by tracking changes (from I to II) in the angle of reflection.

SPR-sensorgrams

A plot of resonance units versus time is termed a "sensorgram" (GE Healthcare, Application Note 83). A sample sensorgram is shown in Fig.11, which schematically depicts the various

phases of SPR-analyses. In the case of the investigations reported here, the stream of buffer solution is brought into contact with the surfaces of immobilized proteins prior to fragment injection, yielding a response baseline. Fragments are then injected into the stream (the association phase) and binding of fragments entrained in the stream to the protein causes a rise in response (binding response, expressed in RU). Once fragments have been injected into the stream, the flow rate is readjusted only in order to contain the flow of buffer solution. Halting the injection of fragments triggers the dissociation phase. As fragments and the protein dissociate and fragments are swept off the latter's surface, signal amplitude will decline to the baseline level.

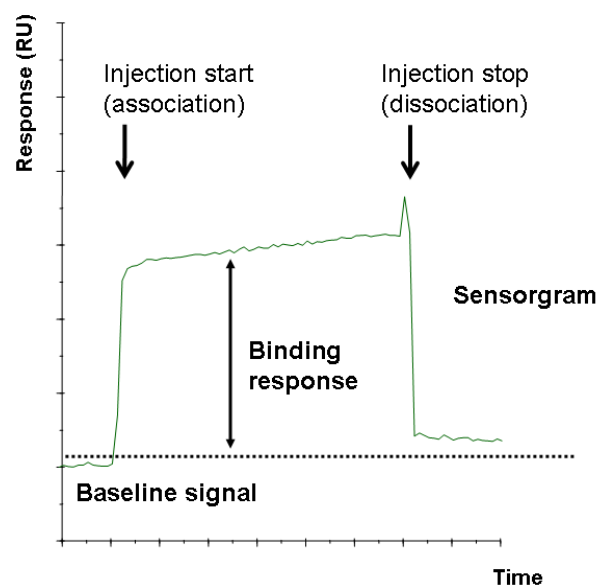


Fig.11. A sample SPR-sensorgram. Sensorgrams plot binding response, expressed in RU, versus time and therefore provide real-time data on overall fragment-protein interactions. The plot shown above is typical of fragments exhibiting transient binding responses. When injection starts, a signal indicating that fragment binding is occurring will be observed. When injection stops, fragment dissociation from the protein's surface will commence and signal amplitude will abruptly drop to the baseline level.

Fragments have low molecular weights and frequently have binding constants falling in the μM to mM range. Binding of a fragment to a surface thus results in relatively small mass increases close to the binding surface and low-level SPR-responses. The resultant low signal/noise ratios thus impose limitations when working with fragments. SPR fragment assays employ high protein and fragment concentrations in order to boost signal amplitudes to levels well above noise levels.

The fragments involved are dissolved in an organic solvent in order to ensure that they will continue to be soluble at high concentrations. A commonly used solvent for small molecules

is DMSO, which has a high refractive index. A slight mismatch in DMSO concentration between the running buffer and sample buffer can thus cause large signal mismatches that can greatly exceed responses generated by fragment-protein interactions. A 0.1 % difference in DMSO concentration corresponds to a response shift of approximately 200 RU. Corrections for response shifts due to changes in the DMSO's refractive index should thus be determined by measuring the signals transmitted on the protein-free reference channel (Cannon, et al., 2004; Huber, 2005). Solvent-correction runs employing buffer injections involving controlled DMSO concentrations will allow correcting for such signal variations.

SPR-signals are sensitive to even the slightest variations in solution refractive index. A reference-spot check may be run in order to determine whether responses are partially attributable to interactions other than fragment-protein interactions. Reference-spot binding responses are then subtracted from protein-spot binding responses in order to obtain just those responses originating from fragment-protein interactions.

Under the experimental procedures employed in the work reported in this dissertation, proteins are immobilized on the sensor's surface prior to fragment injection. Immobilization of proteins on the sensor chip's surface set the protein quantity, or concentration, that should be used in fragment assays. Immobilization of proteins should also ensure that they will be maintained states that will allow them to bind fragments (Huber, 2005). Protein activity levels may be computed by employing a control compound having a known binding stoichiometry, where N represents the total number of bound compound molecules per immobilized protein molecule, i.e., the protein activity level, and is given by

$$N = \frac{R_{protein} \cdot \left(\frac{\delta n}{\delta C}\right)_{reference} \cdot MWT_{reference}}{R_{reference} \cdot \left(\frac{\delta n}{\delta C}\right)_{protein} \cdot MWT_{protein}} \quad (\text{Eq. 4})$$

The protein-binding levels, $R_{protein}$, the saturation response, R_{max} , of the positive control compound, $R_{reference}$, protein molecular weight, $MWT_{protein}$, and the molecular weight of the positive control compound, $MWT_{reference}$, all represent parameters that can be measured. The ratios $(\delta n/\delta C)_{reference}$ and $(\delta n/\delta C)_{protein}$, represent the change in refractive index caused by variations in the concentrations of bound protein or bound compound, and are constants for given molecules and usually unknown. They are therefore neglected in most SPR-applications

(Huber and Mueller, 2006). Measuring protein activity levels following immobilization is recommended. Experience has shown that large variations in protein activity levels between differing protein surfaces can occur (Huber and Mueller, 2006). Protein activity levels are routinely checked several times during fragment-screening campaigns. Control compounds yield the activity levels of individual immobilized surfaces and also provide some degree of control over the stabilities of protein surfaces, since they are employed during several cycles interposed between fragment injections during screening. The variations in activity levels and expected fragment-binding signals occurring throughout screening may then be computed. Unexpected reductions in activity levels can lead to erroneous estimates of the numbers of bound fragment molecules.

2.2.2.1. PKA ASSAY PREPARATION

Sensor-chip quality checks

All SPR-investigation were carried out at 25°C using a BIACORE A-100 instrument (GE Healthcare, Uppsala, Sweden). A fresh CM5 sensor chip was employed on each new experimental setup. The immobilization program employed was that provided by the BIACORE A-100 control software. BIAnormalize solution (BIACORE) and HBS-N buffer (BIACORE) were employed in accordance with the instructions displayed by the software. The control-software settings employed were precisely those specified by the instrument's manufacturer.

BIACORE A-100	BIACORE
Series S sensor chip CM5	BIACORE
BIAnormalize solution	BIACORE
BIAmaintenance kit	BIACORE
HBS-N Buffer	BIACORE

Immobilization

PKA was coupled to the CM5 sensor chip's surface via amine-coupling chemistry. Free carboxylic-acid groups in the dextrane matrix were transformed into N-hydroxysuccinimide esters, which was achieved by injecting carbodiimide (EDC) and N-hydroxysuccinimide (NHS), which reacts with the free carboxylic-acid groups. Coupling occurs largely with the free amino groups of lysine residues. Following immobilization of the protein, ethanolamine was applied to the sensor's surface in order to deactivate any active groups remaining on its surface. The amine coupling reagents EDC, NHS, and ethanolamine (BIACORE), which were kept in storage at -20°C, were withdrawn from storage and thawed. Prior to application, it

was verified that the immobilization reagent to be employed contained no air bubbles. The following protocols list the settings employed in immobilizing PKA on the sensor chip's surface. Fig.12 presents an overview of the instrumental layout for this particular setup of the BIACORE A-100.

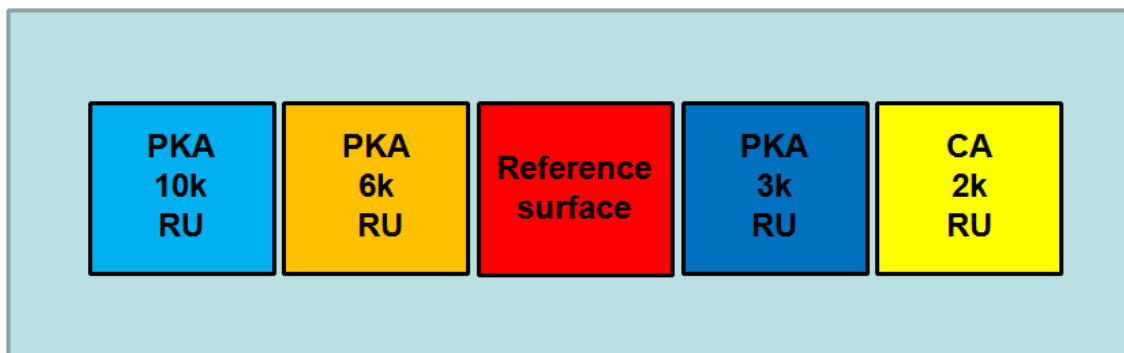


Fig.12. The five detection areas employed in immobilizing protein on the sensor chip. PKA was immobilized on three spots at three, differing, protein-density levels. The immobilized protein levels involved corresponded to response levels of 10 k, 6 k, and 3 k. CA was immobilized on a single spot employed as a reference spot in order to allow investigating nonspecific protein interactions. One spot was employed as a vacant surface and revealed that interactions with the sensor chip's surface were occurring.

BIACORE A-100 control software was employed, where the settings for the immobilizations involved were as follows:

Immobilization conditions

Sensor chip	CM5
Channels/spots	Fc1, Fc2, Fc3, and Fc4; spots 1 – 5
Flow rate	10 μ l/min
Temperature	25°C
Channel	1/2/3/4
Spot(s)	1, 2, and 4
Immobilization mode	Amine coupling
Ligand/protein	Human PKA(10 – 350)
Protein concentration	20 μ g/ml (spots 1 and 2) and 10 μ g/ml (spot 4)
Sample buffer	10 mM bis-tris-propane, pH: 6.5
Sample preparation	1:200 dilution of the ligand in Milli-Q-H ₂ O

Injection time	240 s + 240 s (spot 1) 240 s (spot 2) 120 sec (spot 4)
Running buffer	Immobilization running buffer
BIACORE A-100	BIACORE
Series-S CM5 sensor chip	BIACORE
Normalizing solution	BIACORE
HBS-N buffer	BIACORE
Normalization 1	BIACORE
Normalization 2	BIACORE
EDC	BIACORE
NHS	BIACORE
Ethanolamine	BIACORE
Human PKA protein/protein-immobilization buffer	20.5 mg/ml PKA 5 mM Mes 5 mM bis-tris-propane/HCl 75 mM LiCl 0.1 mM EDTA 1 mM DTT pH: 6.9
CA-protein/protein-immobilization buffer	30 µg/ml CA (BIACORE, S-51 training kit) Acetate buffer, pH: 5.5 (BIACORE)
Protein immobilization running buffer	100 mM HEPES 150 mM NaCl 0.005 % Tween 20 2 mM MgCl ₂ pH: 6.8
PKA-protein immobilization buffer	10 mM bis-tris-propane 200 µM ATP 2 mM MgCl ₂
CA-protein immobilization buffer	Acetate buffer, pH: 5.5 (BIACORE)

2.2.2.2. FRAGMENT SCREENING

Fragment screening involves injecting fragments into a stream of solution at a single concentration in order to determine whether they interact with the protein immobilized on the sensor's surface. The resulting sensorgrams are then analyzed in order to pick out the hits.

An expected maximum response due to fragments binding at equilibrium may be computed for each fragment molecule. During fragment screenings, such computations are utilized for identifying those fragments that interacted with the protein on a 1:1-basis at the molecular level. The theoretical maximum binding responses for such 1:1-interactions, R_{max} , may be computed from the molecular weights of the fragment and protein involved, the quantity of protein immobilized on the sensor chip's surface, and the immobilized protein's activity level, employing the following relation:

$$R_{max} = \text{Immobilized protein level} \cdot \text{protein activity level} \cdot \frac{MWT_{fragment}}{MWT_{protein}} \quad (\text{Eq. 5})$$

Upon binding, chemical scaffolds can cause the occurrence of unexpected refractive-index increments (RII) on the sensor chip's surface (Davis and Wilson, 2000), which can result in the binding responses obtained differing from those expected in the case of certain affinities and molecular weights. Employing an upper cutoff level of $2R_{max}$ as a criterion in hit-classification surveys is therefore recommended in order to preclude inclusion of fragments whose refractive-index increments are due to their molecular properties.

Signal/noise ratios determine the lowest cutoff levels for which fragment binding responses may be regarded as reliable and both represent the minimum response levels that will be reliably detected and define those fragments that will be counted as hits at the fragment concentration employed in screening. Assignments of lower cutoff levels are based on the average responses received from negative controls, plus three standard deviations.

Responses that occur upon fragment binding will be observed in the form of signal transients exhibiting very short rise and fall times (cf. Fig.11). The rates at which steady-state binding, i.e., binding equilibrium, is reached equal the product of the association constant, k_{on} or k_a , and the free-fragment concentration. Under such circumstances, transient binding behavior is

to be expected in the case of virtually all fragments. In this study, such sensorgrams were therefore classified as typical transient-binding sensorgrams.

A compound concentration of 200 μM was employed in fragment screenings. Fragments were flowed onto sensor surfaces bearing immobilized PKA. The fragments involved were prepared by MerckSerono's in-house Compound-Storage Department. The stock solutions employed contained 10-mM fragment concentrations in 100 % DMSO. Those stock solutions were diluted in Eppendorf tubes to sample-preparation-buffer levels in a single operation. The Eppendorf tubes containing the diluted compound solutions were then vortexed for 5 seconds in a VWR International vortexer. Compound solutions were subsequently transferred from the Eppendorf tubes to a BIACORE 386 well plate, which was subsequently sealed using BIACORE sealing film pending usage. Running buffer, sample-preparation buffer, solvent (DMSO) corrections, positive and negative control samples, fragment samples, and surface-regeneration conditioner were all prepared in accordance with the following table:

Running buffer	100 mM HEPES 150 mM NaCl 0.005 % Tween 20 2 mM MgCl_2 pH: 6.8 2 % DMSO
Sample-preparation buffer	100 mM HEPES 150 mM NaCl 0.005 % Tween 20 2 mM MgCl_2 pH: 6.8
PKA positive-control sample	<i>1 mg H-89 dissolved in DMSO to yield:</i> 1 mM 100 % DMSO (stock solution) <i>Diluted in sample-preparation buffer:</i> 2 μM H-89 2 % DMSO

CA positive-control sample	10 mM furosemide (BIACORE, S-51 training kit) 100 % DMSO <i>Diluted in sample preparation buffer:</i> 20 μ M furosemide (BIACORE) 2 % DMSO (Merck)
Negative-control sample	<i>Running buffer</i>
Solvent-correction setup	<i>Sample-preparation buffer containing</i> 1.2 % DMSO 1.4 % DMSO 1.6 % DMSO 1.8 % DMSO 2.0 % DMSO 2.2 % DMSO 2.4 % DMSO 2.6 % DMSO 2.8 % DMSO
Screening compounds	10 mM compound in “remp tubes” 100 % DMSO <i>Diluted in sample preparation buffer:</i> 200 μ M compound 2 % DMSO
Characterization compounds	100 mM compound in stock solutions 100 % DMSO <i>Diluted in sample preparation buffer:</i> 1 mM compound 2 % DMSO <i>1:1-dilution in sample-preparation buffer in ten increments:</i> 1.0 mM compound, 2 % DMSO 500 μ M compound, 2 % DMSO 250 μ M compound, 2 % DMSO 125 μ M compound, 2 % DMSO

	62.5 μ M compound, 2 % DMSO 37.25 μ M compound, 2 % DMSO 15.63 μ M compound, 2 % DMSO 3.91 μ M compound, 2 % DMSO 1.95 μ M compound, 2 % DMSO
--	---

The BIACORE A-100 control software was configured with the following experimental settings:

<i>Chip conditioning</i>	
Solution, flow cell 1	Running buffer A
Solution, flow cell 2	Running buffer A
Solution, flow cell 3	Running buffer A
Solution, flow cell 4	Running buffer A
Contact period, cycles 1 – 5	180 s
Total no. of cycles	5
Extra wash, flow cell 1	50 % DMSO
Extra wash, flow cell 2	50 % DMSO
Extra wash, flow cell 3	50 % DMSO
Extra wash, flow cell 4	50 % DMSO
Stabilization period prior to injection	N/A
Stabilization period following injection	180 s
Flow rate	30 μ l/min
<i>Samples</i>	
Sample buffer, flow cell 1	Sample in running buffer
Sample buffer, flow cell 2	Sample in running buffer
Sample buffer, flow cell 3	Sample in running buffer

Sample buffer, flow cell 4	Sample in running buffer
Running buffer, flow cell 1	Running buffer
Running buffer, flow cell 2	Running buffer
Running buffer, flow cell 3	Running buffer
Running buffer, flow cell 4	Running buffer
Sample type	High-performance kinetics
Flow rate	30 μ l/min
Sample contact period	180 s
Dissociation period	180 s
Extra wash, flow cell 1	50 % DMSO
Extra wash, flow cell 2	50 % DMSO
Extra wash, flow cell 3	50 % DMSO
Extra wash, flow cell 4	50 % DMSO
Stabilization period prior to injection	N/A
Stabilization period following injection	120 s
Analysis temperature	25°C
Tray temperature	25°C
<i><u>PKA positive-control sample (H-89)</u></i>	
PKA positive-control sample	2 μ M H-89 in running buffer
Flow rate	30 μ l/min
Contact period	180 s
Dissociation period	180 s
Extra wash, flow cell 1	50 % DMSO
Extra wash, flow cell 2	50 % DMSO

Extra wash, flow cell 3	50 % DMSO
Extra wash, flow cell 4	50 % DMSO
Stabilization period prior to injection	N/A
Stabilization period following injection	120 s
Analysis temperature	25°C
Tray temperature	25°C
<i><u>Positive-control samples for CA (furose- mide)</u></i>	
Positive-control carbonic anhydrase	20 µM furosemide in running buffer
Flow rate	30 µl/min
Contact period	180 s
Dissociation period	180 s
Extra wash, flow cell 1	50 % DMSO
Extra wash, flow cell 2	50 % DMSO
Extra wash, flow cell 3	50 % DMSO
Extra wash, flow cell 4	50 % DMSO
Stabilization period before injection	N/A
Stabilization period after injection	120 s
Analysis temperature	25°C
Tray temperature	25°C
<i><u>Negative-control samples for PKA and CA</u></i>	
Negative-control sample	Running buffer
Flow rate	30 µl/min
Contact period	180 s
Dissociation period	180 s
Extra wash, flow cell 1	50 % DMSO

Extra wash, flow cell 2	50 % DMSO
Extra wash, flow cell 3	50 % DMSO
Extra wash, flow cell 4	50 % DMSO
Stabilization period prior to injection	N/A
Stabilization period following injection	120 s
Analysis temperature	25°C
Tray temperature	25°C
<u>Solvent correction</u>	
Solvent correction employing DMSO	Running buffer having DMSO-concentrations ranging from 1.2 % to 2.6 % in eight increments of 0.2 %
Flow rate	30 µl/min
Contact period	180 s
Dissociation period	180 s
Stabilization period prior to injection	N/A
Stabilization period following injection	120 s
Analysis temperature	25°C
Tray temperature	25°C
<u>Regeneration</u>	
Regeneration solution 1, flow cell 1	100 mM NaHCO ₃ , pH: 8.7
Regeneration solution 1, flow cell 2	100 mM NaHCO ₃ , pH: 8.7
Regeneration solution 1, flow cell 3	100 mM NaHCO ₃ , pH: 8.7
Regeneration solution 1, flow cell 4	100 mM NaHCO ₃ , pH: 8.7
Contact period	30 s
Stabilization period following injection	120 s

DMSO solvent-correction samples and positive/negative-control samples were injected at intervals of ten compound-injection cycles, for both PKA and for CA.

2.2.2.3. FRAGMENT-HIT CHARACTERIZATION

Fragment-binding steady-state equilibrium may be assessed using the Langmuir adsorption isotherm. The data from the titration curves obtained during hit characterization are fit to the Langmuir isotherm binding model via a nonlinear regression analysis, yielding the values of K_D , R_{max} , and the offsets, which are related by

$$R_{eq} = \frac{c \cdot R_{max}}{(c + K_D)} + offset \quad (\text{Eq. 6})$$

The titration series employed in hit characterization was prepared such that it would cover the expected range of fragment binding affinities. The titration series thus included fragment concentrations ranging from 1 mM, down to approximately 1 μ M.

Titration series involving ten fragment concentrations were prepared. Stock solutions having a compound concentration of 100 mM were prepared by dissolving solid fragment in 100 % DMSO, followed by dilution to 50 mM fragment, 100 % DMSO, in Eppendorf tubes. The compounds were then diluted in sample-preparation buffer to a 1-mM fragment concentration in 2 % DMSO. The compound-buffer solution was vortexed for 5 seconds in a VWR International vortexer and followed by centrifugation for one minute at 6,000 g in an Eppendorf 5415D centrifuge.

Fragment concentrations were prepared via 1:1-dilutions in ten increments (1 mM, 500 μ M, 250 μ M, 125 μ M, 62.5 μ M, 31.25 μ M, 15.625 μ M, 7.8125 μ M, 3.90625 μ M, and 1.953125 μ M). The compound solutions were transferred from the Eppendorf tubes to BIACORE 386 well plates. The plates were then sealed using BIACORE sealing film pending usage.

Running buffer, DMSO-correction samples, positive/negative-control samples and surface-regeneration conditioner were prepared, following the same method employed in the case of SPR-screening.

SPR- data analysis

Fragment binding curves were investigated using BIACORE A-100 evaluation software. Fragment screening data was assessed by following the BIACORE A-100 evaluation software's presettings. Assessments of fragment-hit characterizations were conducted by following the BIACORE A-100 evaluation software's presettings. Data analysis employed affinity-computation and sensorgram-visualization tools. The data was fit to the Langmuir binding isotherm, assuming a 1:1-binding model, which yielded the values of K_D , R_{max} , and the offsets for the fragments employed in hit characterization.

2.2.3. BIOCHEMICAL ASSAYS AT HIGH FRAGMENT CONCENTRATIONS

Employment of high compound concentrations in biochemical assays in order to allow identifying weakly binding fragments represents a further screening option for finding binders and involves extending the concentration range of a typical primary biochemical assay up to the mid- μM or high- μM ranges. Lessened assay volumes and the concomitant decreases in the quantities of biological reagents required are perceived as key factors that have improved the utility of biochemical assays in both HTS and FBLD.

HCA-approaches typically employ the same biochemical assays employed for screening larger-molecule compounds having greater affinities, but are conducted at higher substance concentrations. Fluorescence readout or radioisotope readout are assay techniques that are typically employed in HCA. The major advantages of HCA in FBLD are that the assays involved yield high throughput rates, are, in principle, quantitative, and utilize widely available technologies for detection.

However, pitfalls also arise when utilizing HCA in FBLD. Both false positives and false negatives can occur. For instance, added-fragment concentrations might interfere with the assays via unwanted mechanisms. Prospective causes of problems include compound interference, e.g., fluorescence quenching and/or fluorescence, with assay readout and "nonspecific" binding to, or disruption of, the target protein, or to enzymes causing jumps in signal amplitude. False negatives due to the effective lack of compound solubilities can also occur.

Noteworthy is that there are a number of reports in the literature where fragment molecules have been identified by biochemical assays conducted at high compound concentrations, and,

since high-throughput screening devices are employed, FBLD-studies employing HCA-methods are subject to virtually no limitations on throughput rates, which will allow conducting more extensive explorations of the diversities of fragment chemical spaces.

PKA biochemical assays

MerckSerono's in-house Assay Department was commissioned to setup and run the high-compound-concentration biochemical assays (HCA) involved. In brief, the HCA-fragment screening conducted employed a fragment concentration of 100 μM and runs were set up as competition experiments involving an ATP-concentration of 20 μM .

PKA was diluted to 5 mU – 20 mU in 20-mM MOPS at a pH of 7.5, 1 mM EDTA, 0.01 % Brij35, 0.1 % b-mercaptoethanol, and 1 mg/ml BSA. PKA was assayed against the Kemptide oligopeptide (LRRASLG) in a final volume of 25.5 μl containing 8 mM MOPS at a pH of 7.5, 0.2 mM EDTA, 30 μM substrate peptide, 10 mM magnesium acetate, and 0.005 mM [^{33}P g-ATP] (50 cpm/mole – 1,000 cpm/pmole). 0.5 μl compound in DMSO-solution was added and the mixture incubated for 30 minutes at room temperature. Assays were stopped by adding 5 μl 0.5-M (3 %) orthophosphoric acid and their results harvested onto P81 Unifilter plates employing a wash buffer of 50 mM orthophosphoric acid. Compound concentrations ranged from 200 μM down to 7 nM at the hit-characterization stage. IC_{50} -values were determined following fitting of the inhibition data to a 1:1-binding model.

Protein (PKA)	20 mM MOPS pH: 7.5 0.01 % Brij35 1 mM EDTA 0.1 % b-mercaptoethanol 1 mg/ml BSA
Substrate	30 μM Kemptide (LRRASLG) peptide 8 mM MOPS pH: 7.5 0.2 mM EDTA 10 mM magnesium acetate 0.005 mM [^{33}P g-ATP] (50-1000 cpm/pmole)

	30 min 25°C
Compounds	Titration series covering the range 200 μ M to 7 nM
Assay-stop solution	5 μ l of 0.5 M (3 %) orthophosphoric acid Harvesting onto P81 Unifilter plates Wash buffer: 50 mM orthophosphoric acid.

2.2.4. FRAGMENT-LIBRARY DESIGN

The molecules listed in fragment libraries are employed in various screening and characterization methods in order to detect and characterize fragments' interactions with target proteins. Fragment libraries have been designed to assemble sets of molecules that should be included therein. A molecular weight of less than 300 Da is regarded as the cutoff point for fragments (Congreve, et al., 2003). Examples of the other molecular parameters involved are the number of hydrogen bond donors and acceptors, as well as the solubilities of the fragments at the concentration ranges employed. Several studies and approaches have been employed in designing fragment libraries. Two different fragment libraries have been utilized in the pair of studies reported in this dissertation. A protein-kinase-targeted library was designed for the screening setup involving SPR, HCA, and protein crystallography. In the case of the other study involved, the associated fragment library was configured following a screening of the in-house database for fragments that had exhibited activities with respect to PKA in previous assays. Ready fragment availability was another parameter employed in assembling that fragment library.

The protein-kinase-targeted-fragment library was designed using the ZINC database and MerckSerono's in-house library-design and computational tools. The ZINC database (UCSF, <http://zinc.docking.org/>) was utilized and the following fragment-defining variables applied. The settings employed were in compliance with the rule of three (Congreve, et al., 2003).

- 100 Da \leq molecular weight \leq 300
- clogP \leq 3
- HBA \leq 3
- HBD \leq 3

- NROT ≤ 3
- PSA ≤ 60
- Deliverable within one to three weeks

A computed solubility (clogs, pH 7.4) of 200 μM that was assigned using MerckSerono's in-house solubility-computation tool was employed as a further criterion. The fragment library was exported in the form of sd-files. The fragments involved were manually surveyed using ISIS Base and Accord for Excel for visualizing the structures contained in the sd-files. Fragments for a protein-kinase targeted-chemical library were selected using the "chemical eye" gained from first-hand experience. Fragments containing one or more atoms that theoretically are capable of interacting with the donor-acceptor-donor moiety available in the hinge zone were selected. MerckSerono's in-house database tools were utilized for checking the availability of the compounds involved in MerckSerono's compound-storage facility. The final library contained all fragment compounds that were available in 10-mM concentrations in 100 % DMSO and packaged in vials containing 30 μl per vial. At least five vials were available per compound.

The fragment library based on selections of reported interaction data was assembled following a filtering of MerckSerono's in-house database. That compound database was screened using ISIS Base and the following parameter set:

- Molecular weight ≤ 300 Da
- Computed solubility at pH 7.4 (clogs, pH 7.4) $\geq 2 \times 10^{-4}$ M
- PKA-inhibition ≥ 50 % at 10- μM fragment concentration
- Availability of the compound in solid from MerckSerono's in-house compound-storage facility

Crystallization scaffolds were selected by the manual "chemical eye" method such that one example of each chemical scaffold was represented. Compounds listed in the library were stored in an ISIS Base database. An sdf-file containing the compounds selected and their properties was prepared using Accord for Excel and exported as a csv-file that was imported into the SpotFire program employed for keeping track of the fragments and the empirical data. Fragments listed in the library were ordered from in-house databases for delivery within 24 hours prior to commencement of the experimentation.

Library-generation and virtual-screening software	ZINC (UCSF, http://zinc.docking.org/) ISIS Base (MDL Information Systems, Inc.) ISIS Draw (MDL Information Systems, Inc.) Accord for Excel (Accelrys, Inc.) MOE (Chemical Computing Group, Inc.) SpotFire (Tibco Software, Inc.)
---	---

Chapter 3

RESULTS

3.1. FBLD INVOLVING SPR, HCA, AND PROTEIN CRYSTALLOGRAPHY

Under the approach to FBLD involved here, three different techniques were utilized for investigating fragment-protein interactions, surface-plasmon-resonance (SPR) analyses, high-compound-concentration biochemical assays (HCA) and protein crystallography. The outcomes of those investigations are presented below.

3.1.1. RESULTS OF SURFACE-PLASMON-RESONANCE (SPR) ANALYSES

Immobilization of PKA on the sensor chip's surface was the initial stage of SPR. Carbonic anhydrase II (CA) was also immobilized thereon and employed as a reference protein. Immobilization was carried out using an amine-coupling procedure. Immobilization of PKA resulted in three protein-density levels. The response units for each level were approximately 3,000 RU, 6,000 RU and 10,000 RU. The response-unit level for CA-immobilization was approximately 2,000 RU.

Injections of positive-control compound revealed protein activity levels. H-89 was employed as a positive control in the case of PKA, and furosemide was employed as a positive control in the case of CA. Protein activity levels were assigned under the assumption that the positive control compounds underwent 1:1-stoichiometry interactions with the protein

$$N = \frac{R_{protein} \cdot \left(\frac{\delta n}{\delta C}\right)_{reference} \cdot MW_{reference}}{R_{reference} \cdot \left(\frac{\delta n}{\delta C}\right)_{protein} \cdot MW_{protein}} \quad (\text{Eq. 4})$$

Both PKA and CA exhibited an activity level of approximately 100 %. Fig.13 depicts the sensorgrams obtained from injecting the positive-control compounds onto the surfaces of PKA and CA.

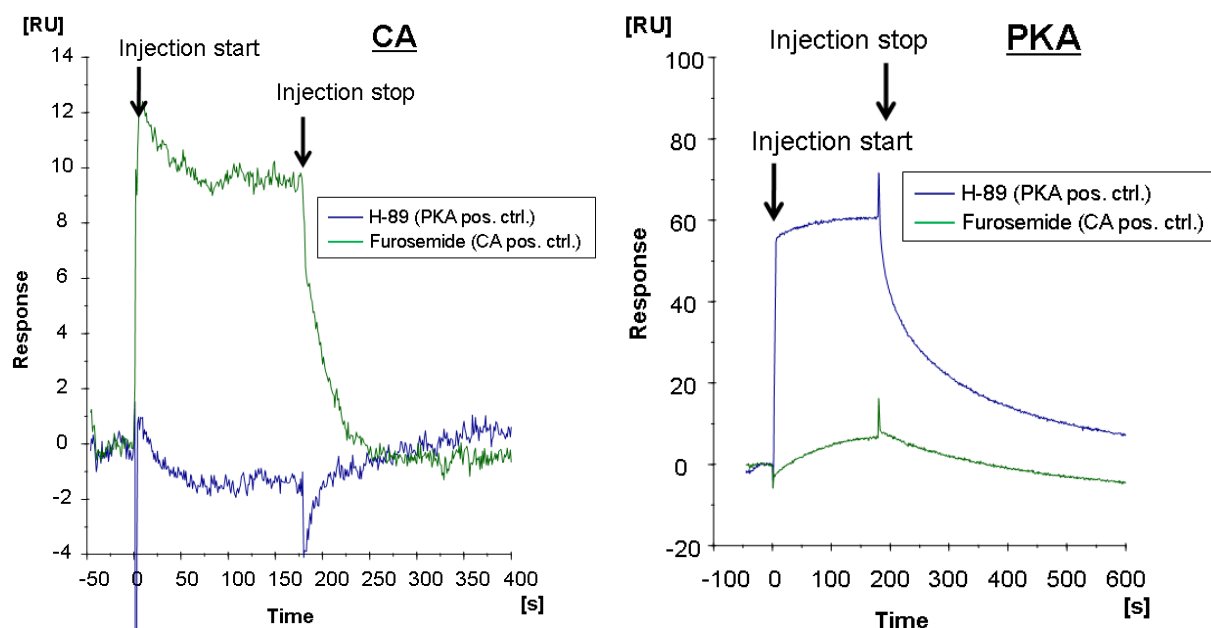


Fig.13. Sensorgrams for the positive-control samples employed in screening and hit characterization. These sensorgrams illustrate the binding of H-89 to PKA and furosemide to CA. Both positive-control compounds were applied in concentrations that saturated the protein's surface. Saturation was exhibited in the form of an abrupt increase in response following the start of injections in the case of both H-89 and furosemide.

Control compounds were injected at intervals of ten fragment-injection cycles during screening runs. Surface activity was maintained during screenings in all but one case, where a single fragment remained attached to the protein's surface following an injection cycle (cf. Fig.17 C), which resulted in a lower PKA activity level, and thus reduced responses from those fragments binding to the surface involved during subsequent injection cycles. New PKA activity levels were assigned to that surface employing the results of subsequent PKA positive-control-compound runs, which allowed conducting an analysis of all screening data.

Maximum response levels, R_{\max} , were employed in assigning cutoff levels to the maximum responses correlated to 1:1, fragment-protein interactions during screening. Those cutoff levels were computed from the associated immobilized-protein level, protein activity level, the molecular weight of the fragment involved, and the protein's molecular weight (cf. Eq. 4). The SPR-evaluation software was utilized for normalizing fragment responses, expressed in RU, referred to the molecular weight of each fragment involved, which resulted in maximum responses of 30 RU for 1:1, fragment-protein binding during the screening of the 257 fragments involved. However, injections of the negative-control samples indicated that variations from the baseline were occurring on the screening setup employed and assigned a lesser cutoff level to detection of fragment binding to low-density PKA-surfaces (those having 3,000-RU immobilized PKA; spot 1 on the sensor chip) during screening, which yielded a

lower cutoff level of 5 RU. Calibration runs employing solvent/DMSO-concentrations ranging from 1.2 % to 2.8 % were employed for correcting for larger mismatches in binding signals caused by variations in DMSO-concentration from sample to sample. Those solvent corrections were applied to all fragments investigated under the screening runs.

The 257 fragments were injected across all flow cells and detection areas at a fragment concentration of 200 μM . Fig.14 presents an overview of the results obtained from screening the 257 fragments, where the high and low cutoff levels for fragment binding are shown. The green spots represent fragments whose binding responses, expressed in RU, fell within the range stipulated for 1:1-interactions. The blue spots represent fragments that failed to exhibit responses exceeding the lower cutoff level. The red spots represent fragments whose responses exceeded that for 1:1 fragment binding, which might indicate either their bonding to multiple sites or a nonspecific binding of fragment aggregates to the protein. The full set of screening results is presented in Appendix 1.

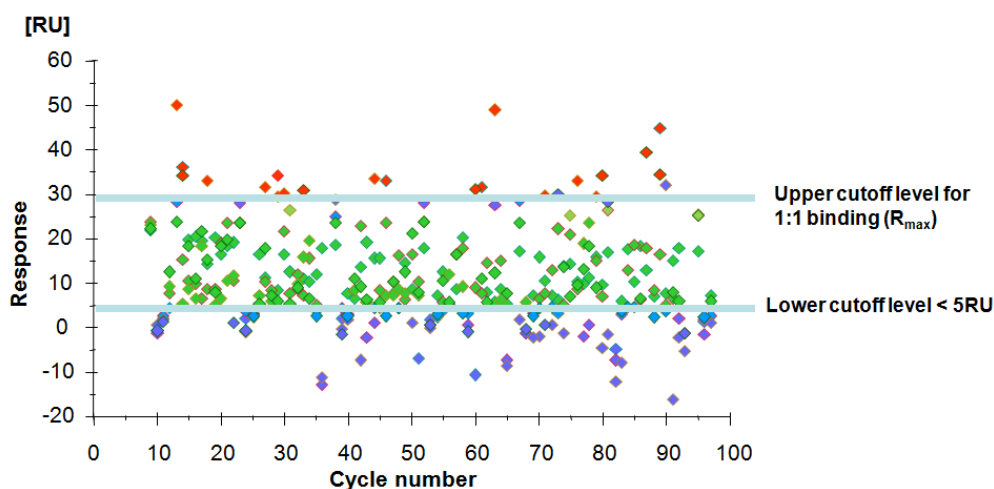


Fig.14. A plot of the responses obtained from fragment screenings. The plot provides an overview of the responses of all 257 fragments screened and has been prepared using BIACORE A-100 evaluation software. Response amplitudes for all 257 fragments are plotted versus cycle numbers and have been adjusted to allow for molecular weight. The upper and lower cutoff levels are indicated by the horizontal lines. The green spots represent fragments whose binding responses fell within the range for 1:1-interactions. The blue spots represent fragments whose responses failed to exceed the lower cutoff level of 5 RU. The red spots represent fragments whose responses indicate superstoichiometric fragment-protein interactions. The 60 hits were selected from among the green spots following manual inspections of their sensorgrams.

Fragments that exhibited binding responses falling between the high and low cutoff levels were manually investigated. The fragment concentration employed in the screenings (200 μM) resulted in transient binding responses from most fragments. Fragment responses

classified as hits were thus confined to those fragments whose sensorgrams exhibited such typical fragment-binding responses (cf. Fig.16).

SPR-responses are proportional to the changes in molecular weight occurring when fragments bond to the protein's surface. A further requirement for classification as a hit was that responses should be proportional to the quantities of immobilized PKA. There thus should be a rise in response correlated to binding on surfaces having higher immobilized-protein densities, and that was the case for all fragments classified as hits under the screenings conducted (cf. Fig.16).

The SPR sensor chip employed utilizes a reference surface, on which the protein carbonic anhydrase II (CA) was immobilized. Screenings detected eleven fragments that interacted with both PKA and CA. Those fragment interactions were excluded from further characterization. Fig.15 depicts the sensorgrams of a fragment that interacted with both PKA and CA.

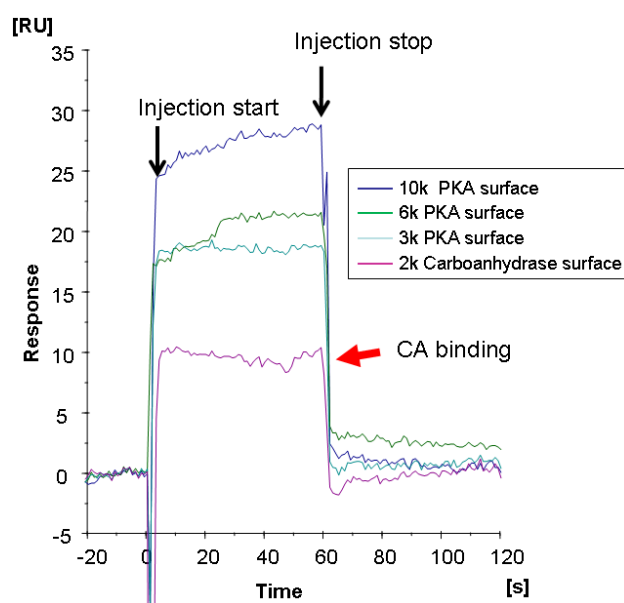


Fig.15. Sensorgrams of a fragment that interacted with both PKA and CA. A comparison of the response curves for PKA and CA indicates that the fragment involved bonded to the surfaces of both PKA and CA. Such fragments were not classified as hits under the screenings conducted.

The criteria for classification as a hit are listed in Table 4. Application of those criteria resulted in 60 fragments being classified as hits under the screenings conducted. The sensorgram of a fragment that met those criteria is illustrated in Fig.16.

Table 4. Criteria for SPR fragment screening hit selection. The table below lists the criteria for classifying fragments as hits in conjunction with the screenings conducted. The upper cutoff level was set to 30 RU and the lower to 5 RU. Increases in binding response varying with protein density/immobilization levels were also required. The binding sensorgrams should resemble those typical of transient fragment binding. A fifth criterion was specificity in binding to PKA.	
Fragment hit-classification criteria	Remarks
Binding responses exceeding a lower cutoff level, where a response of > 5 RU was interpreted as indicating binding to the surface of low-density PKA	Assignments of signal/noise ratios based on the results obtained from injecting negative-control samples yielded a lower cutoff level of 5 RU.
Binding responses remaining below an upper cutoff level, R_{eq}, of < 2 R_{max}	R_{max} , which corresponded to 30 RU in the case of low-density PKA-surfaces, should not be exceeded by more than a factor of two
Transient binding responses	All fragments classified as hits should exhibit typical transient binding.
Binding responses proportional to immobilized PKA-densities	Responses due to binding to higher-density protein surfaces should exceed those for binding to lower-density protein surfaces.
Specificity for binding to PKA	All hit-fragments should exhibit specific binding to PKA. Fragments binding to the reference protein, CA, were rejected.

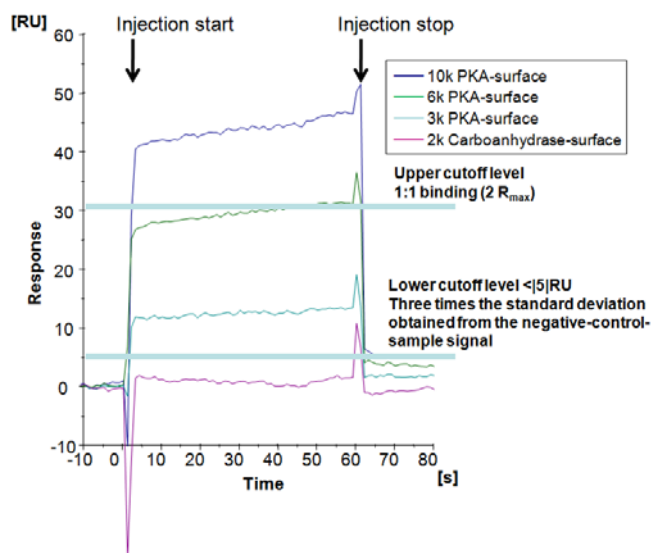


Fig.16. Sensorgrams of a typical hit-fragment. Illustrated above are the sensorgrams obtained from a single flow cell following injections of solutions having a 200- μ M fragment concentration across all five spots. All responses have been corrected to allow for the solvents, molecular weights, and reference levels involved. The fragment in question exhibited transient binding. No binding to the surface of CA was observed. Its responses increased with increasing density of the immobilized protein. Its response on the 3k PKA-surface never fell below 5 RU and never exceeded 30 RU, and thus remained between the upper and lower cutoff levels.

The sensorgrams obtained from the screenings revealed several fragments whose binding failed to correspond to a 1:1-stoichiometry binding model. Such fragments bind in a manner

that has been termed “promiscuous binding” in the SPR-literature (Gianetti, et al., 2008). Forty-five of the 257 fragments exhibited binding responses indicative of promiscuous binding and were identified by manual examinations of the sensorgrams. Three examples of such sensorgrams are shown in Fig.17

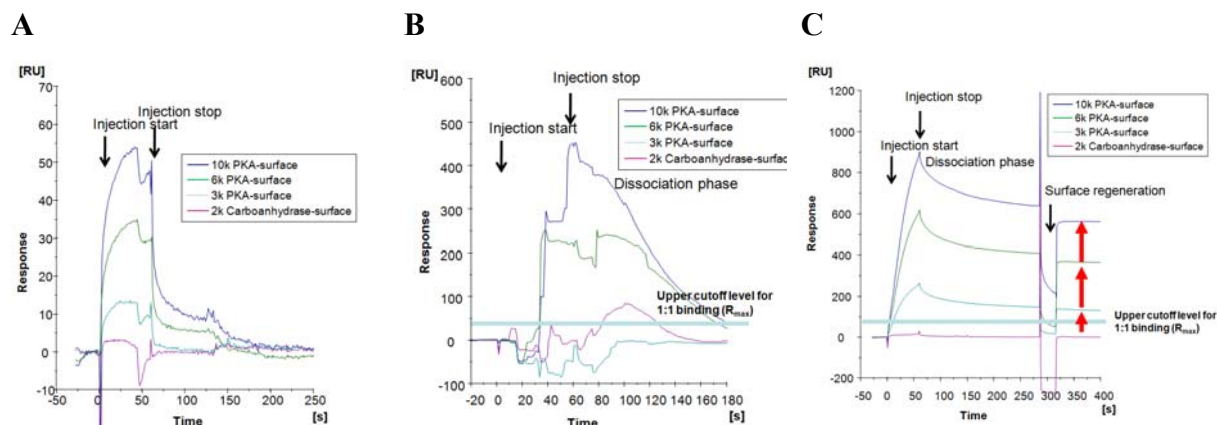


Fig.17. Sensorgrams of fragments exhibiting promiscuous binding. Sensorgrams from the screenings, illustrating the responses of fragments exhibiting promiscuous binding. **(A)** Although the fragment involved yielded responses that remained between the upper and lower cutoff levels, it failed to exhibit any responses similar to typical transient binding. Such binding responses have been reported in the case of micelles that interact with the protein. **(B)** The sensorgrams resulting from fragment injection cannot be characterized as indicative of any particular mode of interaction. The interactions involved were therefore nonspecific and similar to those with the surfaces of CA and PKA. **(C)** Fragment injection resulted in superstoichiometric interactions with the protein. The fragment adhered to the protein’s surface in a pseudo-irreversible manner, resulting in an escalating baseline.

Examinations of the sensorgrams for all 45 fragments involved facilitated classifying promiscuous binding responses, based on the nomenclature proposed by Gianetti and Huber (Gianetti, et al., 2008; Huber, 2005). The various types of promiscuous binding occurring in the sensorgrams shown in Fig.17 were suggestive of either binding of micelles (A), binding of fragments suffering from solubility problems (B), or binding of fragment aggregates that failed to detach from the protein’s surface during the dissociation phase (C).

Those fragment aggregates that failed to detach from the protein’s surface once injection had ceased were detached using regeneration conditioner. NaHCO_3 regeneration conditioner having a pH of 8.5 detached all such aggregates, except those whose sensorgrams are shown in Fig.17C, from its surface.

The 68 screening hits were subsequently characterized employing series of graduated fragment concentrations. All of the hits involved were characterized, based on both SPR and

HCA. In the case of SPR, the fragment concentrations employed ranged from 1 mM to approximately 1 μ M, while for HCA, they ranged from 200 μ M to approximately 1 nM. The responses obtained from SPR-hit characterizations facilitated classifying the 68 fragments into five subgroups. The subgroups and various types of fragment characteristics involved shall be described below and are summarized in Fig.18.

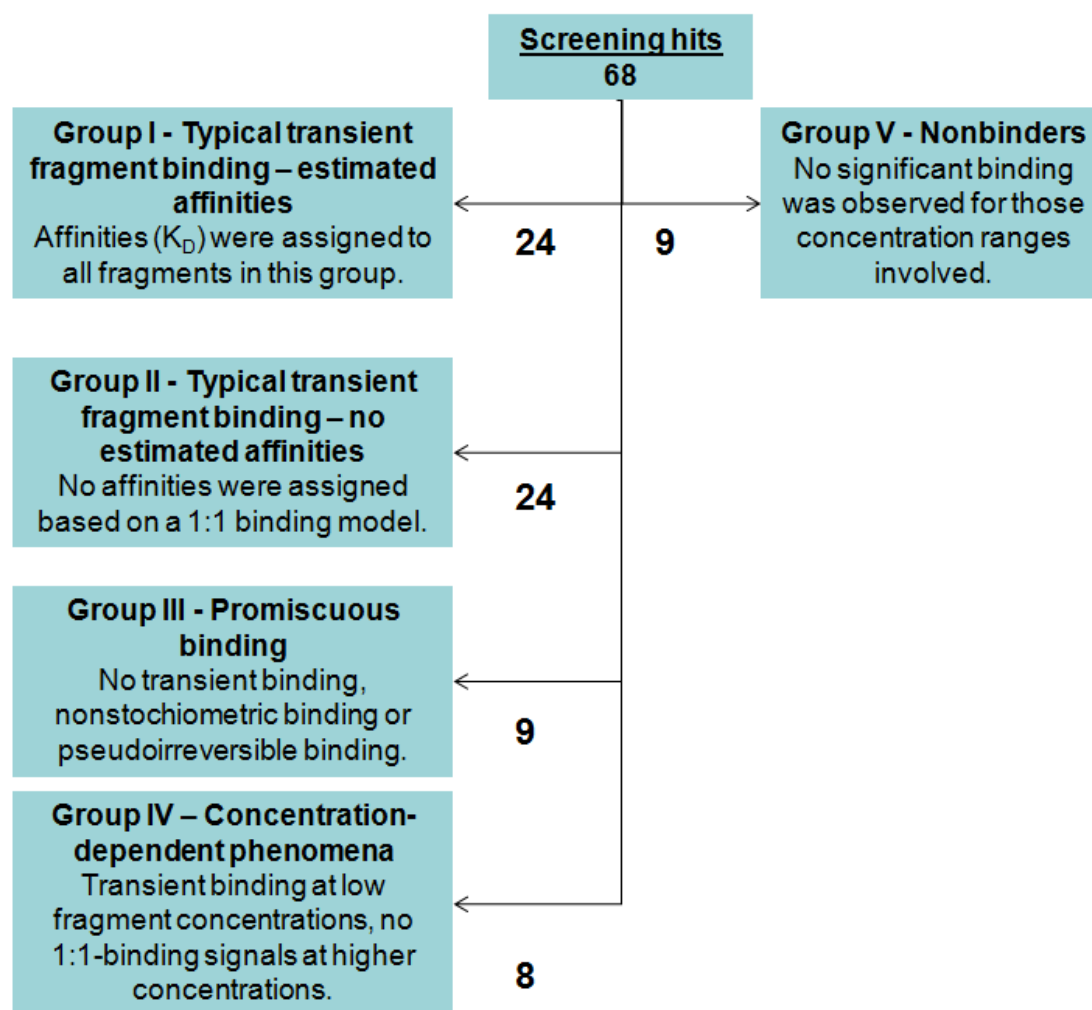


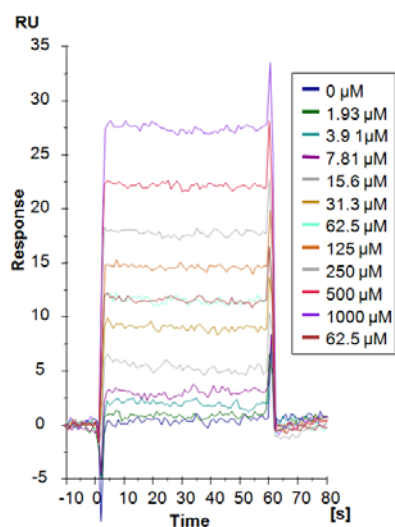
Fig.18. The results of SPR-hit characterizations. SPR-hit characterizations involved fragment concentrations ranging from 1 mM to 1 μ M. The fragments involved were classified into various groups, based on their binding responses. Twenty-four fragments exhibited typical transient binding responses and their affinity constants, K_D , were computed. Another 24 fragments exhibited transient binding responses, but no affinity constants were computed for them. Nine fragments exhibited binding similar to that termed “promiscuous binding” (Gianetti, et al., 2008) and eight fragments exhibited binding behaviors indicating that concentration-dependent aggregations were occurring. Nine fragments exhibited binding responses that remained below the lower cutoff level.

Fragments that had exhibited transient binding responses and whose affinities had been computed were classified as “typical transient-binding, estimated-affinity” fragments (Group I fragments). Fragments exhibiting transient binding, to which no 1:1-binding models or affinities, K_D , were assigned, were classified as “typical transient-binding, no-estimated-

affinity” fragments (Group II fragments). The third group consisted of those fragments whose responses could not be correlated to any 1:1, fragment-protein-interaction models. Such fragments were classified as “fragments exhibiting promiscuous binding” (Group III fragments). Further, those fragments that had exhibited transient, 1:1, binding responses at the lower concentrations, but exhibited nonstoichiometric, or promiscuous, binding responses at the higher concentrations, were classified as “fragments subject to concentration-dependent effects” (Group IV fragments). Sensorgrams similar to those of Group III and Group IV fragments had earlier been described by Huber (2006) and Gianetti, et al. (2008). Finally, fragments that exhibited binding responses that failed to exceed the lower cutoff level were classified as “nonbinders” (Group V fragments).

Fig.19 depicts the sensorgrams of a fragment that was allocated to Group I, since they are typical of transient fragment binding. The occupancies of protein binding sites increased with fragment concentration. A plot of its binding responses versus fragment concentration yielded a curve that asymptotically approaches unity (cf. Fig.19). In the case of such fragments, fitting their response data to the Langmuir-isotherm model yielded the values of their equilibrium binding constant (K_D), R_{max} , and offset. Equilibrium binding constants (affinities) were computed for 24 of the 68 fragments included in the hit characterizations. All 24 selectively interacted with the PKA’s surface and exhibited either no, or only very low, responses due to interactions with the CA’s surface.

(A) Group I fragment



(B) Response-concentration curve for fragment 6

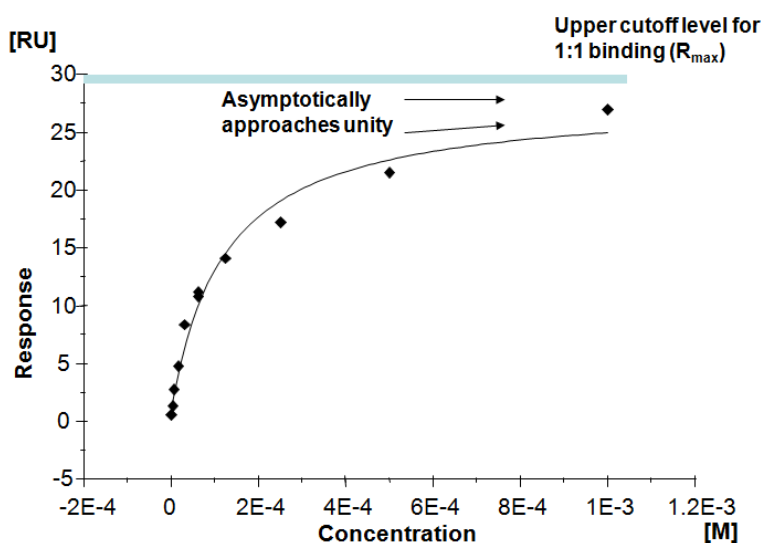
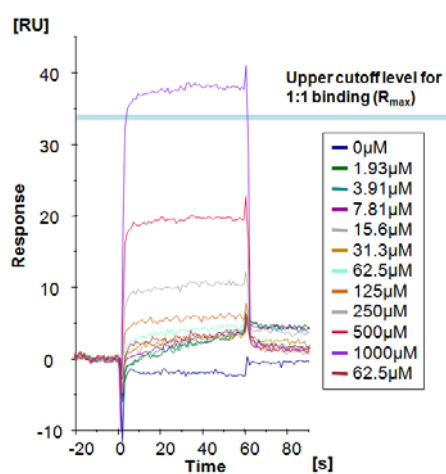


Fig.19. An example of a fragment that exhibited transient binding and was assigned an estimated affinity (Group I fragment). (A) Sensorgrams from the series involving graduated fragment concentrations exhibit the flat response curves indicating that typical transient binding was occurring. (B) A plot of its binding responses

versus fragment concentration yielded a curve that asymptotically approaches unity. The data have been fit to the Langmuir-isotherm binding model employing a nonlinear-regression analysis that yielded the values of K_D , R_{max} , and the offset.

Group II contained 24 fragments. Although they exhibited typical transient binding, their responses exceeded those expected for 1:1, fragment-protein interactions, and no saturation of protein binding sites was observed for them. Since it proved impossible to fit the data to a 1:1-binding model in the case of those fragments involved, no affinities were computed for them. Sample sensorgrams for a fragment from that group are shown in Fig.20.

(A) Group II fragment



(B) Response-concentration curve for fragment 22

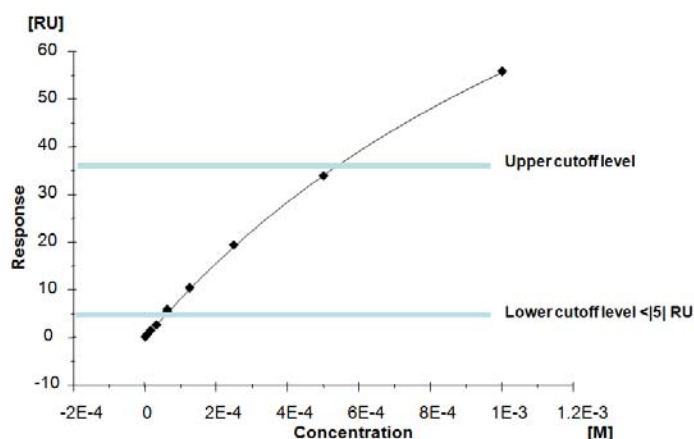
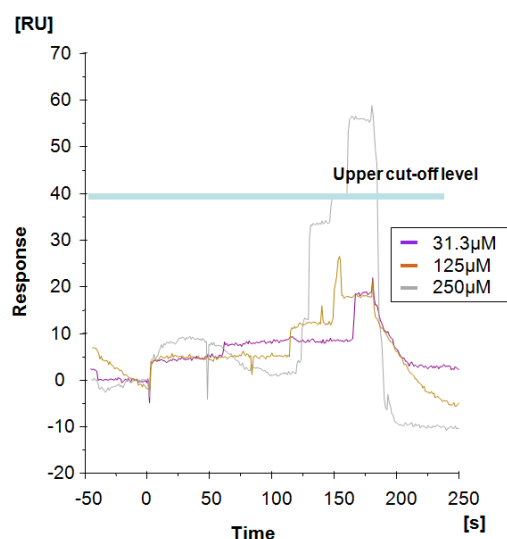


Fig.20. Sensorgrams for a fragment exhibiting transient binding, but for which no K_D was computed. Although the fragment involved yielded sensorgrams typical of transient binding, the R_{max} expected for 1:1, fragment-protein interactions was exceeded. Since saturation of protein binding sites failed to occur, binding isotherms could not be employed for computing such fragments' affinities (K_D).

Group III consisted of fragments exhibiting nonspecific protein interactions. McGovern, et al. (2008) and Gianetti, et al. (2008) had also proposed that the occurrence of such nonspecific interactions should result in the fragments involved being classified as promiscuous binders. Another nine fragments were added to Group III following hit-characterization runs. Two examples of sensorgrams obtained from those runs are shown in Fig.21, where (A) depicts those for a fragment classified in this dissertation as exhibiting “general promiscuous binding,” i.e., to which no particular mode of fragment-protein interaction could be assigned, which meant that their sensorgrams could not be utilized for deriving affinity constants. The sensorgrams obtained for another fragment classified as belonging to Group III are shown in Fig.21 (B). Although its binding responses were typical of transient binding, R_{max} was exceeded by more than a factor of two, indicating occurrence of a class of interactions that has been termed “nonstoichiometric binding.” One possible explanation of that sort of behavior is

that such fragments form oligomers or aggregates that undergo transient interactions with the protein involved.

(A) Group III (general promiscuous binders)



(B) Group III (nonstoichiometric binding)

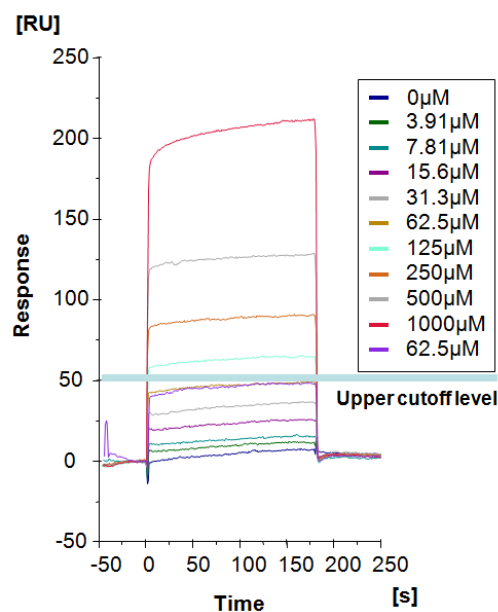


Fig.21. Sensorgrams of fragments exhibiting promiscuous binding. (A) Sensorgrams of a fragment classified as exhibiting general promiscuous binding. Such sensorgrams cannot be correlated any particular mode of fragment-protein interaction. (B) Although the fragment's sensorgrams are typical of transient binding, some of its response curves exceeded R_{max} by more than a factor of two. Its interaction stoichiometry therefore fails to correspond to that of a 1:1-interaction model. This particular fragment is an example of fragments that exhibited nonstoichiometric binding in conjunction with hit characterizations.

A type of response curve that has been described by Gianetti, et al. (2008) as being associated with large aggregates that bind to the protein was observed in the case of three fragments included in the hit characterizations conducted. Such “superstoichiometric binders” yield responses that exceed the maximum for 1:1-interactions by more than a factor of five and have been assigned to a subgroup of promiscuous binders that have been classified as members of Group III. Fig.22 depicts the sensorgrams obtained for one such superstoichiometric binder.

**Group III (superstoichiometric binders);
the case of fragment 100**

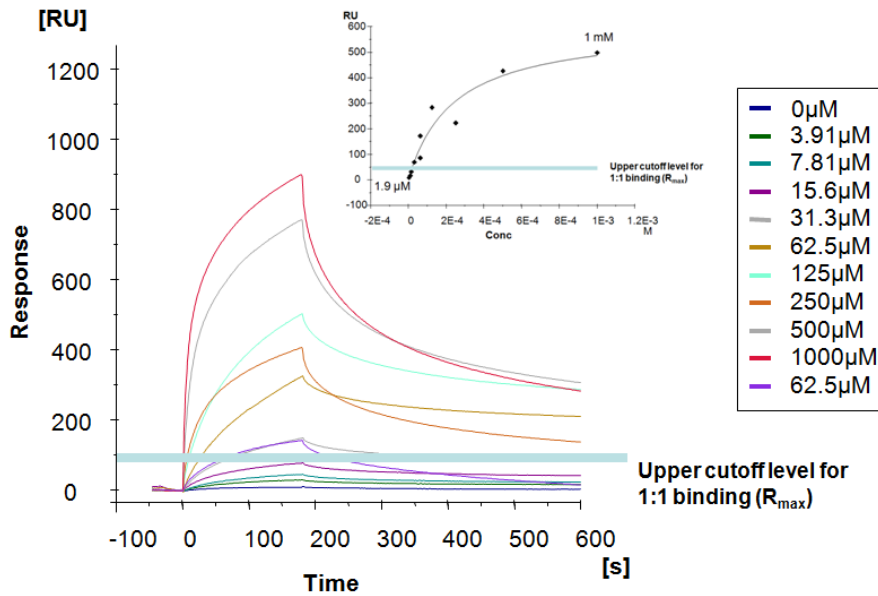


Fig.22. Sensorgrams of a superstoichiometric binder. Fragment binding response exceeded that expected for a 1:1, fragment-protein, interaction model (R_{max}) by more than a factor of five. Such strong binding to the PKA's surface is termed "superstoichiometric promiscuous binding." Such response curves have been correlated to large fragment aggregates that interact with the protein involved.

The SPR-runs conducted covered the association and dissociation phases of the molecular interactions involved, which allowed assessing their reversibilities. The data obtained allowed identifying another subgroup of Group III. That subgroup consisted of those fragments that failed to dissociate from the protein following the conclusions of injection phases. Such interactions are termed "irreversible-binding interactions" or "pseudo-irreversible binding interactions." The hit-characterization runs conducted turned up four fragments exhibiting irreversible or pseudo-irreversible binding. The sensorgrams of one such fragment are shown in Fig.23.

**Group III (pseudo-irreversible binders);
the case of fragment 74**

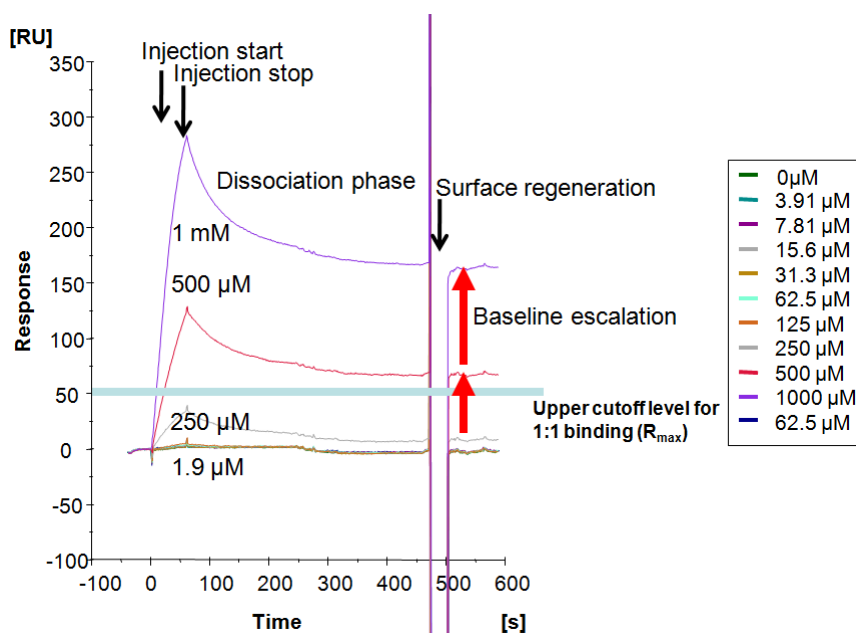


Fig.23. Sensorgrams of a fragment undergoing pseudo-irreversible binding to the protein involved. Its sensorgrams indicate that fragment aggregates form and bond to the PKA's surface. Those fragment aggregates that have formed also accumulated on the protein's surface, which is reflected in an escalating baseline that continues to escalate following the surface-regeneration stage.

Further investigation of the results of hit-characterization runs turned up a distinct, fourth group consisting of eight fragments that exhibited behaviors indicative of the occurrence of concentration-dependent effects. Although the fragments involved exhibited no signs of promiscuous or superstoichiometric binding at the lower compound concentrations, the higher compound concentration yielded either responses that exceeded those expected for the case of 1:1-interactions with the proteins involved or sensorgrams that could not be correlated to 1:1-interactions with them. A closer examination of those fragments showed that they exhibited 1:1-binding behavior with the PKA's surface at the lower compound concentrations. The fragments involved exhibited behaviors similar to those of fragments that were classified by Gianetti, et al. (2008) as belonging to the group subject to "concentration-dependent effects." Nevertheless, in this dissertation, Group IV is defined as consisting of all those fragments exhibiting irregular, concentration-dependent, sensorgrams. The sensorgrams of a fragment subject to concentration-dependent effects are presented in Fig.24.

**Group IV (fragments exhibiting concentration-dependent aggregation);
the case of fragment 19**

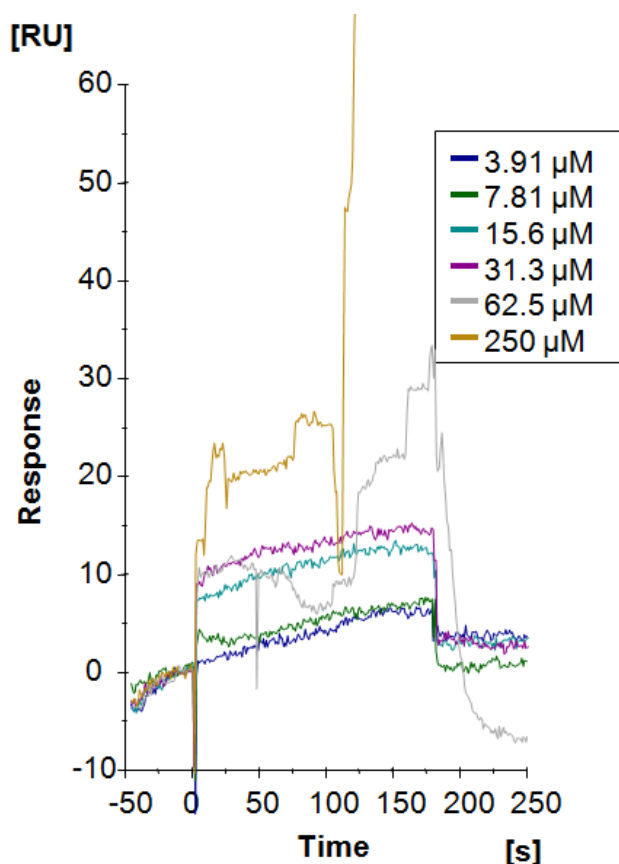


Fig.24. Sensorgrams of a fragment exhibiting concentration-dependent aggregation. Its hit-characterization sensorgrams indicate that it interacts with the protein in accordance with a 1:1-binding model at the lower compound concentrations. However, once compound concentration exceeds 32 μM (the purple curve), the fragment involved starts forming aggregates that exhibit promiscuous binding to the protein. The titration series therefore classifies the fragment as exhibiting concentration-dependent aggregation.

The fifth group consisted of nine fragments whose sensorgrams failed to indicate binding responses exceeding the lower cutoff level of 5 RU.

3.1.2. HIGH-COMPOUND-CONCENTRATION BIOCHEMICAL ASSAYS

Inhibition of PKA-substrate phosphorylation was investigated by means of biochemical-assay screenings at a fragment concentration of 100 μM . The lower cutoff for classification as hits was set to 30 % inhibition. The biochemical-assay screenings conducted resulted in 26 of the total of 257 fragments being classified as capable of inhibiting PKA. The percentage inhibitions of all 257 fragments are listed in Appendix 1. The hit characterizations performed subsequent to the SPR/HCA-screenings yielded the variations in their PKA-inhibitions with concentration, which were deduced from the results of series of runs employing graduated

concentrations (MerckSerono's in-house Assay Department was commissioned to conduct that work). The data obtained were fit to a 1:1-binding model and the inhibition constants, IC_{50} , of the various fragments computed. The HCA hit characterizations resulted in the determination of twelve IC_{50} -values (cf. Appendix 1). Fig.25 depicts the activity curves for two of the fragments involved, based on a 1:1-binding model.

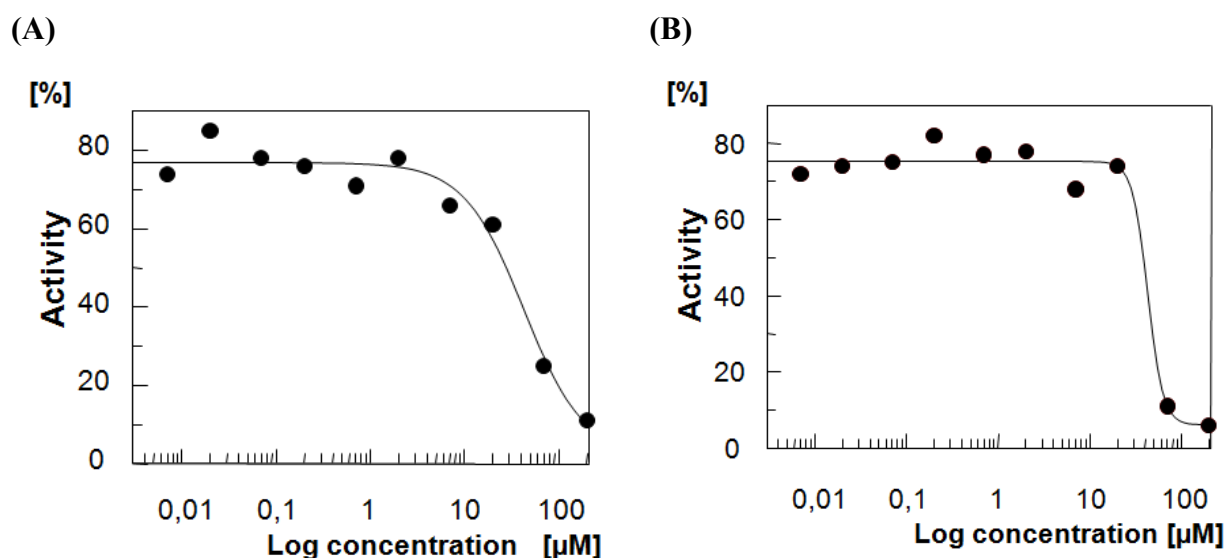


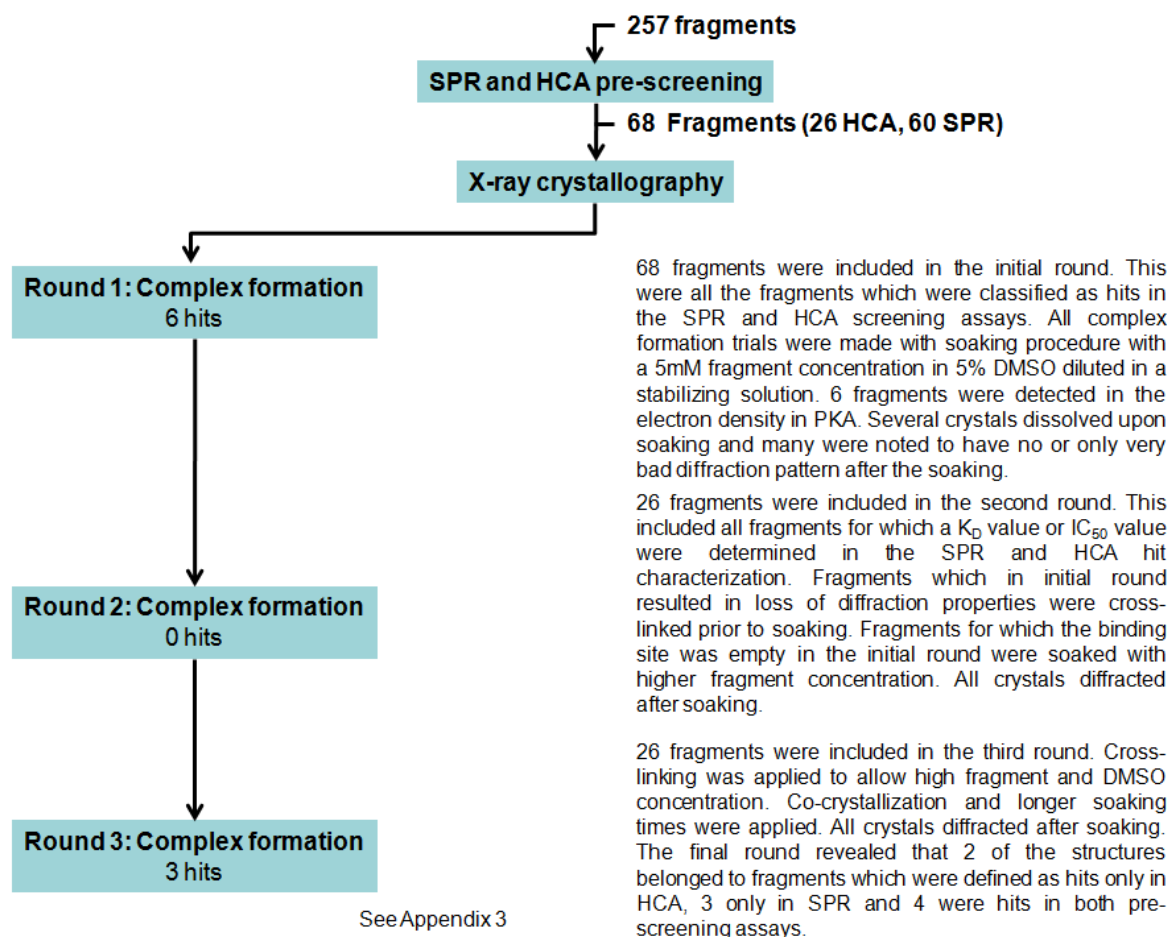
Fig.25. HCA hit-characterization data for two fragments. Activity curves for two sample fragments obtained from the series of graduated-concentration runs conducted in conjunction with hit characterizations, where the y-axis represents the percentage inhibition of PKA-substrate phosphorylation on the x-axis represents the logarithm of fragment concentration, expressed in μM . Fragment concentration ranged from 200 μM to 7 nM. HCA hit characterization was applied to all 68 screening hits and resulted in twelve IC_{50} -values covering the affinity range 23 μM to 110 μM .

3.1.3. PROTEIN CRYSTALLOGRAPHY

The complexes that fragments formed with PKA involved the recombinant, catalytic subunit of cyclic, AMP-dependent, protein kinase (PKA) and the pseudosubstrate, kinase-inhibiting peptide [PKI(5-24)]. All crystals were crystallized in the orthorhombic space group $P2_12_12_1$. Similar cell constants of around 72 Å, 78 Å, and 80 Å were observed for all crystals. Except for those variations in protein conformation reported in the results section of this dissertation, no major structure variations in PKA-conformations were noted. The conformations of PKA's small lobe and large lobe were relatively rigid. Structure patterns, such as the *DFG-motif*, C-helix, and activation loops, were also evident in earlier reports on the conformations of its crystalline structures.

Structure determinations employing protein crystallography were attempted for the 68 hits resulting from both the HCA-screenings and SPR-screenings. In the case of nine hits, the structures of the fragment-PKA complexes involved were determined. Table 5 presents an overview of the protein-crystallography studies conducted under the present approach to FBLD.

Table 5. An overview of the protein-crystallography studies conducted under the present approach to FBLD. The 68 hits from SPR/HCA-screenings were analyzed employing protein crystallography in an initial round in order to determine the modes, by which fragments bond to PKA, which resulted in determinations of the 3D-binding modes of six fragments. The second round of protein-crystallographic analyses involved only those fragments whose affinities or inhibition constants had been determined, but failed to yield the structures of any new, crystalline, fragment-protein complexes. The third round included further optimizations of the protein-crystallographic conditions and resulted in identification of another three structures involving 3D-fragment-protein interactions.



Following the initial soaking, around six fragment-PKA structures were derived from the results of protein crystallography. The fragments involved were unambiguously detected in the electron densities of the ATP binding sites on PKA. Twenty-one soaking attempts resulted

in crystal instabilities. The protein crystals involved either lost their diffractive properties or immediately dissolved upon soaking.

Under the second round, crosslinking with glutaraldehyde was employed for stabilizing the protein crystals, which allowed employing those fragment soakings that had resulted in crystal instabilities and loss of diffractive properties under the initial round for collecting X-ray data. However, all soakings resulted in incidence of vacant binding sites during the second round.

Extended soaking periods, higher fragment and DMSO concentrations, and cocrystallization were employed in the third round and the structures of another three fragment-protein complexes were derived. The detailed results for all nine fragments are presented in Table 10, which has been relegated to Appendix 2.

The structures revealed that all nine fragments bound in the ATP binding pocket of PKA (Fig.26). Table 10, which appears in Appendix 2, includes graphic representations of the fragment binding modes involved and discusses the associated interactions.

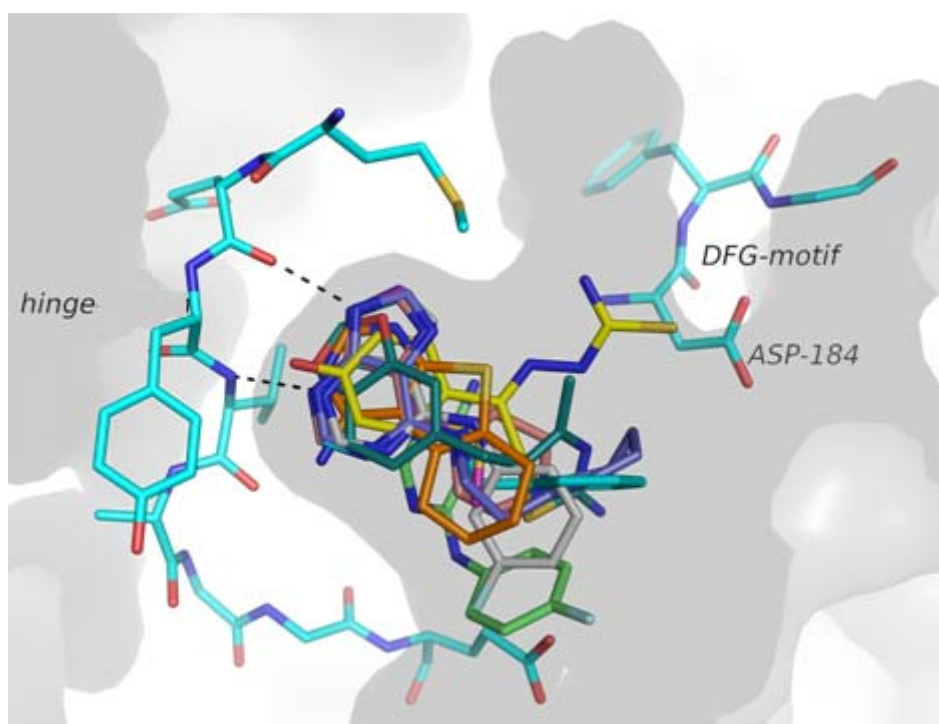


Fig.26. The binding modes of the nine hit-fragments to PKA. The diagram shows the ATP-pocket in PKA, overlain with the binding modes of the nine hit-fragments.

3.1.4. PRESENTATION OF SELECTED RESULTS

Under the present approach, a library of 257 fragments was screened for binders employing SPR and HCA. Sixty-eight of those fragments were classified as hits following screening, 60 of which were turned up by the SPR-runs, and 26 of which were turned up by the HCA-runs. Eighteen hits thus resulted from both screening assays. Selection of the 26 hits resulting from the HCA-runs followed a 100- μ M-concentration screening, where only those fragments that inhibited PKA-substrate phosphorylation by at least 30 % were classified as hits.

A characterization of those hits was subsequently conducted in order to allow further analyses of their interactions with the protein. Affinity constants, K_D , and inhibition constants were computed for 28 fragments and 24 affinity constants, K_D , were derived from the SPR-data, while the IC_{50} -values for twelve fragments were derived from the HCA-data. Values of both IC_{50} and K_D were obtained for eight fragments. The K_D -values obtained ranged from 15 μ M to approximately 1 mM, and the IC_{50} -values obtained ranged from 23 μ M to 110 μ M. Protein crystallography yielded the structures of the complexes formed by six of the twelve fragments that had yielded a value for IC_{50} . X-ray diffraction yielded the structures of the complexes formed by seven of the 24 fragments that had yielded a value for K_D . All nine fragments forming complexes whose structures had been determined from the results of the X-ray-diffraction runs had yielded values of either IC_{50} or K_D , or both.

The results of the first approach, which illustrate the similarities and differences between the various fragments involved and the experimental methods employed under the present approach to FBLD, will be presented below and are summarized in Table 6.

Table 6. Selective interactions observed in conjunction with screenings. Fragment 6 was classified as a hit under the SPR-screenings, but not under the HCA-screenings. The electron density derived from protein crystallography revealed its 3D-binding mode. Fragment 19 was classified as a hit under the HCA-screenings, but failed to exhibit a binding response under the SPR-screenings, so no structure could be derived for it. Although fragment 20 was classified as a hit under the HCA-screenings and yielded a structure for the complex formed, the results of the SPR-screenings conducted did not allow classifying it as a hit. In the case of fragment 57, the results of both the SPR-screenings and the HCA-screenings allowed its classification as a binder over the concentration range employed, but the structures of the complexes it formed, if any, could not be determined

Fragment	SPR-SCREENINGS	HCA-SCREENINGS	X-RAY
Fragment 6	+	-	+
Fragment 19	-	+	-
Fragment 20	-	+	+
Fragment 57	+	+	-

Fragment 6

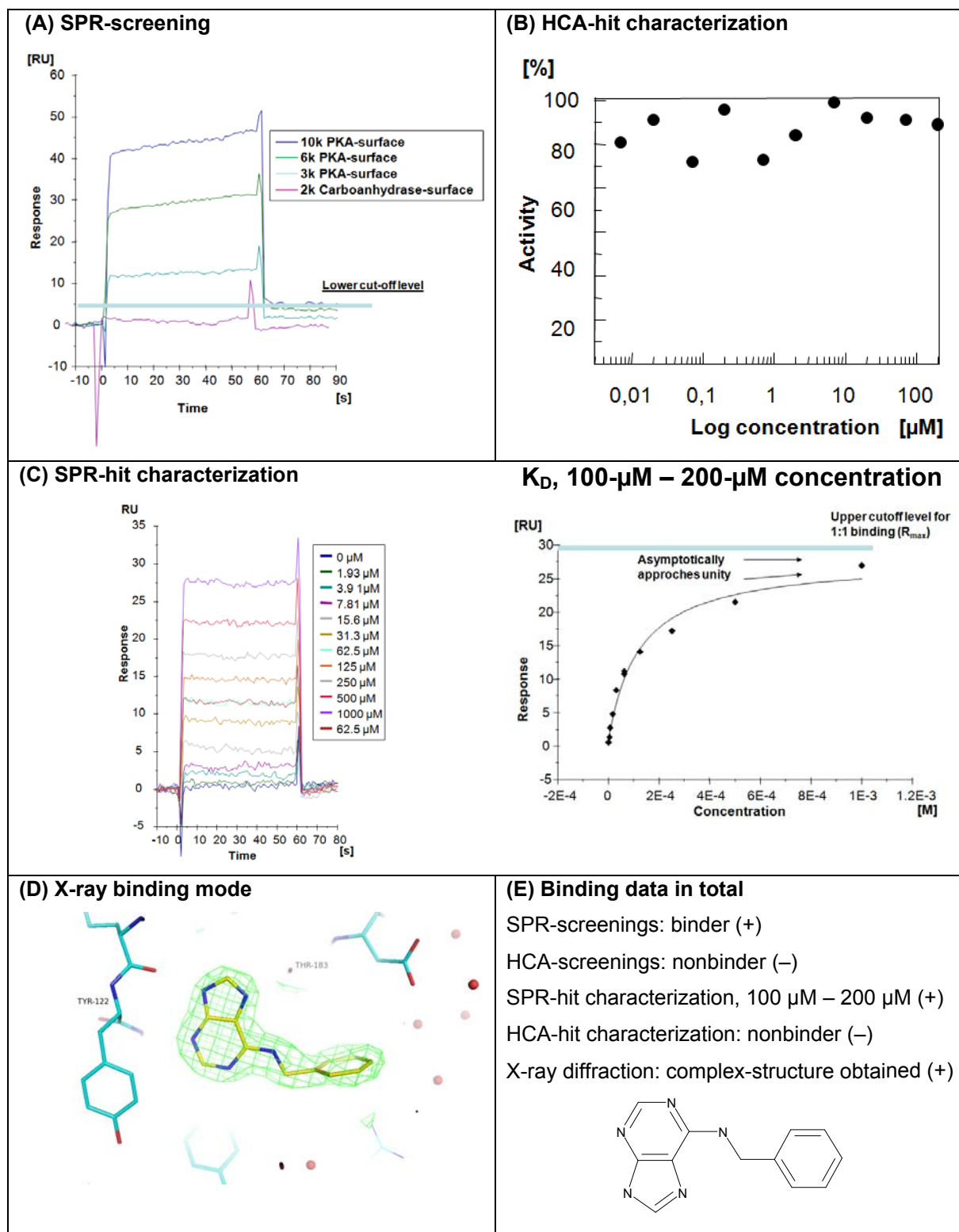
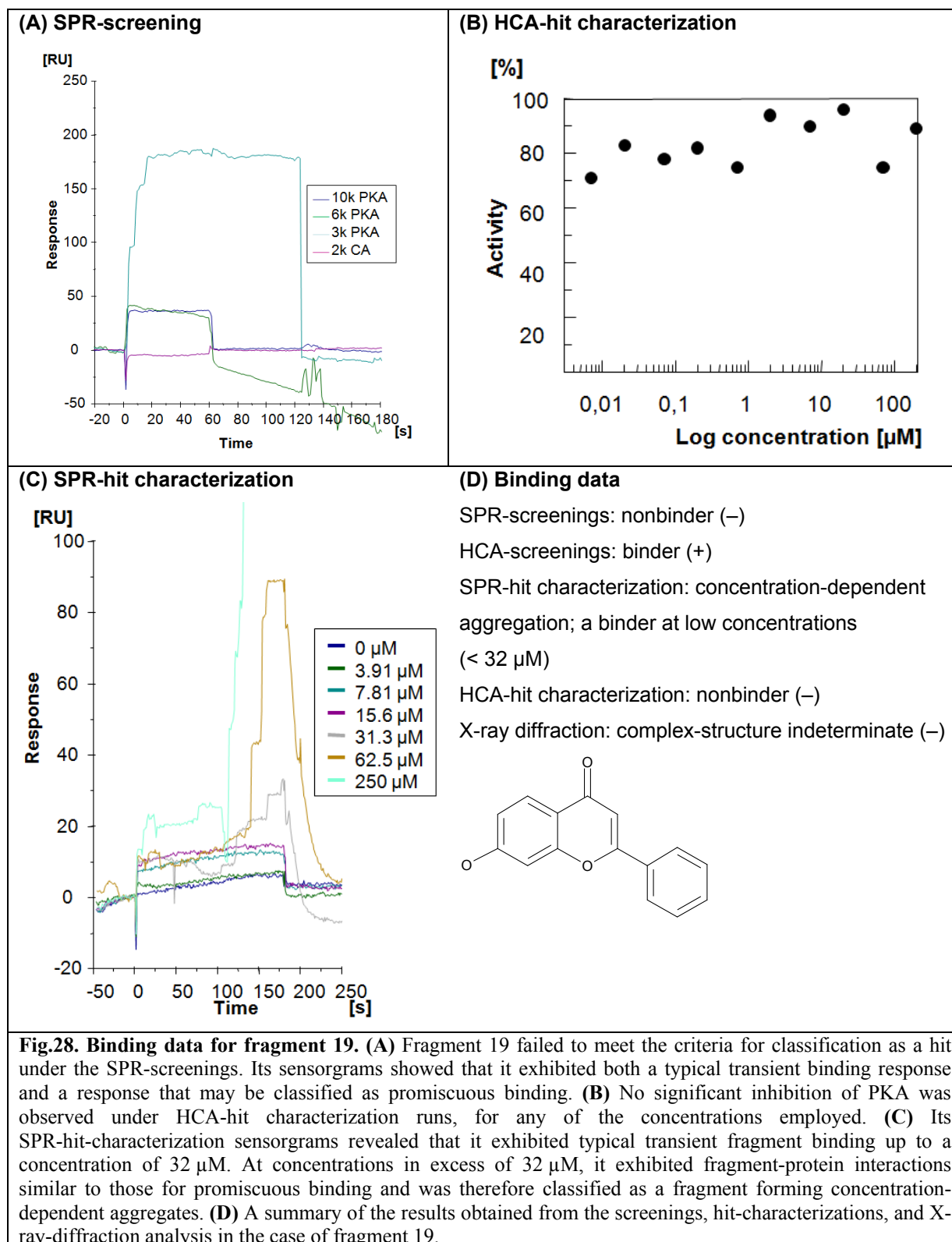


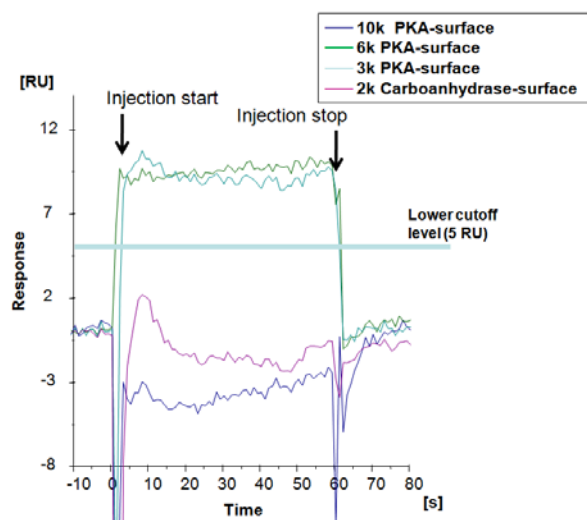
Fig.27. Binding data for fragment 6. (A) Fragment 6 met the criteria for classification as a hit under the SPR-screenings. (B) Under the HCA-hit characterization runs, it exhibited no significant inhibition of PKA for any of the concentrations employed. (C) Its SPR-hit characterization data was fit to the Langmuir binding-isotherm model and its K_D computed. (D) Its binding mode to PKA was determined from protein crystallography. (E) The screening and hit-characterization data obtained from the HCA/SPR-screenings. It was classified as a hit under both SPR-screening and SPR-hit characterization runs. However, neither the HCA-screenings nor the HCA-hit-characterization runs allowed classifying it as a binder/hit. Nevertheless, protein crystallography yielded the structure of the complex it formed with PKA.

Fragment 19

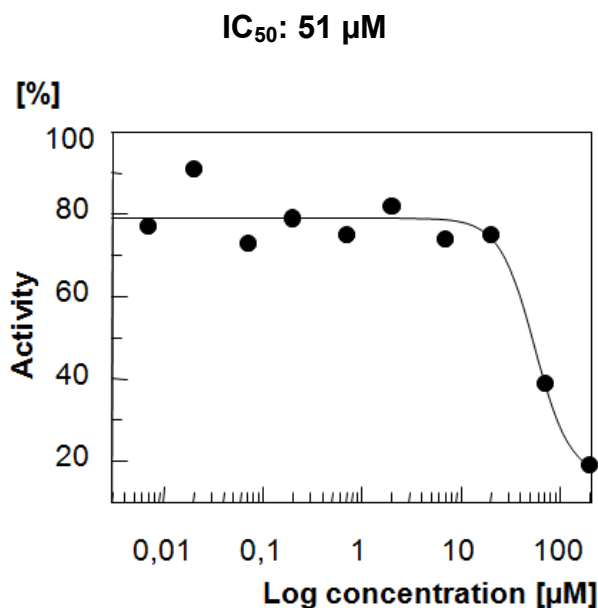


Fragment 20

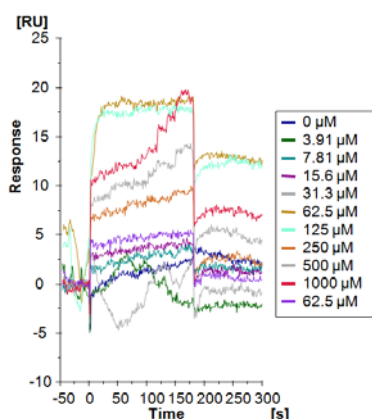
(A) SPR-screenings



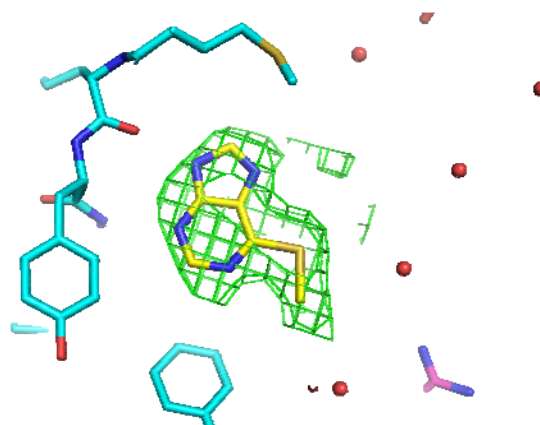
(B) HCA-hit characterization



(C) SPR-hit characterization



(D) Binding mode from X-ray-diffraction data



(E) Binding data

SPR-screenings: nonbinder (-)

HCA-screenings: binder (+)

SPR-hit characterization: binder, but its

SPR-sensorgrams are difficult to interpret (-)

HCA-hit characterization: binder (51 μ M) (+)

X-ray diffraction: complex-structure obtained (+)

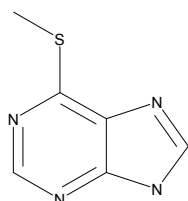
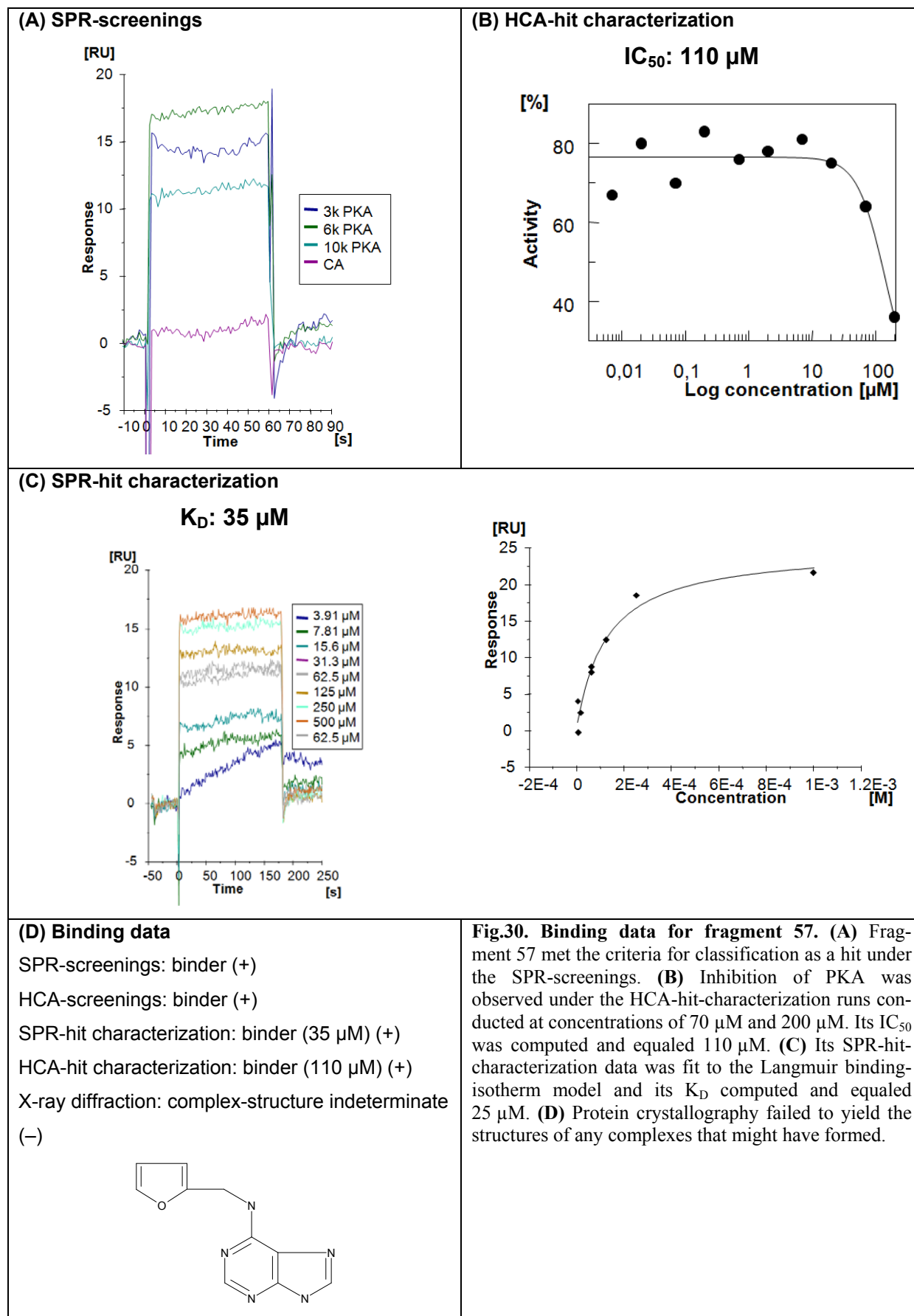


Fig.29. Binding data for fragment 20. (A) Fragment 20 failed to meet the criteria for classification as a hit under the SPR-screenings. Although its sensorgrams exhibited typical transient fragment binding, its responses on the PKA-surfaces involved remained below the background-noise level (5 RU). (B) Inhibition of PKA was observed under the HCA-hit-characterization runs conducted at concentrations of 70 μ M and 200 μ M. Its IC₅₀ was computed and equaled 51 μ M. (C) SPR-hit-characterization runs yielded responses exceeding the lower cutoff and allowed determining its binding mode. However, the sensorgrams involved are difficult to interpret and K_D was not computed for it. (D) Protein crystallography allowed determining its 3D-binding mode to PKA.

Fragment 57



3.2. RESULTS OBTAINED BY EMPLOYING AVAILABLE BIOCHEMICAL-ASSAY DATA IN THE PROTEIN-CRYSTALLOGRAPHIC ANALYSES

MerckSerono's in-house database was screened for compounds having molecular weights of less than 300 Da, computed solubilities exceeding 200 μM , and at least 50 % inhibitions of PKA-substrate phosphorylation under biochemical assays involving a fragment concentration of 10 μM . All of the compounds involved were available in solid form from MerckSerono's compound-storage facility. That screening yielded a library containing 67 fragments. A subset of those 67 fragments was chosen in order to confine further consideration to compounds representative of just those chemical scaffolds available among the 67 fragments. That selection procedure, which employed the researcher's "chemical eye," resulted in 25 fragments being chosen for structure determinations employing protein crystallographic analyses. Fig. 31 depicts the chemical structures of seven of those 25 fragments.

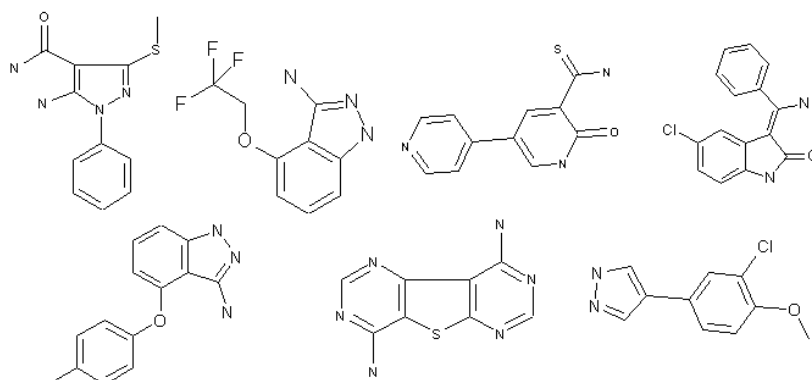


Fig.31. Sample fragments selected for protein crystallography. The chemical-structure diagrams of seven of the 25 fragments chosen for protein-crystallographic analyses illustrate the wide variety of chemical scaffolds found among the 25 fragments involved.

Protein-crystallographic analyses yielded the structures of 21 fragments whose electron densities indicated binding to PKA. The other four fragments failed to exhibit any evidence that they formed complexes with PKA. Table 9 (cf. Appendix 1) presents the results obtained for nine of those 21 fragments, along with illustrations of their binding modes to the protein's binding pocket and descriptions of the fragment-protein interactions involved. All 21 fragments interacted with PKA's ATP binding pocket, which is why the interactions involved have been described using the definitions of the ATP-pocket zones proposed by Liao (Liao,

2007). Those definitions are listed in Fig.7, which depicts the ATP binding pocket of protein kinases and categorizes it into zones designated A, K, R, P, E₀, E₁, BP-I, and BP-II.

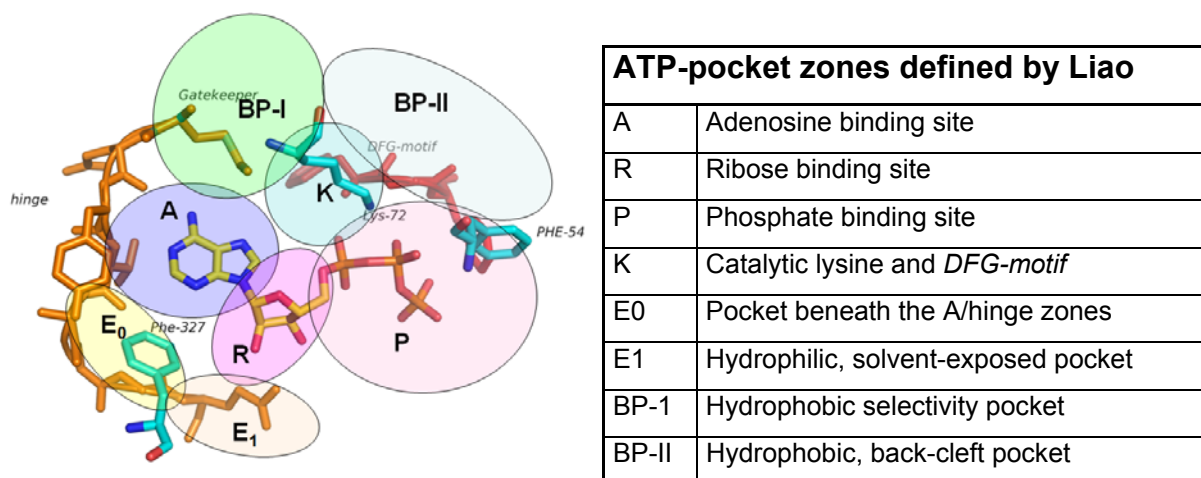


Fig.32. The ATP binding pocket in cAMP-dependent protein-kinase A. An illustration of the zones defined by Liao for describing their ATP-pocket. Their designations are listed in the table at right. When ATP binds, the adenosine moiety is situated in the A-zone. The ribose is situated in the R-zone. Phosphate groups bind in the P-zone. BP-I and BP-II are situated above the A-zone in this view. The K-zone is situated between the A-, R-, BP-I-, and BP-II-zones. The E₀- and E₁-pockets are situated beneath the A- and R-zones, which are described as being hydrophilic, solvent-exposed zones.

Table 7. An overview of fragment-protein interactions. Examples of chemical scaffolds detected in each zone defined by Liao. The scaffolds stated were observed in the structures of the nine fragment-protein complexes described in this dissertation (cf. Appendix 1). The leftmost column lists the symbols assigned to the various zones, and the top row lists the nine fragments involved.

	Fragment 1	Fragment 2	Fragment 3	Fragment 4	Fragment 5	Fragment 6	Fragment 7	Fragment 8	Fragment 9
A (hinge)	phenol	amine-pyrazole	pyrazole	amino-pyrazole	pyrazolo-pyrimidine	amide	pyridine	chloro-indole	amino-pyrimidine
R	-	-	methoxy	-	-	-	-	-	-
P	phenol	-	-	-	-	-	-	-	-
K	linker	-	-	-	-	-	-	-	sulfur
E ₀	-	toluene	chloride	trifluoro methyl	-	phenyl	-	-	-
E ₁	-	-	-	-	-	-	-	-	-
BP-I	-	-	-	-	hydroxy-aniline	mercapto-methyl	sulfur	phenyl	amino-pyrimidine
BP-II	-	-	-	-	-	-	-	-	-

The A-/hinge zone

When ATP binds, the adenine moiety is situated in the A-zone. Adenine forms two hydrogen bonds to the A-/hinge zone. Among the nine fragments, phenol, pyrazole, pyridine, pyrimidine, indole, and amide represent examples of scaffolds that are observed to form

hydrogen bonds to that zone. The majority of small-molecule, kinase inhibitors that have been developed to date target that zone of the ATP binding site (Liu and Gray, 2006). It has also been shown that the hinge-interacting *motif* may be transferred between differing chemical series (Caldwell, et al., 2008). The nine fragment-protein complexes involved incorporated eight, differing scaffolds that form hydrogen bonds to the A-/hinge zone (cf. Fig.33). An overview thereof is presented in Table 7.

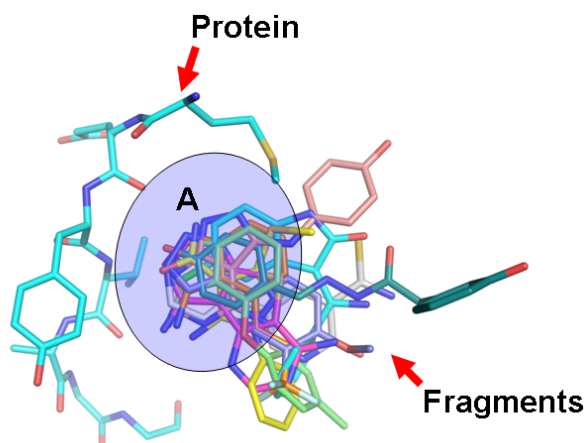


Fig.33. A depiction of the overlappings of fragments bound in the A-zone of PKA. The A-zone, or protein-kinase-hinge zone, binds the adenine moiety when ATP binds. All nine fragments exhibited A-zone interactions.

The BP-I- and K- zones

The BP-I-pocket (selectivity pocket) is relatively small in the case of PKA due to its being “guarded” by the bulky “gatekeeper” residue indicated by the red arrow in Fig.34, which is Met-120 in the case of PKA. In the case of fragments 6 and 7, a sulfur-sulfur interaction between those fragments and the gatekeeper residue occurs (cf. Appendix 1). The K-zone derives its designation from the lysine residue, Lys-72, occurring in PKA. That residue, which is indicated by the green arrow in Fig.34, is vital to the catalytic function occurring on the kinase, persists throughout much of the protein-kinase family. Fragment 1 interacts with the amine in Lys-72 via its carbonyl group.

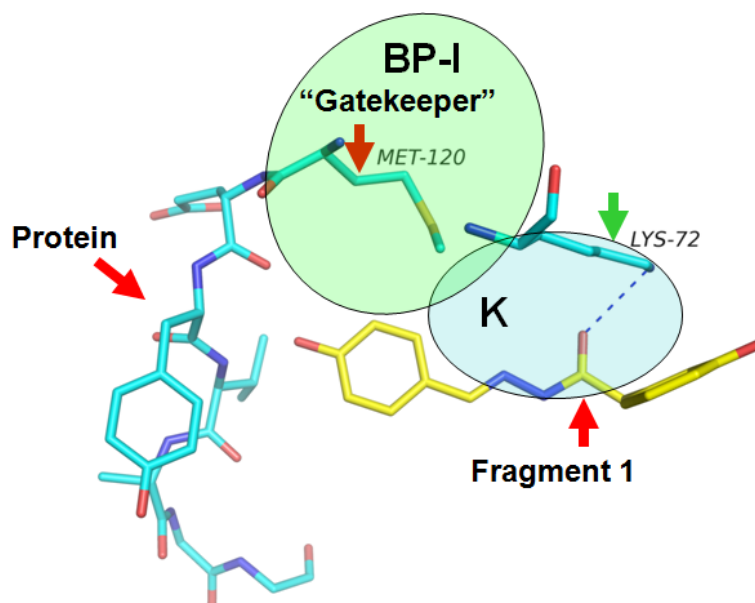


Fig.34. Binding to the BP-I-pocket and K-zone of PKA. The protein is depicted in green and the fragment in yellow. The K-zone contains the catalytic lysine, which is indicated by the green arrow, and is Lys-72 in the case of PKA. The BP-I-pocket in PKA is largely blocked by the bulky “gatekeeper” residue indicated by the red arrow, and is Met-120 in the case of PKA. Fragment 1 picked up an interaction with the amine in Lys-72 via its carbonyl group.

Thr-183 represents another amino acid situated in the K-zone, ahead of the *DFG-motif* (184 - 186 in the case of PKA). In the case of the nine fragments involved, Thr-183 exhibited three, distinct conformations. Fragments 2, 3, 5, 7, and 9 had conformations where Thr-183 was arranged in a vertical orientation, similar to the case of the complex formed with ATP (pdb-code 1ATP) (Zheng, et al., 1993) (cf. Fig.35 (B)), while in the case of fragments 1, 4, 6, and 8, the side chain has a horizontal orientation (cf. Fig.35 (C)).

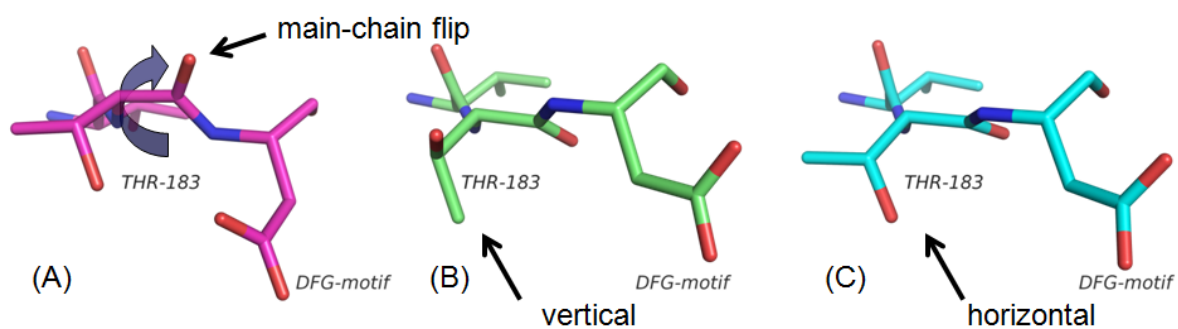


Fig.35. The three conformations of Thr-183 in PKA. (A) depicts the main-chain flip of Thr-183. (B) and (C) depict the two conformations of the Asp-184 side chain (*DFG-motif*).

An interesting conformation of Thr-183 was observed in conjunction with the binding of fragment 6. The bulky, methyl-mercapto moiety occurring in that fragment caused a main-

chain flip that led to a rearrangement of the Thr-183's carbonyl group such that it pointed outward, toward the ATP binding pocket ((A) in Fig.35). That particular main-chain flip is rarely observed. The sole published structure of a complex involving native-PKA and an inhibitor exhibiting that sort of conformational alteration is that involving staurosporine (pdb-code 1STC) (Prade, et al. 1997). The conformation of the carbonyl and trailing DFG-*motif* also led to the kinase acquiring an inactive conformation. The conformation of the DFG-*motif* involved cannot enter into the specific interaction with Mg^{2+} and ATP that is of importance to ATP's transition to ADP. The main-chain flip involved can also be observed in mutant-PKA structures, where Thr-183 is mutated to Ala-183 and observed to form complexes with balanol-series inhibitors (Bonn, et al., 2006).

The E₀- and R-zones

An investigation of the fragments involved turned up chemical scaffolds that interacted with the E₀- and R-zones of the ATP-pocket in PKA. Fig.36 illustrates the interactions occurring in those two zones in the cases of fragments 2, 3, 4, and 6.

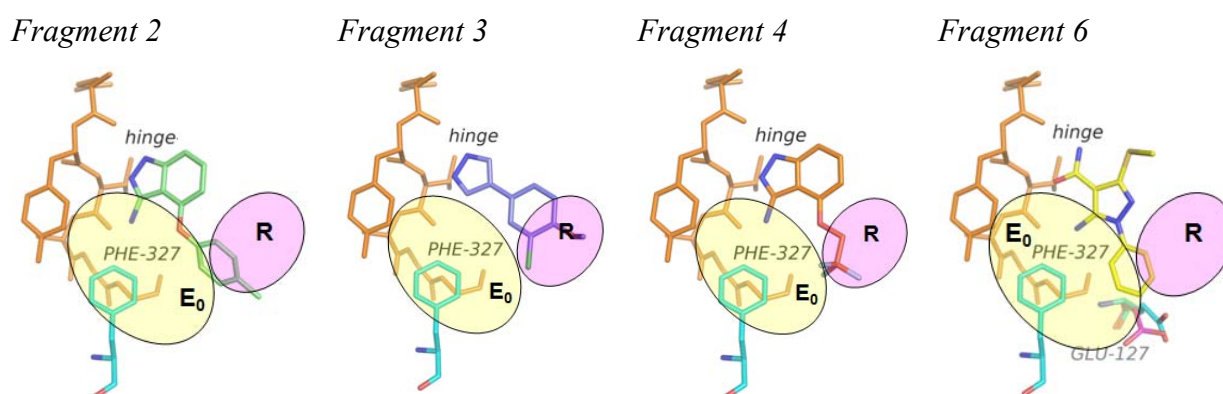


Fig.36. Interactions occurring in the E₀- and R-zones, exemplified by the cases of fragments 2, 3, 4 and 6. Fragments 2, 3, 4, and 6 exhibited signs that chemical-scaffold interactions had occurred in those zones. Scaffolds, such as the toluene in fragment 2, the chloride in fragment 3, the 3-fluoromethyl-group in fragment 4, and the phenyl in fragment 6, were observed to pick up interactions in those two zones. Moreover, the phenyl ring in fragment 6 nudges the side chain of Glu-127, causing it to point away from the R-zone and ATP binding cleft.

The E₀-zone contains the phenylalanine residue, Phe-327, which is shown in blue in Fig.36, specific to the AGC-kinase family. Many protein-kinase inhibitors interact with the E₀-zone. Among those fragments surveyed under the present study, only four had chemical scaffolds situated in that zone. It thus seems that the Phe-327 blocks that zone of the ATP binding site in PKA. The R-zone contains the glutamic-acid residue Glu-127, that shown in red in Fig.36 in the case of Fragment 6. The importance of that amino acid in PKA-substrate recognition

has been discussed by Gibbs and Craig (1991). The phenyl ring in fragment 6 is observed to cause the side chain of Glu-127 to point away from the R-zone and ATP binding cleft.

The P-zone

The glycine-rich loop in the P-zone spans the nucleotide's phosphate-binding sites. The loop is known to be very flexible, and takes on several conformations in the various protein-kinase structures. The overlappings of the nine fragment structures shown in Fig.37 illustrates the incidence of various conformations of that loop. Its flexibility is correlated to the high B-factors of those residues present in the loop, compared to the average B-factors for the protein. Fragment 1 had the most sharply defined glycine-rich loop, where its 4-phenol-group undergoes a π - π -interaction with the Phe-54-residue at its tip, resulting in a stiffening of the loop conformation and reductions of the B-factors of those residues present in the loop.

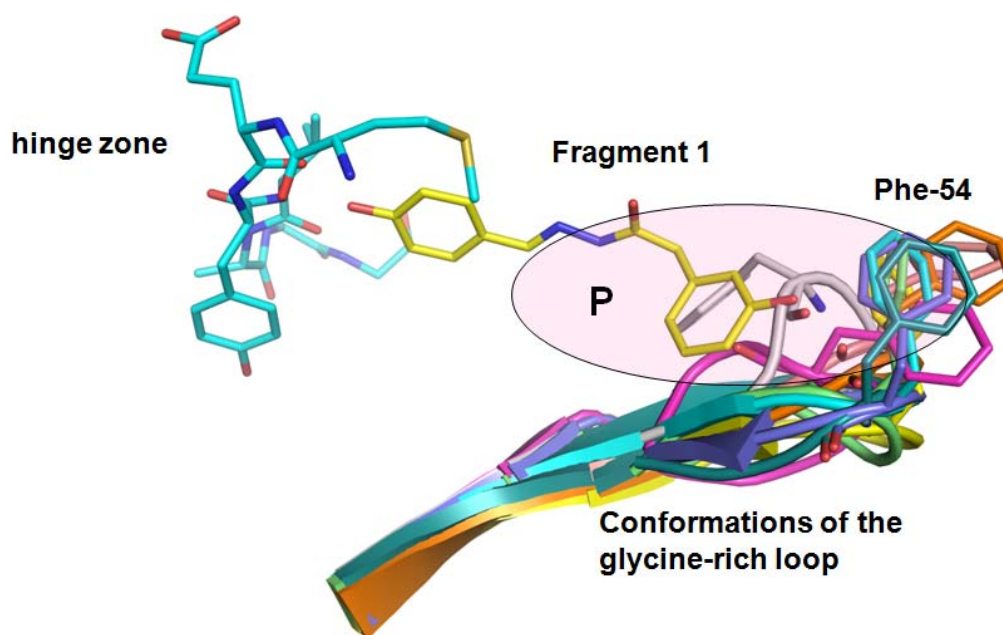


Fig.37. Glycine-rich loop conformations. The various conformations of the glycine-rich loop are shown. At the tip of the loop, the aromatic residue (Phe-54 in the case of PKA) takes on various conformations in the structures of the nine fragments. Binding of fragment 1 (shown in yellow) stabilizes the loop conformation via interactions occurring between its 4-phenol moiety and the Phe-54 residue.

The structures presented in the results section of this dissertation are illustrative of the variety of molecular scaffolds that interact with the ATP binding pocket. The structures obtained from X-ray-diffraction analyses reveal the manners in which all fragments involved bind to PKA's hinge zone, in addition to demonstrating that they pick up interactions in several other zones of the ATP binding pocket. Those structures disclose the relatively high flexibilities of certain zones, such as the glycine-rich loop or the residues surrounding the DFG-motif.

Chapter 4

DISCUSSION

The results obtained exemplify the two FBLD-approaches involved. Both employed PKA as the target protein in studies aimed at characterizing and analyzing protein-fragment interactions. The first approach investigated the fragment-PKA interactions occurring, which were studied utilizing three different techniques, (I) surface-plasmon-resonance (SPR) analyses, (II) high-compound-concentration biochemical assays (HCA), and (III) protein crystallography. Under the second approach, biochemical-assay data was utilized for selecting fragments for structure determinations by means of protein crystallography. The methods employed and the results obtained are summarized in Table 8.

Table 8. The methods employed in, and the results obtained from, the two FBLD-approaches involved. The table below summarizes the results obtained from both FBLD-approaches employed in conjunction with this dissertation. Under Approach 1, a combination of SPR, HCA, and protein crystallography was applied to a library of fragments that were screened, characterized, and had the 3-D-structures of the complexes that they formed analyzed. Approach 2 focused on biochemical assays and protein crystallography in order to determine the 3D-structures of the complexes that formed when fragments bonded to PKA.

	1. Screening (via SPR and HCA)	2. Characterization (via SPR and HCA)	3. 3D-structure determinations (via X-ray diffraction)	4. No. of 3D-structures obtained/(not obtained)
Approach 1	257	68	26	9 (17)
Approach 2	67 (from biochemical assays only)	-	25	21 (4)

SCREENINGS UTILIZING SPR AND HCA

Under the first approach, a library of 257 fragments was screened for binding to PKA utilizing SPR and HCA, and 68 of the fragments involved were classified as hits. SPR was utilized for investigating binding of fragments to PKA under direct-binding assays, where fragments were injected across a sensor surface coated with immobilized PKA, while HCA was utilized for determining the extents to which fragments inhibited PKA-substrate phosphorylation. The results of screenings based on those two methods were only weakly correlated. Only eighteen

of the 60 SPR-hits and 26 HCA-hits showed up as hits under both screenings. Since the experimental techniques involved differ in several ways, including the mechanisms employed for detecting fragment binding, direct comparisons of the results obtained from them are difficult.

Under SPR, the target protein is immobilized on the substrate matrix and binding of fragments to the target protein is measured in a stream of fragments, while under HCA, target-protein activities are quantified in terms of the concentrations of solvated, phosphorylated substrate that result. Since the direct-binding assays employed under the SPR-approach are incapable of measuring the changes in target-protein biological activity that occur upon fragment binding, screening for agonists would be impossible if only SPR were employed. The extents to which fragments that were classified as hits under SPR alone bind to PKA without exhibiting any inhibition under HCA were not studied in conjunction with this dissertation, but would be an interesting subject for further investigations.

Another difference between the two techniques is the fragment concentrations employed during screenings, which are 200 μM in the case of SPR and 100 μM in the case of HCA. High fragment concentrations had to be chosen in order to facilitate detection of low-affinity interactions. Furthermore, the fragment concentrations chosen represented a compromise between affinity range and assay stability in relation to nonspecific fragment interactions, such as binding of fragment precipitates, micelles, or aggregates to various components involved in the assays. At high fragment concentrations, fragment-composition equilibrium points are shifted toward multimeric states and formation of fragment aggregates, which could increase the numbers of both site-specific and nonspecific interactions involved. In fact, increased numbers of nonspecific interactions correlated to high fragment concentrations have already been reported in the case of SPR-investigations (Hämäläinen, et al., 2008). The interaction mechanisms acting between the fragments and target proteins involved are schematically depicted in Fig.38.

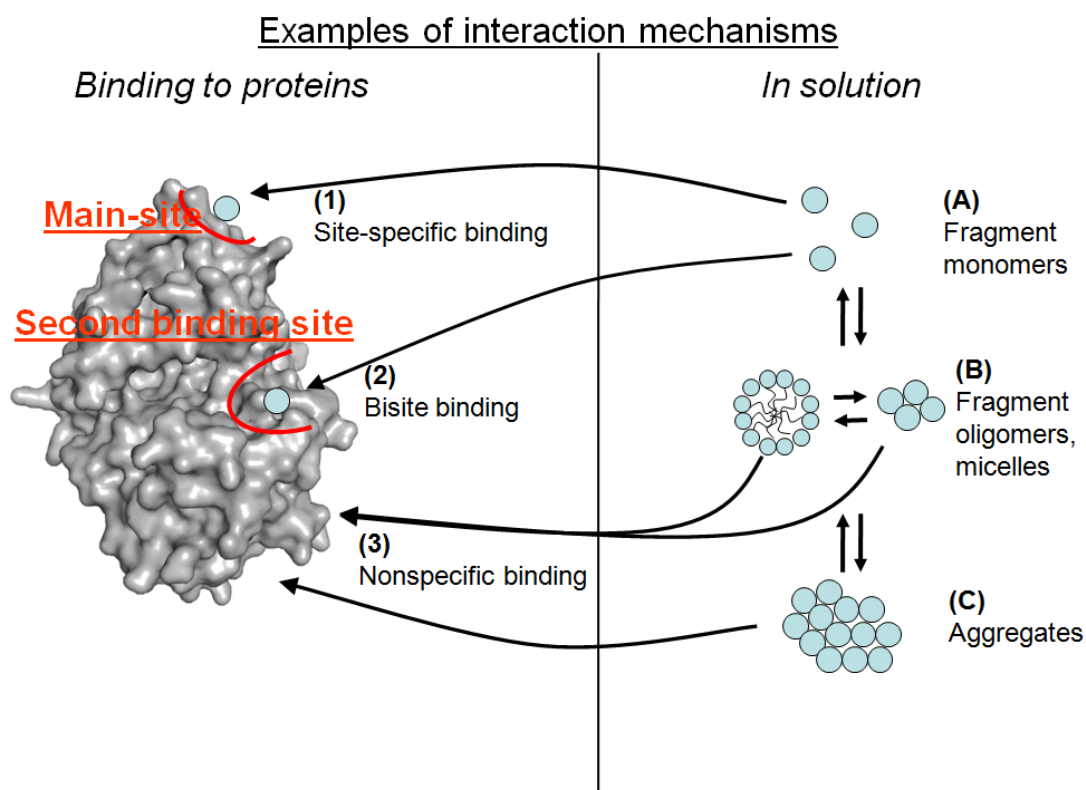


Fig.38. A schematized depiction of fragment-fragment and fragment-protein interactions. (A) Interactions between fragments and the target protein. Solvated fragments should ideally be present in the form of monomers, since they are capable of interacting with the target binding site, although they are also capable of either interacting with multiple binding sites or undergoing nonspecific interactions with the target. (B) Interactions of fragment multimers with the target protein. An equilibrium among solvated fragment monomers, oligomers, and formation of fragment micelles will set in (McGovern, et al., 2003). (C) At higher fragment concentrations, large fragment aggregates may be present. (1) Site-specific binding. Fragment monomers bind to a single binding site. (2) Bisite, or multiple-site, binding, under which fragment monomers bind to several protein binding sites. (3) Nonspecific binding. Fragment oligomers, micelles, or aggregates bind to the protein in a nonspecific manner (McGovern, et al., 2002; Gianetti, et al., 2008).

The monomeric forms of fragments are capable of interacting with the protein-binding site (cf. Fig.38 (1) and (A)). However, they are also capable of undergoing interactions with alternative binding sites (Fig.38 (2) and (A)). Since no competitive experiments were conducted in conjunction with the SPR-approach employed here, no further characterizations of fragments classified as belonging to Group II (cf. p. 71) were possible. Although fragments from that group exhibited typical transient binding, their binding responses exceeded those expected for 1:1, fragment-protein interactions. A certain proportion of weakly soluble fragments will aggregate in solution. Small-molecule aggregates tend to exhibit nonspecific binding to target proteins (cf. Fig.38 (C) and (3)). The two types of assays involved here, SPR and HCA, yielded differing responses to nonspecific binding phenomena, which might be one reason for the differences in the results obtained under them, in accordance with those results reported by Gianetti, et al. (2008), where it was shown that given fragments may exhibit

differing behaviors, depending upon the parameters, such as the presence and type of detergents, buffer composition, pH, presence/absence of cofactors, etc., employed in screening assays. For example, pH-variations might cause changes in the protonation states of the compounds or amino acids present in protein-binding pockets, while detergents might affect compound solubilities. Under HCA, fragment aggregates might interfere with assay readouts due to, e.g., fluorescence quenching or fluorescence, exhibit “nonspecific” binding to the enzymes involved during stages aimed at boosting signal levels, or even cause disruption of the proteins employed in assays (McGovern, et al., 2003). Readouts from screenings that employed the SPR-setup are less sensitive to interference emanating from assays, since they are a measure of direct binding of fragments to the target protein, which means that employing the SPR-setup should allow avoiding the enzymatic, signal-enhancement stages occurring under HCA and reduce the number of prospective sources of interference.

Overall, the outcomes of the screenings conducted yielded a relatively large number of fragments that were classified as hits. The high fragment concentrations employed in the screenings surely increased hit rates, since even very low binding affinities are detectable at high fragment concentrations (Hämäläinen, et al., 2008). Furthermore, employment of a protein-kinase-targeted library probably further increased hit rates. Several chemical scaffolds were identified among the hits resulting from the SPR/HCA-screenings conducted.

HIT CHARACTERIZATION

Hit characterization was undertaken in order to allow more-stringent examinations of the natures of the interactions of the fragments involved with PKA and determinations of their affinity constants, K_D , under SPR, and IC_{50} , under HCA.

Seven binding constants fell within the same range under both assays. One exception is fragment 178, for which a K_D of 750 μM and an IC_{50} of 38 μM was determined. Eight fragments involved in SPR-hit characterization exhibited responses having characteristics that were indicative of concentration-dependent effects occurring within the concentration range involved, particularly at the higher concentrations. Such fragments have been classified as Group IV (cf. p. 71). Fig. 24 (cf. p. 77) depicts the concentration-dependent behavior of fragment 19 during SPR-titration. Similar compounds have been investigated via SPR by Gianetti, et al. (2008) and their results suggest that the fragments involved are poor candidates

for protein-crystallographic studies (Gianetti, et al., 2008), in view of the concentration-dependent aggregates that might occur. However, as stated in the caption to Fig.38, equilibrium between fragments present in the form of oligomers, micelles, or aggregates, and fragments present in the form of solvated monomers will set in. Fragment 20 represents an example of a fragment forming a complex whose crystalline structure could be determined, even though it was classified as being subject to concentration-dependent effects. Furthermore, the number of affinity constants determined under subsequent titrations was reduced from 60 screening hits under SPR and 26 screening hits under HCA to 24 screening hits under SPR and 12 screening hits under HCA, where eight of the latter were classified as hits under both SPR-screenings and HCA-screenings. Under the fragment-library set up, many fragments reached their solubility limits at the higher concentrations. Careful design of the fragment library involved and devoting special attention to fragment solubilities is therefore critical. The fragments involved should ideally have empirically determined solubilities covering ranges extending beyond the highest fragment concentrations employed in titrations.

Subsequent structure determinations employing protein crystallography revealed their binding modes to PKA's hinge zone. The K_D or IC_{50} of every fragment, for which the structure of the complex it formed with PKA could be determined, was computed. On the other hand, no fragment-PKA-complex structures could be determined for those fragments, for which neither SPR- nor HCA-titrations yielded usable results. It should be obvious that conducting measurements at a single concentration, utilizing either SPR or HCA, yields weak selection criteria for use in subsequent crystallographic studies under FBLD. Further titrations will be essential, since they significantly increase the probabilities of obtaining the structures of fragment-target-protein complexes via protein crystallography*.

The outcomes of the experiments conducted in conjunction with this dissertation demonstrated that the SPR-approach is sensitive enough to allow detecting fragment-screening responses, which is in agreement with conclusions reached under earlier SPR-based fragment studies (Nordström, et al., 2008; Hämäläinen, et al., 2008).

* The success rate for determinations of the structures of fragment-PKA complexes increased from 13 % following primary screenings to 30 % following subsequent titrations.

***PROTEIN-FRAGMENT COMPLEX FORMATION AND STRUCTURE
DETERMINATIONS EMPLOYING PROTEIN CRYSTALLOGRAPHY***

Protein crystallography is the method of choice for obtaining detailed data on 3D-fragment-protein interactions. The crystalline structures of fragment-target-protein complexes reveal fragments' chemical environments.

Under the first approach, which involved protein-crystallography analyses, nine of 26 fragments yielded the structures of the complexes involved, while under the second approach, 21 of 25 fragments yielded the structures of the complexes involved. A comparison of the crystallographic results obtained under the two approaches suggests that differences in the designs of the experiments involved are the primary reason for variations in their success rates (cf. Table 8). The much higher success rate under the second approach may be partly explained by the differing concentration ranges employed in the screening and titration runs conducted under the first approach and the conditions under which HTS/biochemical assays were conducted in the case of the second approach. Under the first approach, all fragments had estimated affinities falling in the mid- μM to low-mM range, while, under the second approach, all had estimated affinities falling in the low- μM range or higher, which eliminated many concentration-related issues under the second approach and reduced the number of "false positives."

High occupancies of binding sites are necessary if electron densities are to be reliably detected, which means that certain ligand concentrations in the protein solutions involved must be reached. A rule of thumb is that protein concentrations exceeding K_D by at least a factor of 5 to 10 will be necessary if reasonably well-defined ligand electron densities at binding sites are to be obtained. The ratios of fragments' affinities to their maximum-utilizable concentrations are thus the factors influencing empirical results. The affinity/solubility ratios of weakly soluble fragments affect both the probability that the structures of fragment-protein complexes will be determinable and the probability that fragment binding constants will be derivable from assays. In the case of the investigations conducted here, computed solubilities, $\text{clogS}(7.4)$, were employed as selection parameters in order to increase the likelihood that the structures of fragment-protein complexes would be determined. Nevertheless, computed solubilities are frequently inaccurate and can lead to over/underestimations of solubilities relative to empirically determined solubilities. Empirical assays, such as those

employing optical-dispersion techniques, filtering-assay techniques, or NMR-detection of compound aggregates, may be employed in order to arrive at better estimates of ligands' solubilities in given solutions. Appendix 1 lists examples of empirically determined and computed solubilities (clogs(7.4)), where the data involved was extracted from MerckSerono's in-house database. However, under the second approach, all hit-fragments had IC50-values falling in the low- μ M range and solubility overestimations due to the computational methods employed were much less critical than under the first approach.

In the case of the experimentation conducted in conjunction with this dissertation, higher DMSO-concentrations and detergents were employed in order to increase to affinity/solubility ratios, which, however, increased the stresses exerted on protein crystals and adversely affected the qualities of the diffraction patterns of many of the protein crystals involved. The protein crystals involved were therefore stabilized by crosslinking employing glutaraldehyde, which allowed employing higher fragment concentrations, higher DMSO-concentrations, and longer soaking periods, and facilitated detection of another three fragment-protein complexes. However, crosslinking protein crystals might impose limitations on protein flexibility, thereby preventing the changes in protein conformation essential to formation of some types of fragment-protein complexes. Nevertheless, in the case of several structures, large conformational changes in flexible loops and shifts from alpha helices to other structure conformations were observed, even following crosslinking. In our experience, controlled crosslinking can stabilize protein crystals, while simultaneously permitting conformational changes in the protein contained therein, i.e., can facilitate the formation of fragment-protein complexes.

One major difference in the experimental setups employed in the crystallographic analyses and the SPR/HCA-screenings involving PKA was the presence of 19 amino-acid polypeptide PKI, which was employed as a cocrystallizing agent. Both attempts to conduct SPR/HCA-screenings involving PKA in the presence of PKI, as well as crystallization conditions yielding strongly diffracting crystals, without need for employing PKI, failed. Estimates of the effect of PKI on fragment binding to PKA were thus unobtainable. PKI might have caused reductions of the binding affinities of some fragments, thereby hindering determinations of their crystalline structures.

EMPLOYMENT OF FRAGMENT COMPLEXES

The aim of FBLD is designing lead molecules, based on initial hit-fragments. Data on fragment 3D-binding modes may be employed in various ways in conjunction with that effort. It might be argued that, in the case of the second approach, under which available biochemical-assay data were utilized in selecting hit-fragments, discoveries of new chemical scaffolds will be few and far between. However, fragments are smaller than typical HTS-hits or lead molecules, and therefore subject to fewer structure constraints on their interactions with target proteins. “Old” chemical scaffolds thus can interact with protein binding sites in novel and unexpected ways, thereby promoting arrival at new approaches to designing lead molecules. The investigations conducted in conjunction with this study revealed new interactions occurring in the ATP binding pocket in PKA and identified several novel chemical scaffolds.

Fragment growing, fragment linking, and fragment merging represent techniques commonly employed in FBLD for optimizing fragments in order to obtain more-lead-like molecules having greater affinities. Any fragment-PKA complex identified under this study may be employed as the starting point for those fragment-optimization techniques. Overlappings of fragment structures and known PKA-inhibitors obtained from PDB (cf. Fig.39) suggests that chemical scaffolds might be interchanged between molecules, namely, between two fragments, between two, large inhibitors, and between the fragments involved and the larger inhibitors, and combined in all conceivable manners. Knowledge of fragments’ 3D-binding modes generates new ideas, ideas that may be applied to the design of new, candidate, drug compounds.

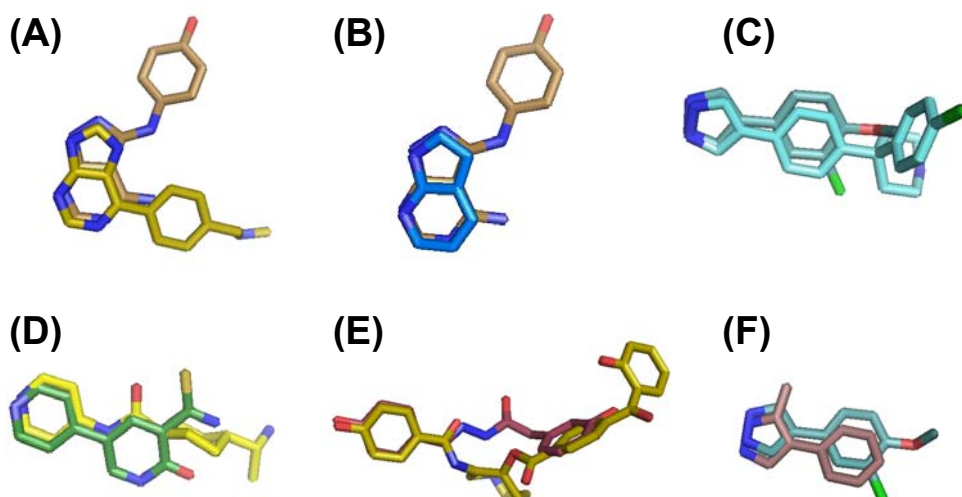


Fig.39. Fragment binding modes overlapped by known PKA-inhibitor molecules. (A) Fragment 5 (shown in brown) and 2UVY-inhibitor, (B) Fragment 5 (shown in brown) and 2UVX-inhibitor, (C) Fragment 3 (shown in dark blue) and 1BX6-inhibitor, (D) Fragment 7 (shown in yellow) and 2GNF-inhibitor, (E) Fragment 1 (shown in brown) and 1RE8-inhibitor, (F) Fragment 3 (shown in dark blue) and 2UW3-inhibitor. These overlappings of fragment structures by the structures of known PKA-inhibitors obtained from PDB suggest that chemical scaffolds might be interchangeable between molecules, between two fragments, between two large inhibitors, and between the fragments involved and the larger inhibitors, and combined in all conceivable manners.

OTHER METHODS EMPLOYED IN FBLD

Protein crystallography is the method most frequently employed for determining the structures of fragment-target-protein complexes. Nevertheless, it is a relatively low-throughput method and unsuitable for screening large numbers of ligands, even if strongly diffracting crystals of the target protein are available. An alternative approach is employing *in-silico*-docking methods for categorizing fragment binding modes (Oblak, et al., 2005; Pickett, et al., 2003). The computational methods involved allow considering multiple sets of compound parameters and assay interaction data in assessments of fragment characteristics. However, since fragments contain fewer functional groups that computational software can employ in categorizing fragments' interactions with target proteins, theoretically predicting fragment binding modes and fragment-protein interactions is difficult. A combination of empirical and computational methods might therefore be the better choice of tool for fragment elaboration in conjunction with FBLD.

4.1 CONCLUSIONS

This work presents the results obtained from two fragment-screening approaches involving cAMP-dependent protein-kinase A (PKA). Under the first approach, fragment-protein interactions were studied employing surface plasmon resonance (SPR), high-concentration biochemical assays (HCA), and protein crystallography, while the second approach employed available biochemical-assay data in the form of HTS-screening data or other activity-assay data for selecting fragment-like molecules to be subjected to crystallographic analyses. The results obtained were in the form of empirically determined binding constants and the 3-dimensional structures of fragment-PKA complexes. The chemical environment of the ATP binding site in PKA was mapped, employing fragment interactions suitable for use as new starting points for lead generation.

Under the first approach, i.e., that employing protein crystallographic analyses, nine of the 26 fragments that had been selected yielded fragment-protein complexes, which demonstrated that ample numbers of fragment-PKA interactions were occurring and that binding characteristics that could be useful in upgrading fragments into lead-like molecules were involved. Although those nine PKA-fragment structures were inadequate to serve as a solid base for statistical analyses, in general, the results obtained indicate that the two screening methods involved, SPR and HCA, yield outcomes that are in a good agreement with one another. The residual differences involved may be largely attributed to two factors, the presumed formation of fragment aggregates and their nonspecific binding to PKA and/or the narrow width ($< 200 \mu\text{M}$) of the screening window employed in the case of HCA.

Direct comparisons of the results obtained from the two screening methods are difficult, particularly if the differences in the experimental setups involved are taken into account. SPR may be set up in the form of a label-free assay well suited to the primary screening of fragment libraries and capable of detecting hit-fragments having millimolar affinities. The advantage of employing SPR as a screening method is that it consumes relatively small quantities of proteins and provides responsivities and throughput rates sufficient to allow screening libraries consisting of hundreds to thousands of fragments for binding to target proteins within days. Furthermore, analyses of SPR titration data allow rapidly identifying nonstoichiometric binders and prospective aggregates. On the other hand, although the concentration ranges involved in most HCA-screenings remained below millimolar levels,

HCA might well be employed a high-throughput mode, and therefore might be a means for readily screening tens of thousands to hundreds of thousands of fragments per day.

Under the second approach, 21 of the 25 fragments involved yielded the structures of their protein complexes. That high success rate may be attributed to the conservative selection criteria (> 50 % inhibition at 10 μ M fragment concentration) employed in identifying hit-fragments. If similar selection criteria had been applied to the results of typical HTS-runs, much higher hit ratios would be expected, which would have led to many novel chemical scaffolds being identified as new, prospective, starting points for lead-discovery investigations.

The two approaches involved thus provided interaction data and crystalline structures that can serve as bases for developing PKA-inhibitors. The methods employed here are generally applicable to the study of other enzymes and therefore useful in FBLD.

BIBLIOGRAPHY

Akamine, P., Madhusudan, W. J., Xuong, N. H., Ten Eyck, L. F. and Taylor, S. S. (2003): Dynamic Features of cAMP-dependent Protein Kinase Revealed by Apoenzyme Crystal Structure, *J Mol Biol*, **327**, 159–171.

Albert, J. S., Blomberg, N., Breeze, A. L., Brown, A., Burrows, J. N., Edwards, P. D., Folmer, R. H., Geschwindner, S., Griffen, E. J., Kenny, P. W., Nowak, T., Olsson, L., Sanganee, H. and Shapiro, A. B., (2007): An Integrated Approach to Fragment-Based Lead Generation: Philosophy, Strategy and Case Studies from AstraZeneca's Drug Discovery Programmes, *Curr Top in Med Chem*, **7**, 1600-1629.

Barker, J., Courtney, S., Hestekamp, T., Ullmann, D. and Whittaker, M. (2006): Fragment screening by biochemical assay, *Expert Opin Drug Disc*, **1**, 225-236.

Bemis, G. W. and Murcko, M. A. (1996): The properties of known drugs. 1. Molecular frameworks, *J Med Chem*, **39**, 2887–2893.

Bemis, G. W. and Murcko, M. A. (1999): The properties of known drugs. 2. Side chains. *J Med Chem*, **42**, 5095–5099.

Bernstein, F. C., Koetzle, T. F., Williams, G. J. B., Meyer, E. F. Jr., Brice, M. D., Rogers, J. R., Kennard, O., Shimanouchi, T. and Tasumi, M. (1977): The Protein Data Bank: a computer-based archival file for macromolecular structures, *J Mol Biol*, **112**, 535-542.

Blume-Jensen, P. and Hunter, T., (2001): Oncogenic kinase signaling, *Nature*, **411**, 355-365.

Blundell, T. (2001): High-throughput crystallography for Lead Discovery in Drug Design. *Nat Rev Drug Discov*, **1**, 45-54.

Bohacek R. S., Martin, C and Guida, W. C., (1996): The art and practice of structure-based drug design: A molecular modelling approach, *Med Res Rev*, **16**, 3–50.

Bohm, H-J., Flohr, A. and Stahl, M. (2004): Scaffold hopping, *Drug Discov Today Tech*, **1**, 217-224.

Bohm, H. J., Banner, D. W. and Weber, L. (1999): Combinatorial docking and combinatorial chemistry: design of potent non-peptide thrombin inhibitors, *J Comput Aided Mol Des*, **13**, 51–56.

Boehm, H-J., Boehringer, M., Bur, D., Gmuender, H., Huber, W., Klaus, W., Kostrewa, D., Kuehne, H., Luebbers, T., Meunier-Keller, N. and Mueller, F. (2000): Novel Inhibitors of DNA Gyrase: 3D Structure Based Biased Needle Screening, Hit Validation by Biophysical Methods, and 3D Guided Optimization. A Promising Alternative to Random Screening. *J Med Chem*, **43**, 2664-2674

Bonn, S., Herrero, S., Breitenlechner, C. B., Erlbruch, A., Lehmann, W., Engh, R. A., Gassel, M. and Bossemeyer. (2006): Structural analysis of protein kinase A mutants with Rho-kinase inhibitor specificity, *J Biol Chem*, **281**, 24818-24130.

Bosch, J., Robien, M.A., Mehlin, C., Boni, E., Riechers, A., Buckner, F. S., Van Voorhis, W. C., Myler, P. J., Worthey, E. A., DeTitta, G., Luft, J. R., Lauricella, A., Gulde, S., Anderson, L.A., Kalyuzhniy, O., Neely, H. M., Ross, J., Earnest, T. N., Soltis, M., Schoenfeld, L., Zucker, F., Merritt, E. A., Fan, E., Verlinde, C. L. and Hol, W (2006): Using Fragment Cocktail Crystallography To Assist Inhibitor Design of Trypanosoma brucei Nucleoside 2-Deoxyribosyltransferase, *J Med Chem*, **49**, 5939-5946.

Bragg W. L. and Bragg W. H. (1913) The diffraction of X-rays by crystals. *Proc Roy Soc Sect A*, **88**, 428-438.

Breitenlechner, C., Bossemeyer, D. and Engh, R. A. (2005): Crystallography for protein kinase drug design: PKA and SRC case studies, *Biochim Biophys Acta*, **1754**, 38 – 49.

Brewerton, S.C. (2008): The use of protein-ligand interaction fingerprints in docking, *Curr Opin Drug Discov Dev*, **11**, 356-364.

Brünger, A. T. (1992): Free R-value: a novel statistical quantity for assessing the accuracy of crystal structures, *Nature*, **355**, 472-475.

Brünger, A. T. (1997): Free R-value: Cross-validation in crystallography, *Methods Enzymol*, **277**, 366-396.

Brünger, A. T., Adams, P. D., Clore, G. M., Delano, W. L., Gros, P., Grossekunstleve, R. W., Jiang, J. S., Kuszewski, J., Nilges, M., Pannu, N. S., Read, R. J., Rice, L. M., Simonson, T. and Warren, G. L. (1998): Crystallography and NMR System - a New Software Suite for Macromolecular Structure Determination, *Acta Crystallogr D*, **54**, 905-921.

Bruno, I. J., Cole, J. C., Lommerse, J. P. M., Rowland, R. S., Taylor, R. and Verdonk M. L. (1997): Isostar: A library of information about non-bonded interactions, *J Comput Aided Mol Des*, **11**, 525-537.

Broennimann, C., Eikenberry, E. F., Henrich, B., Horisberger, R., Huelsen, G., Pohl, E., Schmitt, B., Schulze-Briese, C., Suzuki, M., Tomizaki, T., Toyokawa, H. and Wagner, A. (2006): The Pilatus 1M-Detector, *J Synchrotron Rad*, **13**, 120-130.

Cannon, M. J., Papalia, G. A., Navratilova, I., Fisher, R.J., Roberts, L. R., Worthy, K. M., Stephen, A.G., Marchesini, G. R., Collins, E. J., Casper, D., Qiu, H., Satpaev, D., Liparoto, S.F., Rice, D.A., Gorshkova, I. I., Darling, R.J., Bennett, D. B., Sekar, M., Hommema, E., Liang, A.M., Day, E. S., Inman, J., Karlicek, S. M., Ullrich, S. J., Hodges, D., Chu, T., Sullivan, E., Simpson, J., Rafique, A., Luginbühl, B., Westin, S. N., Bynum, M., Cachia, P., Li, Y. J., Kao, D., Neurauter, A., Wong, M., Swanson, M. and Myszka, D. G. (2004): Comparative analyses of a small molecule/enzyme interaction by multiple users of Biacore technology, *Anal Biochem*, **330**, 98-113.

Cannon, M. J. and Myszka, D. G. (2003): Analysing the binding of low molecular mass compounds using Biacore S51, *Recent Res Devel Biophys Biochem*, **3**, 333-344.

Caldwell, J. J., Davies, T. G., Donald, A. McHardy, T., Rowlands, M. G., Aherne, W., Hunter, L. K., Taylor, K., Ruddle, R., Raynaud, F. I., Verdonk, M., Workman, P., Garrett, M. D. and Collins, I. (2008): Identification of 4-(4-Aminopiperidin-1-yl)-7H-pyrrolo[2,3-d]pyrimidines as Selective Inhibitors of Protein Kinase B through Fragment Elaboration, *J Med Chem*, **51**, 2147–2157.

Carr, R., Congreve, M., Murray, C. and Rees, D. (2005): Fragment-based lead discovery: leads by design, *Drug Discov Today*, **10**, 987-992.

Cherry, M. and Williams, D. H. (2004): Recent Kinase and Kinase Inhibitor X-ray Structures: Mechanism of Inhibition and Selectivity Insights, *Curr Med Chem*, **11**, 663-673.

Kim, C., Vigil, D. Anand, G. and Taylor, S.S. (2006): Structure and dynamics of PKA-signaling proteins, *Eur J Cell Biol*, **85**, 651–654.

Ciulli, A. and Abell, C. (2007): Fragment-based approaches to enzyme inhibition, *Curr Opin Biotechnol*, **18**, 1-8.

Cohen-Hadar, N., Wine, Y., Nachliel, E., Huppert, D., Gutman, M., Frolow, F. and Freeman, A. (2006): Monitoring The Stability of Crosslinked Protein Crystals Biotemplates: A Feasibility Study, *Biotechnol Bioeng*, **94**, 1005-1011.

Cohen, M.S., Zhang, C., Shokat, K. M. and Taunton, J. (2005): Structural Bioinformatics-Based Design of Selective, Irreversible Kinase Inhibitors, *Science*, **308**, 1318-1321.

Cohen, P. (2002): Protein kinases – the major drug targets of the twenty-first century?, *Nat Rev Drug Discov*, **1**, 309-315.

Congreve, M., Carr, R., Murray, C. and Jhoti, H. (2003): A ‘rule of three’ for fragment-based lead discovery?, *Drug Discov Today*, **8**, 876-877.

Congreve, M. S., Davis, D. J., Devine, L., Granata, C., O’Reilly, M., Wyatt, P. G. and Jhoti, H. (2003): Detection of ligands from a dynamic combinatorial library by X-ray crystallography, *Angew Chem, Int Ed*, **42**, 4479-4482.

David, C. R., Miles, C., Christopher, W. M., & Robin, C. (2004): Fragment-based Lead Discovery, *Nat Rev Drug Discov*, **3**, 660-672.

Davies, S. P., Reddy, H., Caivano, M. and Cohen, P. (2000): Specificity and mechanism of action of some commonly used protein kinase inhibitors, *Biochem J*, **351**, 95–105.

Davis, T. M., and Wilson, W. D. (2000): Determination of the refractive index increments of small molecules for correction of surface plasmon resonance data, *Anal. Biochem.* **284**, 348–353.

Dean, P.M., Lloyd, D. G. and Todorov, N. P. (2004): De novo drug design: Integration of structure-based and ligand-based methods, *Curr Opin Drug Discov Devel*, **7**, 347-353.

Deinum, J., Gustavsson, L., Gyzander, E., Kullman-Magnusson, M., Edstrom, A. and Karlsson, R. (2002): A thermodynamic characterization of the binding of thrombin inhibitors

to human thrombin, combining biosensor technology, stopped-flow spectrophotometry and microcalorimetry, *Anal Biochem*, **300**, 152-162.

DeLano, W. L. and Brünger, A. T. (1995): The direct rotation function: Rotational Patterson correlation search applied to molecular replacement, *Acta Crystallogr D*, **51**, 740-748.

DeLano, W. L. (2002): The PYMOL Molecular Graphics System, *DeLano Scientific, San Carlos, CA, USA*.

Di, L. and Kerns, E. H. (2006): Biological assay challenges from compound solubility: Strategies for bioassay optimization, *Drug Discov Today*, **11**, 446-451.

Alastair, D., McHardy T., Rowlands, M. G., Hunter, L. J. .K., Davies, T. G., Berdini, V., Boyle, R. G., Aherne, G. W., Garrett, M. D. and Collins, I. (2007): Rapid Evolution of 6-Phenylpurine Inhibitors of Protein Kinase B through Structure-Based Design, *J Med Chem*, **50**, 2289-2292.

Edwards, P. D., Albert, J. S., Sylvester, M., Aharony, D., Andisik, D., Callaghan, O., Campbell, J. B., Carr, R. A., Chessari, G., Congreve, M., Frederickson, M., Folmer, R. H., Geschwindner, S., Koether, G., Kolmodin, K., Krumrine, J., Mauger, R. C., Murray, C. W., Olsson, L. L., Patel, S., Spear, N. and Tian, G. (2007): Application of Fragment-Based Lead Generation to the Discovery of Novel, Cyclic Amidine α -Secretase Inhibitors with Nanomolar Potency, Cellular Activity, and High Ligand Efficiency, *J Med Chem*, **50**, 5912-5925.

Engh, R. A., Girod, A., Kinzel, V., Huber, R. and Bossemeyer, D. (1996): Crystal Structures of Catalytic Subunit of cAMP-dependent Protein Kinase in Complex with Isoquinolinesulfonyl Protein Kinase Inhibitors H7, H8, and H89, *J Biol Chem*, **271**, 26157-26164.

Emsley, P. and Cowtan, K. (2004): Coot: model-building tools for molecular graphics, *Acta Crystallogr D*, **60**, 2126-2132.

Erlanson, D.A. (2006): Fragment-based lead discovery: a chemical update, *Curr Opin Biotechnol*, **17**, 643-652.

Erlanson, D.A., McDowell, R. S. and O'Brien, T. (2004): Fragment-Based Drug Discovery, *J Med Chem*, **47**, 3463-3482.

Ewald, P. P. (1921): Das „reziproke“ Gitter in der Strukturtheorie, *Z Kristallogr*, **56**, 129-156.

Fejzo, J., Lepre, C. and Xie, X. (2003): Application of NMR screening in drug discovery, *Curr Top Med Chem*, **3**, 81-97.

Frederickson, M., Callaghan, O., Chessari, G., Congreve, M., Cowan, S.R., Matthews, J. E., McMenamin, R., Smith, D. M., Vinković, M. and Wallis, N. G. (2008): Fragment-Based Discovery of Mexiletine Derivates as Orally Bioavailable Inhibitors of Urokinase-Type Plasminogen Activator, *J Med Chem*, **51**, 183-186.

Fägerstam, L. G., Frostell-Karlsson, A., Karlsson, R., Persson, B. and Rönnberg, I. (1992): Biospecific interaction analysis using surface plasmon resonance detection applied to kinetic, binding site and concentration analysis, *J Chromatogr*, **597**, 397-410.

Geschwindner, S., Olsson, L. L., Albert, J. S., Deinum, J., Edwards, P. D., de Beer, T. and Folmer, R. H. (2007): Discovery of Novel Warhead against β -Secretase through Fragment-Based Lead Generation, *J Med Chem*, **50**, 5903-5911.

Gianetti, A. M., Koch, B. D. and Browner, M. F. (2008): Surface Plasmon Resonance Based Assay for the Detection and Characterization of Promiscuous Inhibitors, *J Med Chem*, **51**, 574-580.

Gibbs, C. and Craig, S. (1991): Identification of Electrostatic Interaction That Determine the Phosphorylation Site Specificity of the cAMP-Dependent Protein Kinase, *Biochem*, **30**, 5329-5334.

Gilbert, M. and Albala, J. S. (2002): Accelerating code to function: sizing up the protein production line, *Curr Opin Chem Biol*, **6**, 102-105.

Gill, A., Cleasby, A. and Jhoti, H. (2005): The Discovery of Novel Protein Kinase Inhibitors by Using Fragment-Based High- Throughput X-ray Crystallography, *Chem Bio Chem*, **6**, 506-512.

Gill, A. L., Frederickson, M., Cleasby, A., Woodhead, S. J., Carr, M. G., Woodhead, A. J., Walker, M. T., Congreve, M.S., Devine, L.A., Tisi, D., O'Reilly, M., Seavers, L.C., Davis, D. J., Curry, J., Anthony, R., Padova, A., Murray, C. W., Carr, R. A. and Jhoti, H. (2005): Identification of Novel p38r MAP Kinase Inhibitors Using Fragment-Based Lead Generation, *J Med Chem*, **48**, 414-426.

Gillet, V. J. (2008), New directions in library design and analysis, *Curr Opin Chem Biol*, **12**, 372-378

Gribbon, P., and Sewing, A., (2003): Fluorescence readouts in HTS: no gain without pain?, *Drug Discov Today*, **8**, 1035-1043.

Hajduk, P. J. (2006): Fragment-Based Drug Design: How Big Is Too Big?, *J Med Chem*, **49**, 6972-6976.

Hajduk, P. J. and Greer, J., (2007): A decade of fragment-based drug design: strategic advances and lessons learned, *Nat Rev Drug Discov*, **6**, 211-219.

Hajduk, P. J., Gomtsyan, A., Didomenico, S., Cowart, M., Bayburt, E. K., Solomon, L., Severin, J., Smith, R., Walter, K., Holzman, T. F., Stewart, A., McGaraughty, S., Jarvis, M. F., Kowaluk, E. A. and Fesik, S. W. (2000): Design of adenosine kinase inhibitors from the NMR-based screening of fragments, *J Med Chem*, **43**, 4781-4786.

Hanks S. K., Quinn, A.M. and Hunter, T. (1988): The protein kinase family: conserved features and deduced phylogeny of the catalytic domains, *Science*, **241**, 42-52.

Hanks, S. K. and Hunter, T. (1995): Protein kinases 6. The eukaryotic protein kinase superfamily: kinase (catalytic) domain structure and classification, *FASEB J*, **9**, 576-596.

Hahn, M. M., Tudor, I. O. (2004): Pursuing the leadlikeness concept in pharmaceutical research, *Curr Opin Chem Biol*, **8**, 255-263.

Hann, M. M., Leach, A. R. and Harper, G. (2001): Complexity and Its Impact on the Probability of Finding Leads for Drug Discovery, *J Chem Inf Comput Sci*, **41**, 856-864.

Hartshorn, M. J., Murray, C. W., Cleasby, A., Frederickson, M., Tickle, I. J. and Jhoti, H. (2005): Fragment-Based Lead Discovery Using X-ray Crystallography, *J Med Chem*, **48**, 403-413.

Hassell, A.M., An, G., Bledsoe, R. K., Bynum, J. M., Carter, H. L., Deng, S. J., Gampe, R. T., Grisard, T. E., Madauss, K. P., Nolte, R. T., Rocque, W. J., Wang, L., Weaver, K. L., Williams, S. P., Wisely, G. B., Xu, R. and Shewchuk, L. M. (2007): Crystallization of protein-ligand complexes, *Acta Crystallogr D*, **63**, 72-79.

Hendlich, M., Bergner, A., Günther, J. and Klebe, G. (2003): Relibase - Design and Development of a Database for Comprehensive Analysis of Protein-Ligand Interactions, *J Mol Biol*, **326**, 607-620.

Heinemann, U., Illing, G. and Oschkinat, H. (2001): High-throughput three-dimensional protein structure determination, *Curr Opin Biotechnol*, **12**, 348-354.

Hesterkamp, T. and Whittaker, M. (2008): Fragment-based activity space: smaller is better, *Curr Opin Chem Biol*, **12**, 260-268.

Hohwy, M., Spadola, L., Lundquist, B., Hawtin, P., Dahmén, J., Groth-Clausen, I., Nilsson, E., Persdotter, S., von Wachenfeldt, K., Folmer, R. H. and Edman, K. (2008): Novel Prostaglandin D Synthase Inhibitors Generated by Fragment-Based Drug Design, *J Med Chem*, **51**, 2178-2186.

Hoppe, W. (1957): Die Faltmolekülmethode: eine neue Methode zur Bestimmung der Kristallstruktur bei ganz oder teilweise bekannten Molekülstrukturen, *Acta Crystallogr*, **10**, 750-751.

Howard, N., Abell, C., Blakemore, W., Chessari, G., Congreve, M., Howard, S., Jhoti, H., Murray, C. W., Seavers, L.C. and van Montfort, R. L. (2006): Application of Fragment Screening and Fragment Linking to the Discovery of Novel Thrombin Inhibitors, *J Med Chem*, **49**, 1346-1355.

Huber, R. (1965): Die automatisierte Faltmolekülmethode, *Acta Crystallogr*, **19**, 353-356.

Huber, W. and Mueller, F. (2006): Biomolecular interaction analysis in drug discovery using surface plasmon resonance technology, *Curr Pharm Design*, **12**, 3999-4021.

Huber, W. (2005): A new strategy for improved secondary screening and lead optimization using high-resolution SPR characterization of compound-target interactions, *J Mol Recog*, **18**, 273-281.

Hunter, T. (1995): Protein kinases and phosphatases: the yin and yang of protein phosphorylation and signaling, *Cell*, **80**, 225-236.

Hunter T., (2000): Signalling-2000 and Beyond, *Cell*, **7**, 113-127.

Hünenberger, P. H., Helms, V., Narayana, N., Taylor, S.S. and McCammon, J. A. (1999): Determinants of Ligand Binding to cAMP-Dependent Protein Kinase, *Biochem*, **38**, 2358-2366.

Hämäläinen, M. D., Zhukov, A., Ivarsson, M., Fex, T., Gottfries, J., Karlsson, R. and Björsne, M. (2008): Label-Free Primary Screening and Affinity Ranking of Fragment Libraries Using Parallel Analysis of Protein Panels, *J Biomol Screening*, **13**, 202-209.

Irwin, J. J. and Shoichet, B. K. (2005): ZINC - A Free Database of Commercially Available Compounds for Virtual Screening, *J Chem Inf Model*, **45**, 177-182.

Jahnke, W. and Erlanson, D.A. (2006): Fragment-based approaches in Drug Discovery, Wiley-VCH Verlag GmbH & Co. KGaA.

Jhoti H. (2005): A new school for screening, *Nat Biotechnol*, **23**, 184-186.

Jhoti, H., Cleasby, A., Verdonk, M. and Williams, G. (2007): Fragment-based screening using X-ray crystallography and NMR spectroscopy, *Curr Opin Chem Biol*, **11**, 485-493.

Kabsch, W. J. (1993): Automatic processing of rotation diffraction data from crystals of initially unknown symmetry and cell constants, *J Appl Cryst*, **26**, 795-800.

Karle, J. and Hauptman, H. (1950): The phases and magnitudes of the structure factors, *Acta Crystallogr*, **3**, 181-187.

Karlsson, R., Kullman-Magnusson, M., Hämäläinen, M.D., Remaeus, A., Andersson, K., Borg, P., Gyzander, E. and Deinum, J. (2000): Biosensor analysis of drug-target interactions: Direct and competitive binding assays for investigation of interactions between thrombin and thrombin inhibitors, *Anal Biochem*, **278**, 1-13.

Katayama, N., Orita, M., Yamaguchi, T., Hisamichi, H., Kuromitsu, S., Kurihara, H., Sakashita, H., Matsumoto, Y., Fujita, S. and Niimi, T. (2008): Identification of a key element for hydrogen bonding patterns between protein kinases and their inhibitors, *Proteins*, **73**, 795-801.

Kemp, B. E., Graves, D. J., Benjamini, E. and Krebs, E.G. (1997): Role of Multiple Basic Residues in Determining the Substrate Specificity of Cyclic AMP-dependent Protein Kinase, *J Biol Chem*, **252**, 4888-4894.

Krebs, E. G. and Beavo, J. A. (1979): Phosphorylation-dephosphorylation of enzymes, *Annu Rev Biochem*, **48**, 923-959

Kuhn, P., Wilson, K., Patch, M. G. and Stevens, R. C. (2002): The genesis of high-throughput structure-based drug discovery using protein crystallography, *Curr Opin Chem Biol*, **6**, 704-710.

Leach, A. R., Hann, M. M., Burrows, J. N. and Griffen, E. J. (2006): Fragment screening: an introduction, *Mol Biosyst*, **2**, 429-446.

Leslie, A. G. W. (1992): Joint CCP4 + ESF-EAMCB Newsletter on Protein Crystallography, No. 26.

Lesley S. A. (2001): High-throughput proteomics: protein expression and purification in the postgenomic world, *Protein Expr Purif*, **22**, 159-164.

Liao, J. L. (2007): Molecular Recognition of Protein Kinase Binding Pockets for Design of Potent and Selective Kinase Inhibitors, *J Med Chem*, **50**, 409-424.

Liebeschuetz, J. W., Jones, S. D., Morgan, P. J., Murray, C. W., Rimmer, A. D., Roscoe, J. M., Waszkowycz, B., Welsh, P. M., Wylie, W. A., Young, S. C., Martin, H., Mahler, J., Brady, L. and Wilkinson, K. (2002): PRO_SELECT: combining structure-based drug design and array-based chemistry for rapid lead discovery. 2. The development of a series of highly potent and selective factor Xa inhibitors, *J Med Chem*, **45**, 1221-1232.

Liu, Y. and Gray, N. S. (2006): Rational design of inhibitors that bind to inactive kinase conformations, *Nature Chem Biol*, **7**, 358-364.

Lindsay M. A. (2005): Finding new drug targets in the 21st century, *Drug Discov Today*, **10**, 1683-1687.

Lundqvist, T. (2005): The devil is still in the details - driving early drug discovery forward with biophysical experimental methods, *Curr Opin Drug Discov Devel*, **8**, 513-519.

Lusty C. J. (1999): A gentle vapor-diffusion technique for cross-linking of protein crystals for cryocrystallography, *J Appl Cryst*, **32**, 106-112.

Malmqvist, M. (1993): Biospecific interaction analysis using biosensor technology, *Nature*, **361**, 186-187.

Manning, G., Whyte, D. B., Martinez, R., Hunter, T. and Sudarsanam, S. (2002): The protein kinase complement of the human genome, *Science*, **298**, 1912-1934.

Mausser, H. and Guba, W. (2008): Recent developments in *de novo* design and scaffold hopping, *Curr Opin Drug Discov Devel*, **11**, 365-374.

Marcou, G. and Rognan, D. (2007): Optimizing fragment and scaffold docking by use of molecular interaction fingerprints, *J Chem Inf Model*, **47**, 195-207.

McDonnell, J. M. (2001): Surface plasmon resonance: towards an understanding of the mechanisms of biological molecular recognition, *Curr Opin Chem Biol*, **5**, 572-577.

McGovern S. L., Caselli, E., Grigorieff, N. and Shoichet, B. K. (2002): A Common Mechanism Underlying Promiscuous Inhibitors from Virtual and High-Throughput Screening, *J Med Chem*, **45**, 1712-1722.

McGovern, S. L., Helfand, B. T., Feng, B. and Shoichet, B. K. (2003): A Specific Mechanism of Nonspecific Inhibition, *J Med Chem*, **46**, 4265-4272.

McPherson, A., Malkin, A. J. and Kuznetsov, Y. G. (1995): The science of macromolecular crystallization, *Structure*, **3**, 759-768.

McPherson A. (1982): The preparation and analysis of protein crystals, *John Wiley & Sons*, New York.

Melnikova, I. and Golden, J. (2004): Targeting protein kinases, *Nat Rev Drug Discov*, **3**, 993-994.

Metz, G., Otteleben, H. and Vetter, D. (2003): Small molecule screening on chemical microarrays, *Meth Principles Med Chem*. **19**, 213-236.

Myszka, D. (1997): Kinetic analysis of macromolecular interactions using surface plasmon resonance biosensors, *Curr Opin Biotechnol*, **8**, 50-57.

Neumann, T., Junker, H-D., Keil, O., Burkert, K., Otteleben, H., Gamer, J., Sekul, R., Deppe, H., Feurer, A., Tomandl, D. and Metz, G. (2005): Discovery of thrombin inhibitor fragments from chemical microarray screening, *Lett Drug Des Discovery*, **2**, 590-594.

Nienaber, V. L., Richardson, P. L., Klighofer, V., Bouska, J. J., Giranda, V. L. and Greer, J. (2000): Discovering novel ligands for macromolecules using X-ray crystallographic screening, *Nature Biotech*, **18**, 1105-1108.

Nordin, H., Jungnelius, M., Karlsson, R. and Karlsson, O. P. (2005): Kinetic studies of small molecule interactions with protein kinases using biosensor technology, *Anal Biochem*, **340**, 359-368.

Nordström, H., Gossas, T., Hämäläinen, M., Källblad, P., Nyström, P., Nyström, S., Wallberg, H. and Danielson, U. H. (2008): Identification of MMP-12 Inhibitors by Using Biosensor-Based Screening of a Fragment Library, *J Med Chem*, **51**, 3449-3459.

Norman, P. (2007): Fragments 2007 – What has fragment-based drug discovery delivered for medicinal chemistry?, *IDrugs*, **10**, 313-316.

Oblak, M., Grdadolnik, S. G., Kotnik, M., Jerala, R., Filipic, M. and Solmajer, T. (2005): In silico fragment-based discovery of indolin-2-one analogues as potent DNA gyrase inhibitors, *Bioorg Med Chem Lett*, **15**, 5207-5210.

Otwinowski, Z. and Minor, W. (1997): Processing of X-ray Diffraction Data Collected in Oscillation Mode, *Methods in Enzymology, Macromolecular Crystallography, Part A*, **276**, 307-326.

Papalia, G. A., Leavitt, S., Bynum, M.A., Katsamba, P.S., Wilton, R., Qiu, H. W., Steukers, M., Wang, S. M., Bindu, L., Phogat, S., Giannetti, A. M., Ryan, T. E., Pudlak, V. A., Matusiewicz, K., Michelson, K. M., Nowakowski, A., Pham-Baginski, A., Brooks, J., Tieman, B. C., Bruce, B. D., Vaughn, M., Baksh, M., Cho, Y. H., De Wit, M., Smets, A., Vandersmissen, J., Michiels, L. and Myszka, D. G. (2006): Comparative analysis of 10 small molecules binding to carbonic anhydrase II by different investigators using Biacore technology, *Anal Biochem*, **359**, 94-105.

-
- Pawson T. (1994): Introduction: Protein Kinases, *The FASEB Journal*, **8**, 1112-1113.
- Perutz, M. (1985): Early days of protein crystallography, *Methods Enzymol*, **114**, 3-18.
- Pflugrath, J. W. (1999): The finer things in X-ray diffraction data collection, *Acta Crystallogr D*, **55**, 1718-1725.
- Pickett, S.D., Sherborne, B. S., Wilkinson, T., Bennett, J., Borkakoti, N., Broadhurst, M., Hurst, D., Kilford, I., McKinnell, M. and Jones, P.S. (2003): Discovery of Novel Low Molecular Weight Inhibitors of IMPDH Via Virtual Needle Screening, *Bioorg Med Chem Lett*, **13**, 1691-1694.
- Prade, L. (1997): Staurosporin-induced conformational changes of cAMP-dependent protein kinase catalytic subunit explain inhibitory potential, *Structure*, **5**, 1627-1637.
- Reed, J. (1999): Dysregulation of Apoptosis in Cancer, *J Clin Onc*, **17**, 2941-2953.
- Reynolds, C. H., Tounge, B. A. and Bembenek, S. D. (2008): Ligand Binding Efficiency: Trends, Physical Basis, and Implications, *J Med Chem*, **51**, 2432-2438.
- Roche, O., Schneider, P., Zuegge, J., Guba, W., Kansy, M., Alanine, A., Bleicher, K., Danel, F., Gutknecht, E. M., Rogers-Evans, M., Neidhart, W., Stalder, H., Dillon, M., Sjögren, E., Fotouhi, N., Gillespie, P., Goodnow, R., Harris, W., Jones, P., Taniguchi, M., Tsujii, S., von der Saal, W., Zimmermann, G. and Schneider, G. (2002): Development of a virtual screening method for identification of "Frequent Hitters" in compound libraries, *J Med Chem*, **45**, 137-142.
- Rodems, S. M., Hamman, B. D., Lin, C., Zhao, J., Shah, S., Heidary, D., Makings, L., Stack, J. H. and Pollok, B. A. (2002): A FRET-based assay platform for ultra-high density drug screening of protein kinases and phosphatases, *Assay Drug Dev Technol*, **1**, 9-19.
- Roy J. J. and Abraham, T. E. (2004): Strategies in Making Cross-Linked Enzyme Crystals, *Chem Rev*, **104**, 3705-3722.
- Rupasinghe, C. N. and Spaller, M. R. (2006): The interplay between structure-based design and combinatorial chemistry, *Curr Opin Chem Biol*, **10**, 188-193.
- Sanders, W. J., Nienaber, V. L., Lerner, C. G., McCall, J. O., Merrick, S. M., Swanson, S. J., Harlan, J. E., Stoll, V. S., Stamper, G. F., Betz, S. F., Condroski, K. R., Meadows, R. P., Severin, J. M., Walter, K. A., Magdalinos, P., Jakob, C. G., Wagner, R. and Beutel, B. A. (2004): Discovery of Potent Inhibitors of Dihydroneopterin Aldolase Using CrystaLEAD, High-Throughput X-ray Crystallographic Screening and Structure-Directed Lead Optimization, *J Med Chem*, **47**, 1709-1718.
- Saxty, G., Woodhead, S. J., Berdini, V., Davies, T. G., Verdonk, M. L., Wyatt, P. G., Boyle, R. G., Barford, D., Downham, R., Garrett, M. D. and Carr, R. A. (2007): Identification of Inhibitors of Protein Kinase B Using Fragment-Based Lead Discovery, *J Med Chem*, **50**, 2293-2296.

Sharff, A. and Harren, J. (2003): High-throughput crystallography to enhance drug discovery, *Curr Opin Chem Biol*, **7**, 340–345.

Shoji, S., Titani, K., Demaille, J. G. and Fischer, E. H. (1979): Sequence of two phosphorylated sites in the catalytic subunit of bovine cardiac muscle adenosine 3':5'-monophosphate-dependent protein kinase, *J Biol Chem*, **54**, 6211–6214.

Schnur, D. M., (2008): Recent trends in library design: 'Rational design' revisited, *Curr Op Drug Disc Dev*, **11**, 375-380.

Allen, F. H. (2002): The Cambridge Structural Database: a quarter of a million crystal structures and rising, *Acta Crystallogr B*, **58**, 380-388.

Traxler, P. and Furet, P. (1999): Strategies toward the Design of Novel and Selective Protein Tyrosine Kinase Inhibitors, *Pharmacol Ther*, **8**, 195-206.

Taylor, J. D., Gilbert, P. J., Williams, M. A., Pitt, W. R. and Ladbury, J. E. (2007): Identification of novel fragment compounds targeted against the pY pocket of v-Src SH2 by computational and NMR screening and thermodynamic evaluation, *Proteins*, **67**, 981-990.

Taylor, S.S., Yang, J., Wu, J., Haste, N.M., Radzio-Andzelm, E. and Anand, G. (2004): PKA: a portrait of protein kinase dynamics, *Biochim Biophys Acta*, **1697**, 259– 269.

Vagin, A. and Teplyakov, A. (1997): MOLREP: an Automated Program for Molecular Replacement, *J Appl Cryst*, **30**, 1022-1025.

Vangrevelinghe, E. and Rüdissler, S. (2007): Computational approaches for fragment optimization, *Curr Comput Aided Drug Design*, **3**, 69–83.

Vriend, G. (1990): WHAT IF: A molecular modeling and drug design program, *J Mol Graph*, **8**, 52-56.

Wade, R. C. Henrich, S. and Wang, T. (2004): Using 3D protein structures to derive 3D-QSARs, *Drug Discov Today Tech*, **1**, 241-246.

Warner, S. L., Bashyam, S., Vankayalapati, H., Bearss, D. J., Han, H., Mahadevan, D., Von Hoff, D. D. and Hurley, L. H. (2006): Identification of a lead small-molecule inhibitor of the Aurora kinases using a structure-assisted, fragment-based approach, *Mol Cancer Ther*, **5**, 1764-1773.

Wlodawer, A., Minor, W., Dauter, Z. and Jaskolski, M. (2008): Protein crystallography for non-crystallographers, or how to get the best (but not more) from published macromolecular structures, *FEBS Journal*, **275**, 1–21.

Yonemoto, W., McGlone, M. L., Grant, B. and Taylor, S. S. (1997): Autophosphorylation of the catalytic subunit of cAMP-dependent protein kinase in *Escherichia coli*, *Protein Eng*. **10**, 915–925.

Zartler, E. R. and Shapiro, M. J. (2005): Fragonomics: fragment-based drug discovery, *Curr Opin Chem Biol*, **9**, 366–370.

Zheng, J., Trafny, E. A., Knighton, D. R., Xuong, N. H., Taylor, S. S., Ten Eyck, L. F. and Sowadski, J. M. (1993): 2.2 A refined crystal structure of the catalytic subunit of cAMP-dependent protein kinase complexed with MnATP and a peptide inhibitor, *Acta Crystallogr D*, **49**, 362-365.

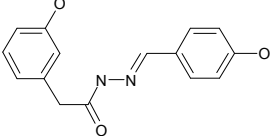
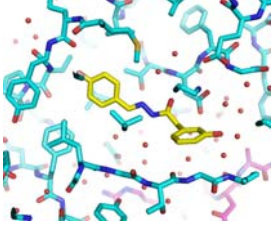
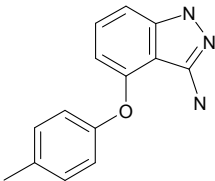
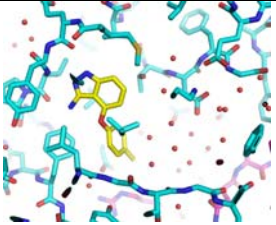
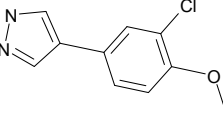
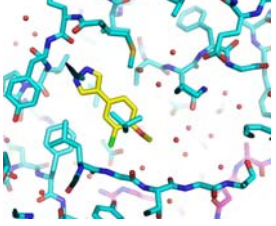
Internet references

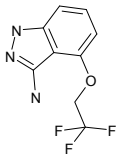
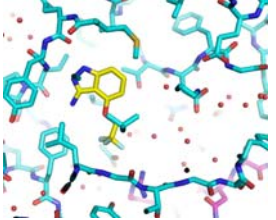
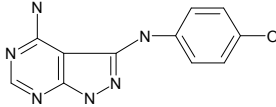
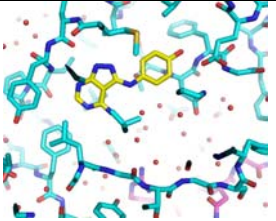
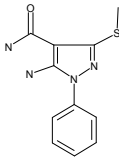
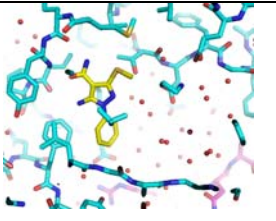
SLS - <http://sls.web.psi.ch/view.php/beamlines/px/index.html>

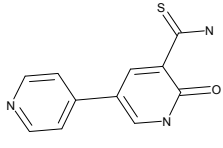
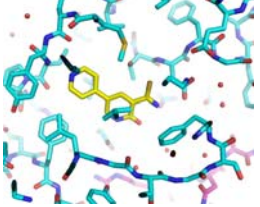
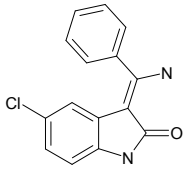
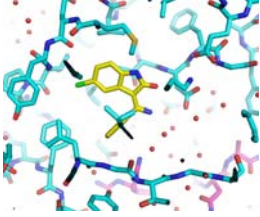
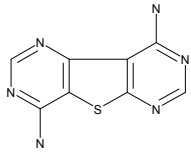
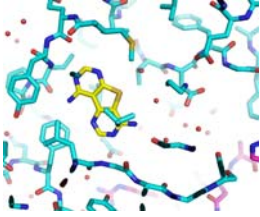
The Scripps Research Institute - <http://www.scripps.edu/~arvai/adv.html>

APPENDIX 1

Table 9. Binding modes for the nine fragments involved. The table below covers all nine fragments, and presents supplementary data on their molecular weights, biochemical-inhibition factors, and computed and measured solubilities. Also included are diagrams depicting their binding modes and brief descriptions of the fragment-protein interactions involved.

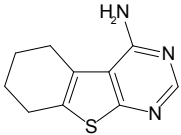
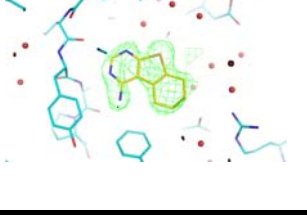
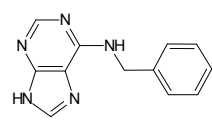
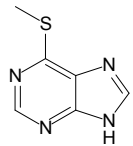
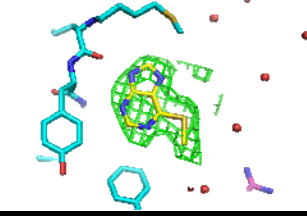
<p>Fragment 1</p> 	<p>MWT: 270.29 Inhibition: 41 % at 10 μM fragment concentration Solubility (computed pH: 7.4): 12.9 mM Solubility (kinetic): > 200 μM</p>
	<p>Fragment 1 binds to the kinase's A-/hinge zone, with its 4-phenol group acting as a donor/acceptor. Its pair of nitrogen atoms interacts with the DFG-<i>motif</i> in the K-zone and the glycine-rich loop in the kinase's P-zone. The carboxylic acid interacts directly with the (K-zone) Lys-72. Closer to the solvent, the fragment's 4-phenol group interacts with the tip of the (P-zone) glycine-rich loop, where the Phe-54-residue undergoes a π-π-interaction with the 4-phenol group.</p>
<p>Fragment 2</p> 	<p>MWT: 239.28 Inhibition: 9 % at 10 μM fragment concentration Solubility (computed pH: 7.4): 0.362 mM Solubility (kinetic): > 200 μM</p>
	<p>Fragment 2 forms three hydrogen bonds with the kinase's A-/hinge zone, one via its amine group, which interacts with the main-chain carboxyl-group of Val-123, and two to the Glu-121 hinge residue, via the indazole. Its toluene group is directed toward the (E₀-zone) aromatic residue, Phe-327, specific to AGC-kinases.</p>
<p>Fragment 3</p> 	<p>MWT: 208.65 Inhibition: 44 % at 10 μM fragment concentration Solubility (computed pH: 7.4): 1.26 mM Solubility (kinetic): 100 μM</p>
	<p>Fragment 3 forms two hydrogen bonds with the kinase's A-/hinge zone, where the two nitrogen atoms on its pyrazole group act as donor and acceptor, respectively, and interact with the Glu-121 and Val-123. The 3-chloro radical on its methoxy-phenyl group is situated near the kinase's (E₀-zone) Phe-327, at precisely the same location as the trifluoro group on fragment 4 and the toluene ring on fragment 2.</p>

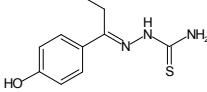
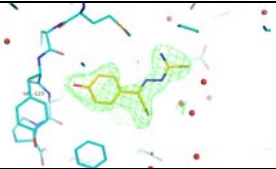
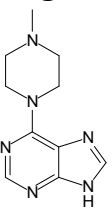
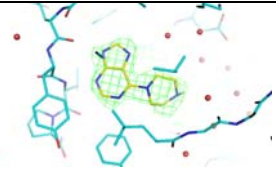
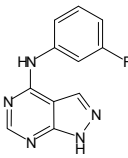
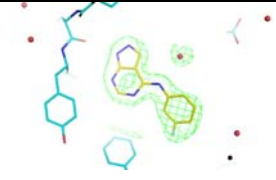
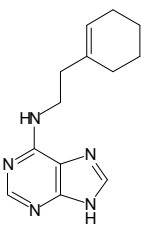
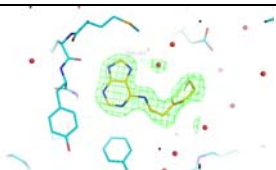
<p>Fragment 4</p> 	<p>MWT: 231.18 Inhibition: 13 % at 10 μM fragment concentration Solubility (computed pH: 7.4): 10 mM Solubility (kinetic): > 200 μM</p>
	<p>Fragment 4's indazole-amine group forms three hydrogen bonds with the kinase's A-/hinge zone. Its trifluoro group is situated within interaction range of the kinase's (E₀-zone) Phe-327, whose π-electrons interact with its electronegative fluorine atoms. Superimposing the diagram for fragment 4 on that for fragment 3 reveals that the trifluoro group on fragment 4 coincides with the chlorine atom on fragment 3, and therefore interacts with the protein in a similar manner.</p>
<p>Fragment 5</p> 	<p>MWT: 242.24 Inhibition: 20 % at 10 μM fragment concentration Solubility (computed pH: 7.4): 4.13 M Solubility (kinetic): > 200 μM</p>
	<p>Fragment 5's pyrazole-pyrimidine group forms two hydrogen bonds with the kinase's A-/hinge zone. Its hydroxyl-aniline group is directed toward the kinase's gatekeeper and BP-I/specificity pockets. An interaction between its aniline group's π-electron cloud and the electrons of the sulfur atom in the gatekeeper residue, Met-120, was observed.</p>
<p>Fragment 6</p> 	<p>MWT: 248.31 Inhibition: 33 % at 10 μM fragment concentration Solubility (computed pH: 7.4): 24.3 mM Solubility (kinetic): > 200 μM</p>
	<p>Fragment 6 has an amide group that acts as a hinge-binder in the kinase's A-zone. Its phenyl group is situated in the pocket close to the (E₀-zone) Phe-327, and its mercapto-methyl group is directed toward the (BP-I-pocket) gatekeeper residue, Met-120. Interestingly, the main chain flips 180° at the location of the (K-zone) Thr-183, which is probably due to the bulkiness of the sulfur atom on the ligand present in that zone. Also noteworthy is that the gatekeeper residue (Met-120) is thrust "upward" into the BP-I pocket, compared to the case for the other PKA-structures presented here and published in the pdb-database.</p>

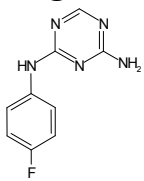
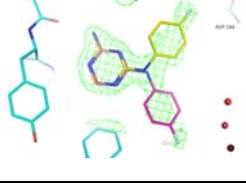
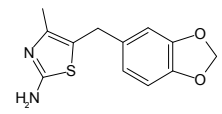
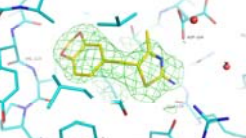
<p>Fragment 7</p> 	<p>MWT: 231.28 Inhibition: 43 % at 10 μM Solubility (computed pH: 7.4): 83.4 mM Solubility (kinetic): 50 μM</p>
	<p>Fragment 7 binds via a hydrogen bond that binds its pyridine group to the kinase's A-/hinge zone. Its thiocarbonyl group interacts with the aspartic-acid residue situated in the (Asp-184/K-zone) DFG-<i>motif</i>. Its sulfur group is directed toward the specificity/BP-I-pocket gatekeeper residue, Met-120. The nitrogen atom on its pyridine ring interacts with the Glu-327 present in the kinase's P-zone. The glycine-rich loop is not clearly differentiated from the protein's structure, which might be due to its relatively large, compared to the average for the protein, B-factors and diffuse electron density.</p>
<p>Fragment 8</p> 	<p>MWT: 270.72 Inhibition: 33 % at 10 μM fragment concentration Solubility (computed pH: 7.4): 708 μM Solubility (kinetic): 25 μM</p>
	<p>Fragment 8 binds to PKA, where its chlorine atom interacts with the kinase's A-/hinge zone. Its phenyl group is situated in the same pocket as that on fragment 1, i.e., that close to the (E_0-zone) Phe-327 residue. Its indole-carbonyl group points outward, toward the solvent/P-zone.</p>
<p>Fragment 9</p> 	<p>MWT: 218.24 Inhibition: 22 % at 10 μM fragment concentration Solubility (computed pH: 7.4): 379 μM Solubility (kinetic): > 200 μM</p>
	<p>The amino-pyrimidine groups on fragment 9 bind to the kinase's A-/hinge zone. One has its sulfur atom pointing toward the gatekeeper residue (the Met-120 situated between the kinase's A-zone and BP-I pocket), and the other points toward the solvent (P-zone) and picks up interactions with surrounding residues via interactions with water molecules.</p>

APPENDIX 2

Table 10. The results of the X-ray-crystallographic investigations conducted. The table below covers all nine fragments detected in the electron density of the ATP binding pocket in PKA, and includes their molecular structures, binding affinities, and inhibition constants, brief descriptions of the interactions occurring between the respective fragments and protein, and diagrams illustrating the 3D-binding modes involved.

<p>Fragment 178</p> 	<p>MWT: 205.28 HCA IC₅₀: 38 μM SPR K_D: 500 μM – 1 mM</p>
	<p>Fragment-protein interactions: Fragment 178 binds to PKA via two hinge interactions. Its 6-nitrogen acts as an acceptor, and its amide nitrogen acts as a donor with respect to the main-chain amide and carboxyl group on the hinge residue, Val-123. Its electron-rich sulfur atom is readily apparent in the electron density and points upward, toward the Met-120 residue, yielding a sulfur-sulfur interaction. Its saturated pyrimidine ring is not readily evident in the electron-density distribution.</p>
<p>Fragment 6</p> 	<p>MWT: 225.6 HCA IC₅₀: - SPR K_D: 100 μM – 200 μM</p>
	<p>Fragment-protein interactions: Fragment 6 binds to the protein, where its purine moiety forms two hydrogen bonds to the hinge zone at the ATP binding site. The benzene group is rotated 90° relative to the purine scaffold and is situated in the ribose-binding pocket.</p>
<p>Fragment 20</p> 	<p>MWT: 166.21 HCA IC₅₀: 51 μM SPR K_D: Binding occurred at low concentrations and concentration-dependent aggregation was observed at the higher fragment concentrations (> 70 μM); its affinity (K_D) was not computed.</p>
	<p>Fragment-protein interactions: Fragment 20 bonds to the protein, where its purine moiety forms two hydrogen bonds to the hinge zone at the kinase-ATP-binding site. The 5-sulfur atom is clearly visible in the electron-density distribution and directed toward the ribose pocket.</p>

<p>Fragment 23</p> 	<p>MWT: 223.30 HCA IC₅₀: - SPR K_D: 500 μM – 1 mM</p>
	<p>Fragment-protein interactions: Fragment 23 binds to the protein, where its phenol moiety acts as both a donor and an acceptor with respect to the hinge zone in the ATP-pocket. Its ethyl radical points downward, toward the ribose pocket, and its sulfonamide group points upward, toward the DFG-residue, Asp-184, and the gatekeeper residue, Met-120.</p>
<p>Fragment 103</p> 	<p>MWT: 218.26 HCA IC₅₀: 100 μM SPR K_D: 70 μM</p>
	<p>Fragment-protein interactions: Fragment 103 binds to the protein, where its purine moiety forms two hydrogen bonds to the hinge zone at the kinase-ATP-binding site. Its methyl-piperidine group takes on a chair conformation and is situated in the ribose pocket.</p>
<p>Fragment 154</p> 	<p>MWT: 229.22 HCA IC₅₀: 27 μM SPR K_D: a weak binder (K_D > 1 mM)</p>
	<p>Fragment-protein interactions: Fragment 154 binds to the protein, where its pyrazole-pyrimidine moiety forms two hydrogen bonds to the latter's hinge zone. Its fluorophenyl group points downward, toward the ribose pocket, and interacts with the Phe-327-residue's π-electrons. That residue is specific to just a few members of the AGC-protein-kinase family and blocks part of the ATP binding pocket, where many small-molecule, protein-kinase inhibitors are frequently observed to interact.</p>
<p>Fragment 162</p> 	<p>MWT: 243.31 HCA IC₅₀: 86 μM SPR K_D: 100 μM</p>
	<p>Fragment-protein interactions: The purine in fragment 162 forms two hydrogen bonds to the ATP-pocket's hinge zone. An interaction with the Thr-183-residue is picked up from the nitrogen in its purine ring, via a water molecule. Its cyclohexane ring points away from the hinge, toward the solvent zone.</p>

Fragment 192 	MWT: 205.20 HCA IC₅₀: - SPR K_D: 400 μ M
	Fragment-protein interactions: Interestingly, fragment 192 exhibited two, distinct binding modes, both of which were readily apparent in the electron-density distribution obtained following collection of protein-crystallographic data. Both conformations have the aminoamide as their hinge-binding structure. However, in one of those conformations, the fluorephenyl group points toward the DFG- <i>motif</i> , and, in the other, it points toward the ribose pocket.
Fragment 236 	MWT: 248.30 HCA IC₅₀: 59 μ M SPR K_D: 70 μ M
	Fragment-protein interactions: Fragment 236 binds to the protein, where its benzofuran group interacts with the kinase's hinge zone. Its thiophene ring is directed toward the solvent and its amine group picks up an interaction with the Glu-127-residue situated in the ribose-binding pocket.

APPENDIX 3

Table 11. Characterization data for all those fragments contained in the library. The first column lists the fragment number, the second column contains a +/- indicating whether the fragment involved was classified as a hit/no hit, respectively, under the SPR-screenings conducted, the third column lists the values of K_D determined from those SPR-screenings, the fourth column lists the fragment binding affinities determined in conjunction with SPR-hit characterization, the fifth column contains a +/- indicating whether the fragment involved was classified as a hit/no hit, respectively, under the HCA-screenings conducted, and the sixth column 6 the values of IC50 determined in conjunction with HCA-hit characterization. The seventh column contains a +/- indicating whether an X-ray-diffraction structure determination was conducted for the fragment involved. The column listing binding affinities states the respective ranges involved, where “cd” indicates that concentration-dependent aggregation occurred, “ns” indicates that nonstoichiometric binding occurred, “ss” indicates that superstoichiometric binding occurred, and “i” indicates that irreversible/pseudo-irreversible interactions were involved. Characterization as a “weak binder” indicates that although the fragment involved exhibited typical transient binding, its binding affinity was not computed. Fragments characterized as “general promiscuous” or “nonbinder” have also been included.

FRAGMENT NO.	SPR-SCREENING	SPR-KD [μ M]	BINDING AFFINITY	HCA-SCREENING	HCA-IC50 [μ M]	X-RAY
1	—			—		—
2	—			—		—
3	—			—		—
4	—			—		—
5	—			—		—
6	+	150	100 μ M – 200 μ M	—		+
7	—			—		—
8	—			—		—
9	—			—		—
10	—			—		—
11	—			—		—
12	—			—		—
13	—			—		—
14	—			—		—
15	—			—		—
16	—			—		—
17	—			—		—
18	—			—		—
19	—		cd, weak binder	+		—
20	—		cd/i, binder	+	51	+
21	+		Weak binder	—		—
22	+		Weak binder	—		—
23	+	750	500 μ M – 1 mM	—		+
24	—		cd, binder	+		—

25	+		weak binder	—		—
26	—			—		—
27	—			—		—
28	—			—		—
29	—			—		—
30	—			—		—
31	+		weak binder	—		—
32	—			—		—
33	—			—		—
34	—			—		—
35	—			—		—
36	—			—		—
37	—			—		—
38	—			—		—
39	—			—		—
40	—			—		—
41	—			—		—
42	—			—		—
43	—			—		—
44	—			—		—
45	—			—		—
46	—			—		—
47	—			—		—
48	—			—		—
49	+		general promiscuous	—		—
50	—			—		—
51	—			—		—
52	—			—		—
53	—			—		—
54	—			—		—
55	—			—		—
56	—			—		—
57	+	35	20 μ M – 50 μ M	+	110	—
58	+		nonbinder	—		—
59	+	300	200 μ M – 400 μ M	—		—
60	+		weak binder	—		—
61	—			—		—
62	—			—		—
63	—			—		—

64	—			—		—
65	+	65	60 μ M – 70 μ M	+	73	—
66	+		weak binder	—		—
67	—			—		—
68	—			—		—
69	—			—		—
70	—			—		—
71	—			—		—
72	—			—		—
73	+		nonbinder	—		—
74	+		ns/i	—		—
75	—			—		—
76	—			—		—
77	—			—		—
78	—			—		—
79	+		ns/i	+	38	—
80	+		cd, weak binder	+		—
81	—			—		—
82	—			—		—
83	+		weak binder	—		—
84	—			—		—
85	—			—		—
86	—			—		—
87	+		ns	+		—
88	+		weak binder	—		—
89	+	100	100 μ M	+		—
90	—			—		—
91	—			—		—
92	—			—		—
93	—			—		—
94	—			—		—
95	—			—		—
96	+	15	15 μ M	+		—
97	—			—		—
98	+		nonbinder	—		—
99	+			—		—
100	—		ss/i	+		—
101	—			—		—
102	—			—		—

103	—	70	70 μ M	+	100	+
104	—			—		—
105	—			—		—
106	—			—		—
107	—			—		—
108	—			—		—
109	—			—		—
110	+		weak binder	—		—
111	—			—		—
112	—			—		—
113	—			—		—
114	+		weak binder	—		—
115	—			—		—
116	—			—		—
117	—			—		—
118	—			—		—
119	+		cd, weak binder	—		—
120	—			—		—
121	—			—		—
122	+	750	0.5 mM – 1 mM	+		—
123	+	700	700 μ M	+		—
124	—			—		—
125	—		ns	+		—
126	—			—		—
127	—			—		—
128	—			—		—
129	—			—		—
130	+		nonbinder	—		—
131	—			—		—
132	—			—		—
133	—			—		—
134	—			—		—
135	—			—		—
136	—			—		—
137	—			—		—
138	—			—		—
139	+	150	100 μ M – 200 μ M	+	64	—
140	+	100	100 μ M	+	23	—
141	—			—		—

142	—			—		—
143	—			—		—
144	—			—		—
145	—			—		—
146	—			—		—
147	—			—		—
148	—			—		—
149	+		ss/l, cd/l, weak binder	—		—
150	+		nonbinder	—		—
151	—			—		—
152	—			—		—
153	—			—		—
154	+		weak binder	+	27	+
155	—			—		—
156	—			—		—
157	—			—		—
158	—			—		—
159	—			—		—
160	—			—		—
161	—			—		—
162	+	100	100 µM	+	86	+
163	—			—		—
164	—			—		—
165	—			—		—
166	—			—		—
167	—			—		—
168	+		weak binder	—		—
169	—			—		—
170	—			—		—
171	—			—		—
172	—			—		—
173	—		nonbinder	+		—
174	—			—		—
175	—			—		—
176	—		ns/i	+		—
177	+		weak binder	—		—
178	+	750	500 µM	+	38	+
179	—			—		—
180	—			—		—

181	—			—		—
182	+		weak binder	—		—
183	—			—		—
184	—			—		—
185	—			—		—
186	—			—		—
187	—			—		—
188	—			—		—
189	—			—		—
190	—			—		—
191	—			—		—
192	+	400	400 μ M	+		+
193	+	80	80 μ M	—		—
194	—			—		—
195	+		weak binder	—		—
196	—			—		—
197	+	1000	1 mM	—		—
198	—			—		—
199	+	650	600 μ M – 700 μ M	—		—
200	—			—		—
201	—			—		—
202	—			—		—
203	+	300	300 μ M	—		—
204	—			—		—
205	+	600	600 μ M	—		—
206	—			—		—
207	—			—		—
208	—			—		—
209	+	800	700 μ M – 900 μ M	—		—
210	—			—		—
211	+		nonbinder	—		—
212	—			—		—
213	—			—		—
214	+		weak binder	—		—
215	—			—		—
216	—			—		—
217	—			—		—
218	—			—		—
219	+	300	300 μ M	—		—

220	—			—		—
221	—			—		—
222	—			—		—
223	—			—		—
224	—			—		—
225	—			—		—
226	+	300	300 μ M	+		—
227	—			—		—
228	—			—		—
229	—			—		—
230	—			—		—
231	—			—		—
232	+		weak binder	—		—
233	—			—		—
234	—			—		—
235	—			—		—
236	+	70	70 μ M	+	59	+
237	—			—		—
238	—			—		—
239	—			—		—
240	+		cd, binder	+	65	—
241	—			—		—
242	—			—		—
243	+		nonbinder	—		—
244	+		weak binder	—		—
245	—			—		—
246	—			—		—
247	—			—		—
248	—			—		—
249	—			—		—
250	—			—		—
251	+		nonbinder	—		—
252	—			—		—
253	+		cd, weak binder	—		—
254	—			—		—
255	—			—		—
256	+		weak binder	—		—
257	—			—		—